SOUTHWEST RESEARCH INSTITUTE
Post Office Drawer 28510, 6220 Culebra Road
San Antonio, Texas 78284

METALLURGICAL INVESTIGATION OF CRACKING IN A REACTOR VESSEL NOZZLE SAFE-END

FINAL REPORT

SwRI Project 02-5389-001

To

Iowa Electric Light and Power Co.
IE Tower
200 First Street S.E.
Cedar Rapids Iowa 52406

December 26, 1978

Prepared by:
H. C. Burghard, Jr.
A. J. Bursle

Approved:

U. S. Lindholm, Director
Department of Materials Sciences

TABLE OF CONTENTS

1.0 INTRODUCTION

A safe-end forging removed from a recirculation inlet nozzle of the reactor vessel at the Duane Arnold Energy Center was submitted to Southwest Research Institute by Iowa Electric Light and Power Company. Through-wall cracking of this component had developed in service. A diagram of the recirculation inlet nozzle with the attached safe-end and thermal sleeve is shown in Figure 1-1.

The safe-end sample, shown in Figure 1-2, was identified as recirculation inlet nozzle 2A. Penetration of the wall of the safe-end had occurred over approximately 85° of the outside surface (from 75° clockwise to 160°). The appearance of the crack on the outside surface is shown in Figure 1-3.

The safe-end and thermal sleeve materials were specified as Inconel 600 to meet the requirements of ASME SB 166. The thermal sleeve attachment weld was reported to have been made with Inconel 182 stick electrodes. In the initial fabrication of the safe-end a repair weld was made on the outside of the forging to correct a machining error. This repair weld was visually evident on the outside of the sample, see Figures 1-2 and 1-3.

A metallurgical examination of the safe-end was initiated to establish the nature and extent of the cracking and to identify the mechanism and cause of failure. This investigation included ultrasonic inspection of the safe-end sample, chemical analysis of the safe-end and thermal sleeve materials, and metallographic examinations of representative sections through the thermal sleeve attachment area. Fractographic examinations of representative crack surface specimens and analyses of surface deposits were also performed.

The locations of the metallographic sections and the crack surface specimens examined in this investigation are indicated in Figure 1-4. All saw cutting operations performed in the removal of these specimens were performed without lubricants to prevent contamination of the sample. The sample was radioactively contaminated so that it was necessary to perform all saw cutting and specimen grinding operations in a special radiation containment facility.

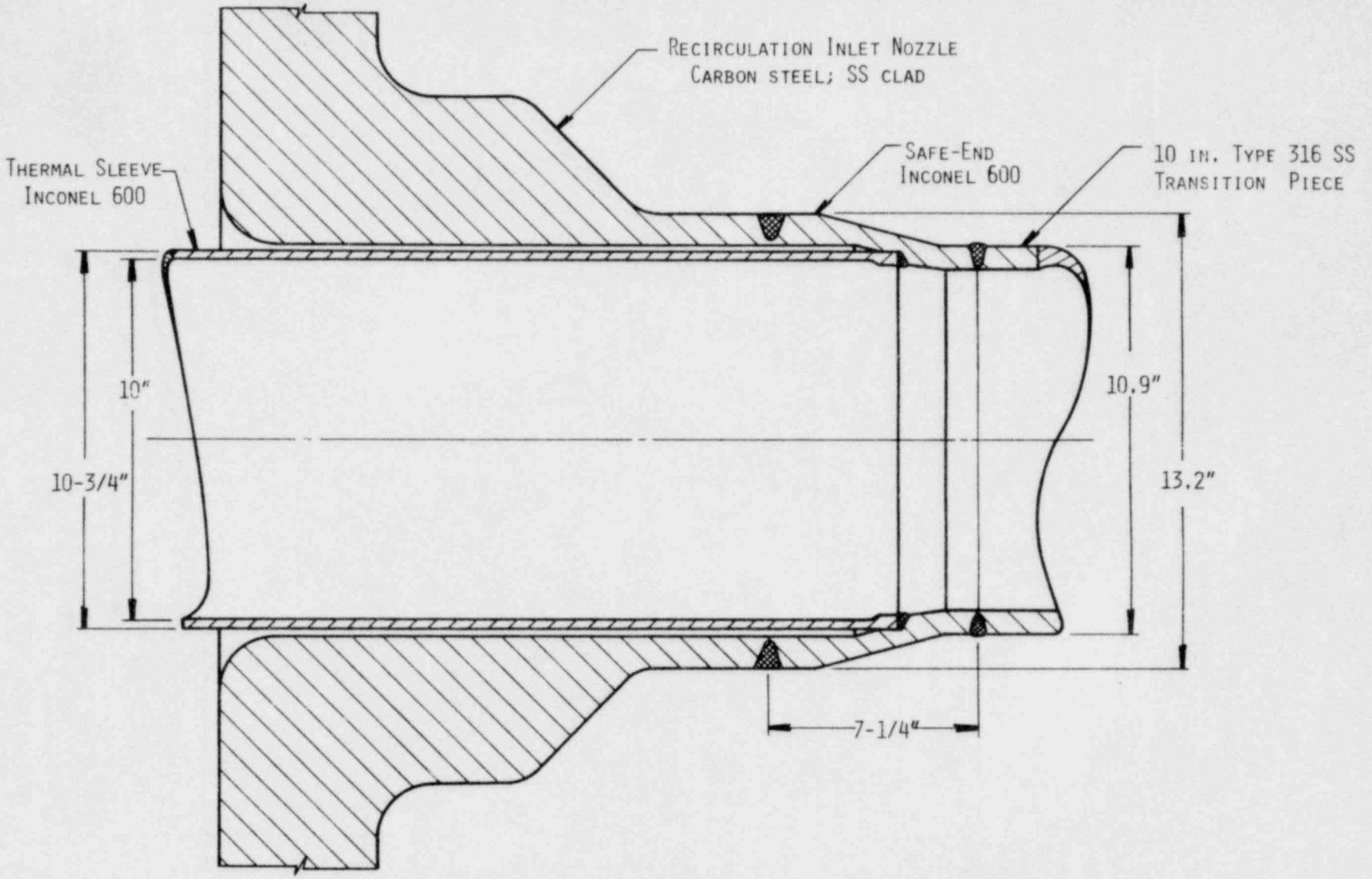

FIGURE 1-1. RECIRCULATION INLET NOZZLE

2-34314

FIGURE 1-2. SAFE-END SAMPLE. Arrows mark the ends of the through-wall-crack.

2-34320

(a) At 150°

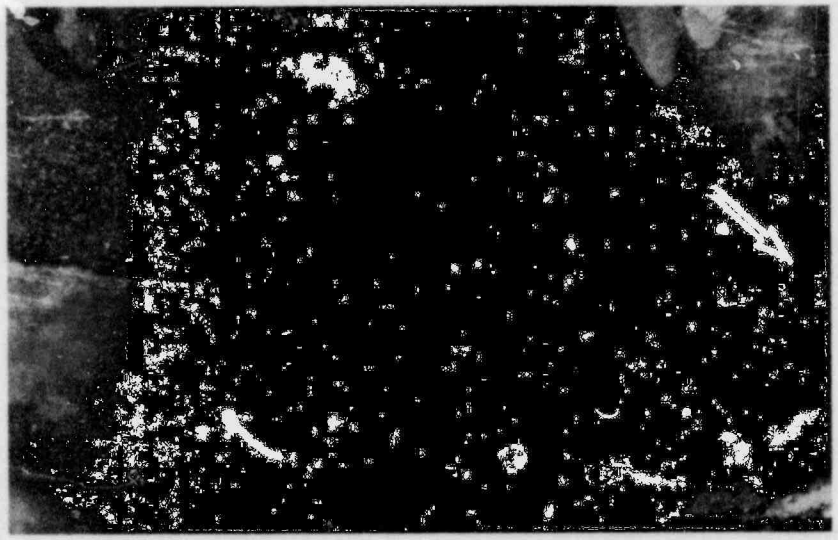

2-34322

(b) At 90°

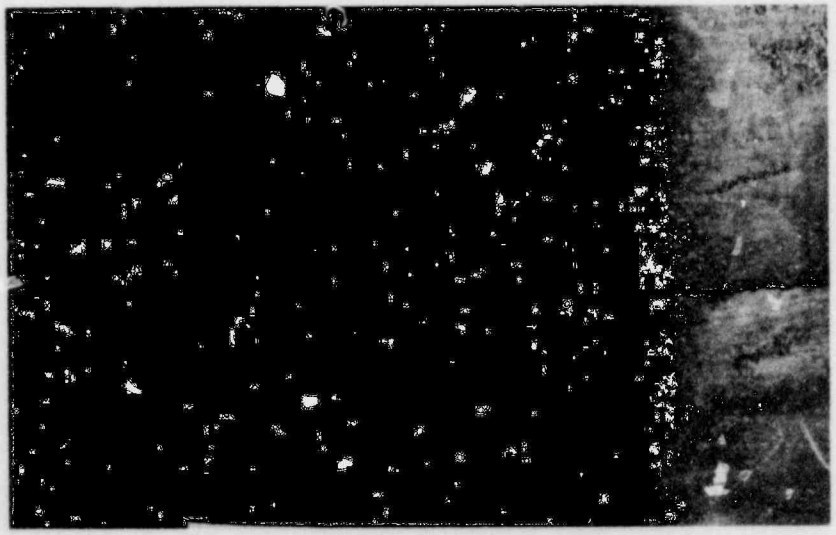

2-34321

(c)

FIGURE 1-3. CRACK ON OUTSIDE SURFACE OF SAFE-END. Arrows indicate end of through-wall crack. Note shift in crack path in (c). Actual size.

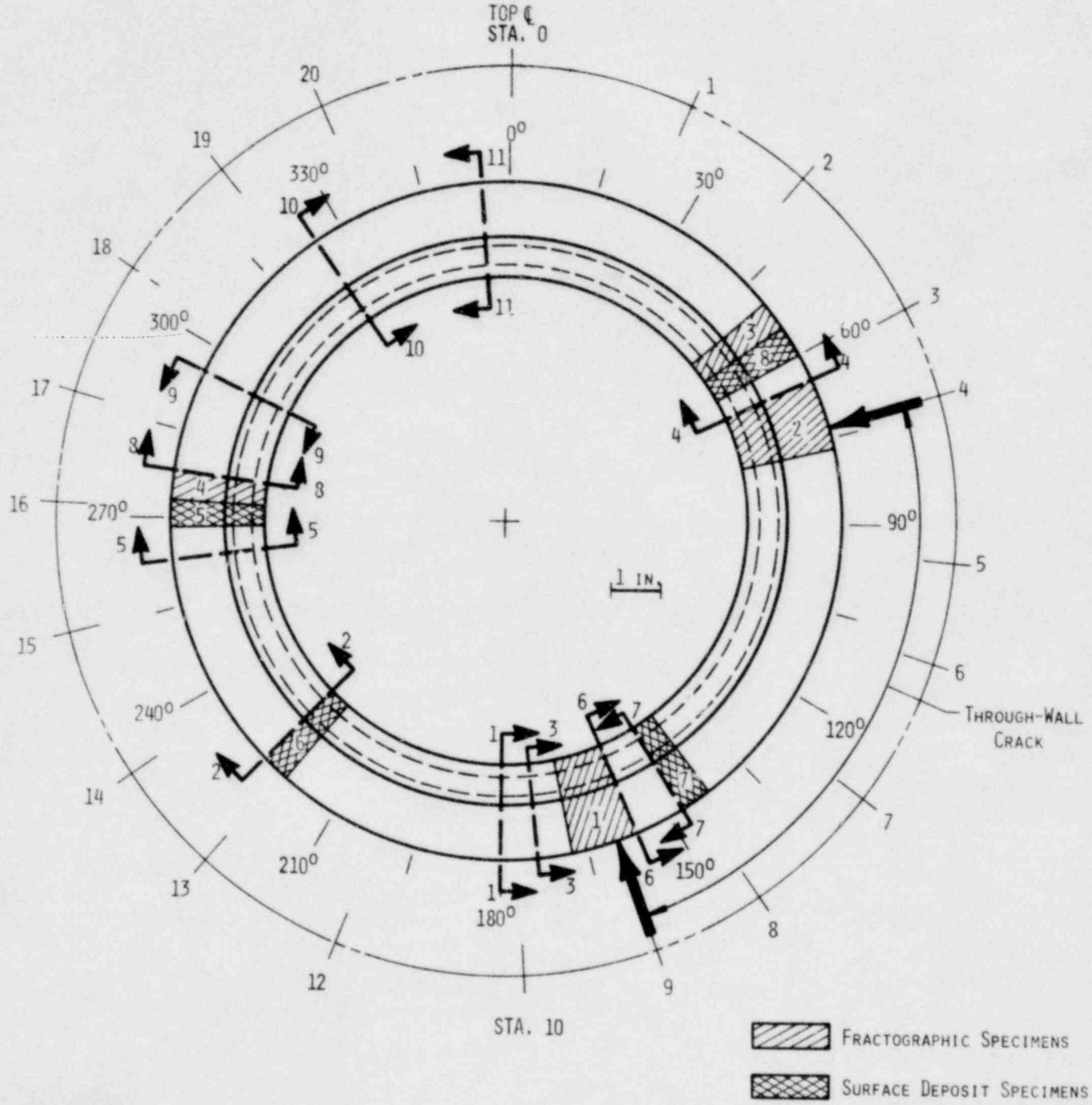

FIGURE 1-4. SPECIMEN LOCATIONS

2.0 MACROSCOPIC ASPECTS OF CR CKING

2.1 Nondestructive Inspections

A radiographic inspection of the safe-end was performed on site at t e Duane Arnold Energy Center after removal of the safe-end sample from the reactor vessel. This inspection identified major cracking over approximately 280° of the circumference. No identifiable crack indications were noted in the region extending from 270° to 345°. Copies of representative portions of the radiographs are included in Appendix A.

A limited ultrasonic inspection of the safe-end sample was performed after receipt at SwRI. A 1.5 MHz transducer was employed in the inspection and the sound beam was directed from the large end toward the smaller end. The cracking in the safe-end was readily detectable by this technique. Particular attention was paid to the zone in which no definite radiographic crack indications were obtained. Definite ultrasonic crack indications were noted over the entire segment from 270° to 0°, establishing that major cracking extended completely around the inside surface of the safe-end.

2.2 Crack Location and Configuration

A total of eleven longitudinal sections were examined macroscopically to establish the general location and confi ration of cracking. As shown in Figure 1-4, the particular sections included locations near each end of the through-wall portion of the crack and sections selected on the basis of the radiographic crack indications to provide for evaluation over the complete circumference.

A diagram of a typical longitudinal section, showing the relative positions of the attachment weld, crevice, and repair weld is shown in Figure 2-1. Macrographs of representative sections are shown in Figures 2-2 through 2-5. Additional macrographs are included in Appendix B.

Major cracking was evident in all of the sections examined. At all locations, the crack originated near the tip of the crevice adjacent to the attachment weld and extended outward through the safe-end wall. In that portion of the through-wall crack extending from approximately 125° to 160°,

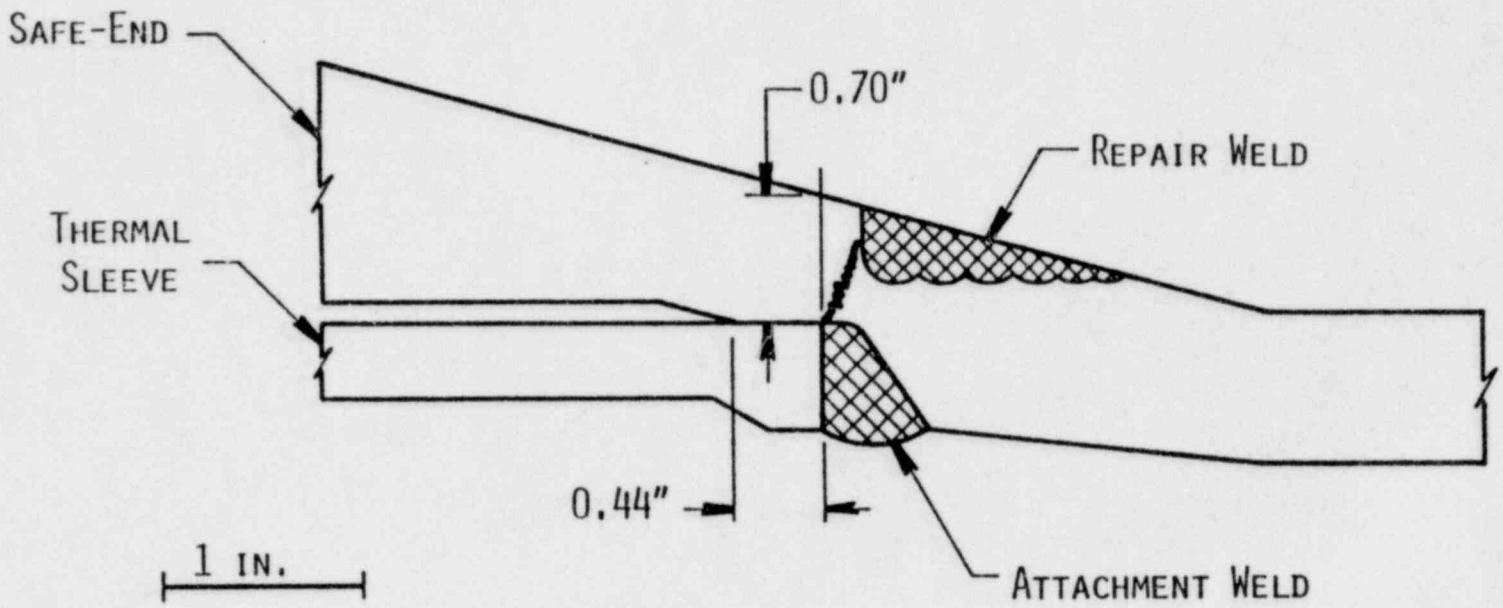

FIGURE 2-1. TYPICAL LONGITUDINAL SECTION THROUGH THERMAL SLEEVE ATTACHMENT AREA

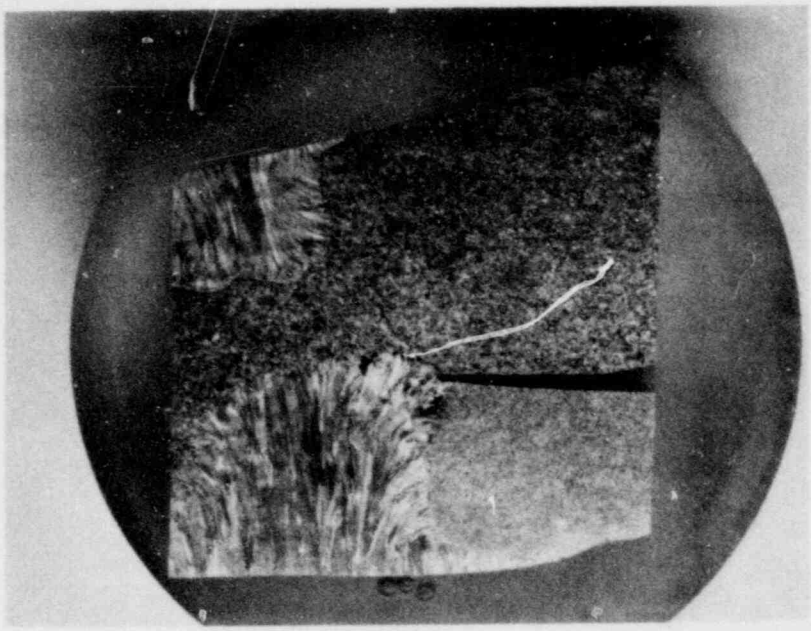

2-34348 2X

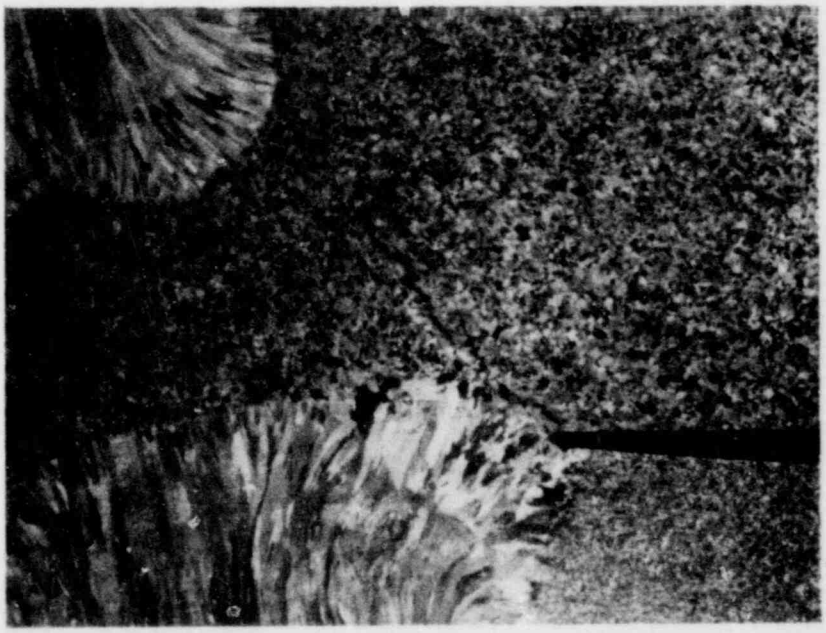

2-34349 5X

FIGURE 2-2. LONGITUDINAL SECTION AT THERMAL SLEEVE ATTACHMENT. Section 1-1, Figure 1-4. Lapito's etch.

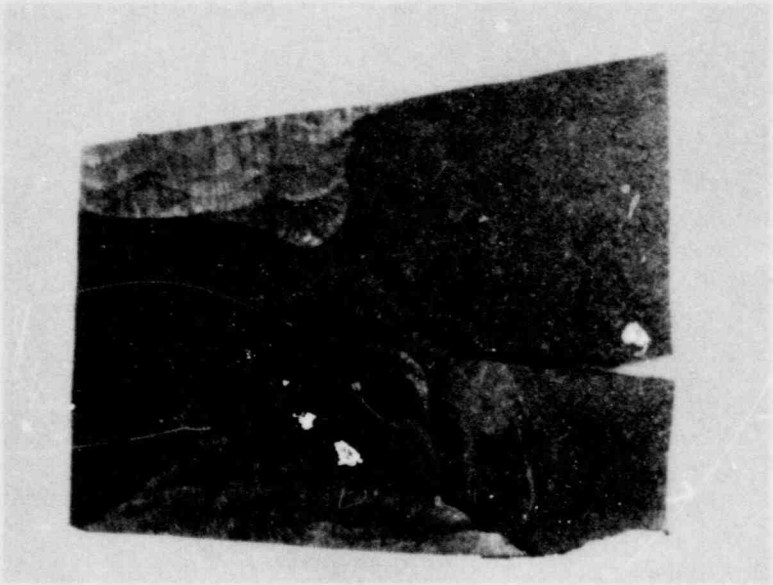

2-34461 2X

2-34462 5X

FIGURE 2-3. LONGITUDINAL SECTION AT THERMAL SLEEVE ATTACHMENT. Section 4-4, Figure 1-4. Lapito's etch.

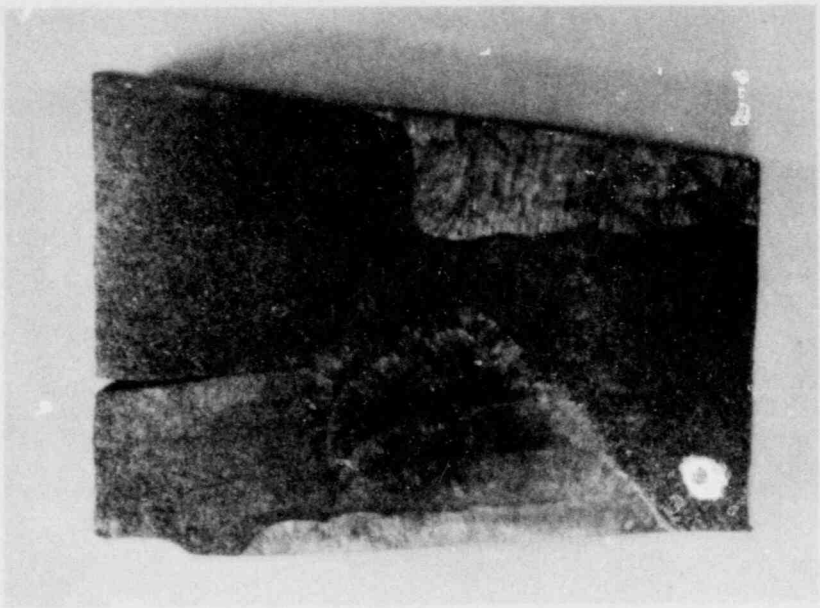

2-34447 2X

Lapito's etch

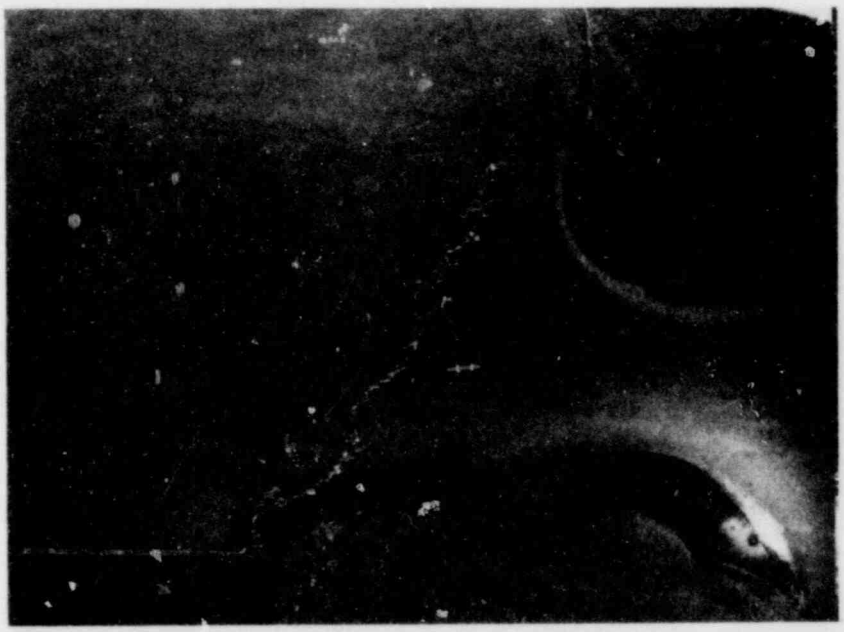

2-34492 5X

Etchant: 8:1
Phosphoric acid

FIGURE 2-4. LONGITUDINAL SECTION AT THERMAL SLEEVE ATTACHMENT.
Section 5-5, Figure 1-4.

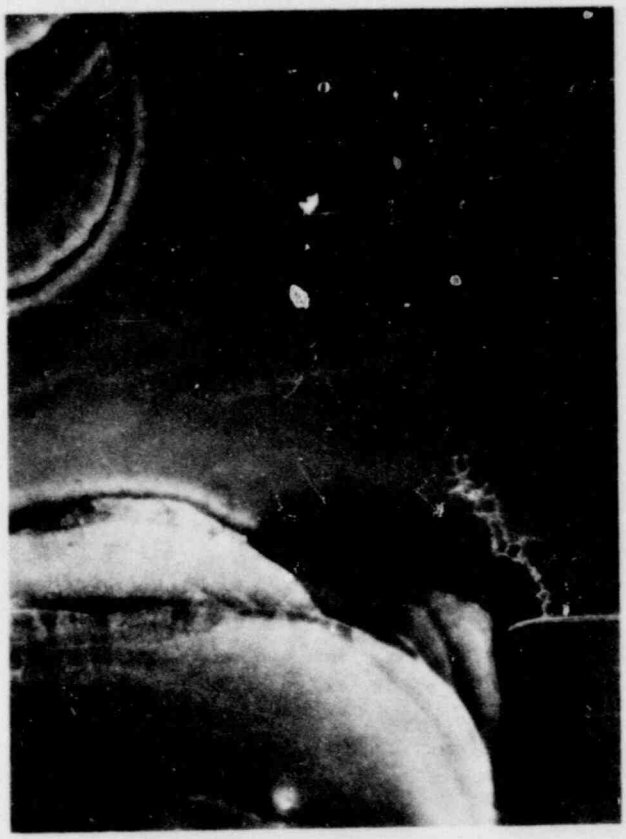

2-34868

FIGURE 2-5. LONGITUDINAL SECTION AT THERMAL SLEEVE ATTACHMENT. Section 9-9, Figure 1-4. Etchant: 8:1 Phosphoric acid. 7X

the later stages of cracking propagated through the repair weld, see Figures 2-2, B-1(b), B-1(c) and B-1(d). In the zone from approximately 75° to 125° crack propagation occurred completely within the safe-end base metal and penetrated the outside surface adjacent to the fusion line of the repair weld, (Figure 2-3).

The crack length a' remaining ligament (radial distance from the crack tip to the outside surface) were measured in all eleven sections. The results are plotted in Figure 2-6. Examination of sections 5-5, 8-8, 9-9, 10-10 and 11-11 verified the existence of major cracking in the zone from 270° to 330°. The radiographic inspection of this area did not reveal definite crack indications.

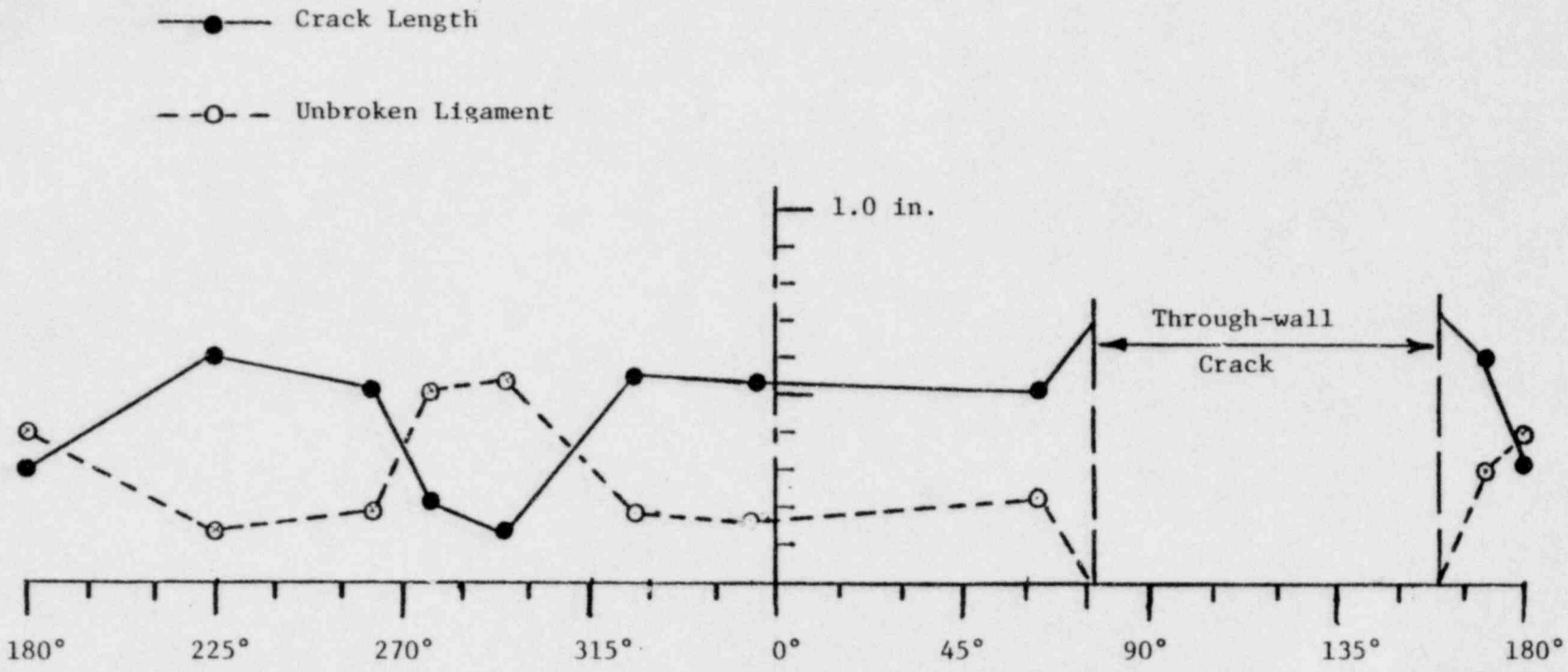

FIGURE 2-6. CRACK LENGTH AND UNBROKEN LIGAMENT VS ANGULAR POSITION

3.0 MATERIALS CHARACTERIZATION

3.1 Chemical Composition

Samples of the safe-end, thermal sleeve, attachment weld metal and repair weld metal were analyzed to determine the bulk chemical composition. The results of these analyses are presented in Table 3-1 together with the composition limits specified by ASME SB 166 for wrought Inconel 600 and by AWS-5.11-76 for as deposited Inconel 182 weld metal.

These analyses established that both the safe-end forging and the thermal sleeve material conform to the compositional requirements of SB 166. It was reported that Inconel 182 stick electrodes were employed for the weld repair and thermal sleeve attachment weld. The composition of the attachment weld conforms to the specified composition for deposited ENiCrFe-3 weld deposit metal (Inconel 182) in all respects. The composition determined for the repair weld meets the requirements for ENiCrFe-3 except for a slightly low manganese content.

3.2 Microstructure

The typical microstructure of the safe-end forging, as observed at locations remote from the welds, is shown in Figure 3-1. The micrographs shown illustrate the microstructural features revealed by dual etching. The specimens were polished and etched in 10% nital and examined on the optical metallograph. Subsequently, the specimens were repolished, reetched in 8:1 phosphoric acid, and examined at the identical location to provide a direct comparison of microstructural features revealed by the two etching techniques.

The 10% nital etch will delineate grain boundaries in Inconel 600 regardless of the heat treating condition. The phosphoric acid etch selectively attacks precipitated carbides in the microstructure. As a result, grain boundaries and other microstructural features are delineated by this etch only if they are decorated with precipitated carbides. Thus, the lack of any grain boundary etching effect with the phosphoric acid etch, at a location where grain boundaries have been identified by a nital etch, is a specific indication of a fully solution treated microstructure.

TABLE 3-1

CHEMICAL COMPOSITION

Item	Composition - Wt.%								
	Ni	Cr	Fe	Co	C	Mn	Cu	Si	S
Safe-end	74.82	15.18	8.61	0.06	0.07	0.18	0.13	0.29	0.005
Thermal Sleeve	77.42	14.86	6.98	0.04	0.07	0.28	0.01	0.15	0.005
ASME SB-166	72.0 Min.	14.0-17.0	6.0-10.0	Incl. w/Ni	0.15 Max.	1.00 Max.	0.50 Max.	0.50 Max.	0.015 Max.
Repair Weld	70.46	14.54	8.21	0.04	0.05	4.80	0.06	0.53	0.008
Attachment Weld	67.90	14.48	8.16	0.03	0.05	7.10	0.16	0.51	0.018
AWS-5.11-76 ENiCrFe-3	59.0 Min.	13.0-17.0	10.0 Max.	0.12 Max.	0.10 Max.	5.0-9.5	0.5 Max.	1.0 Max.	0.015

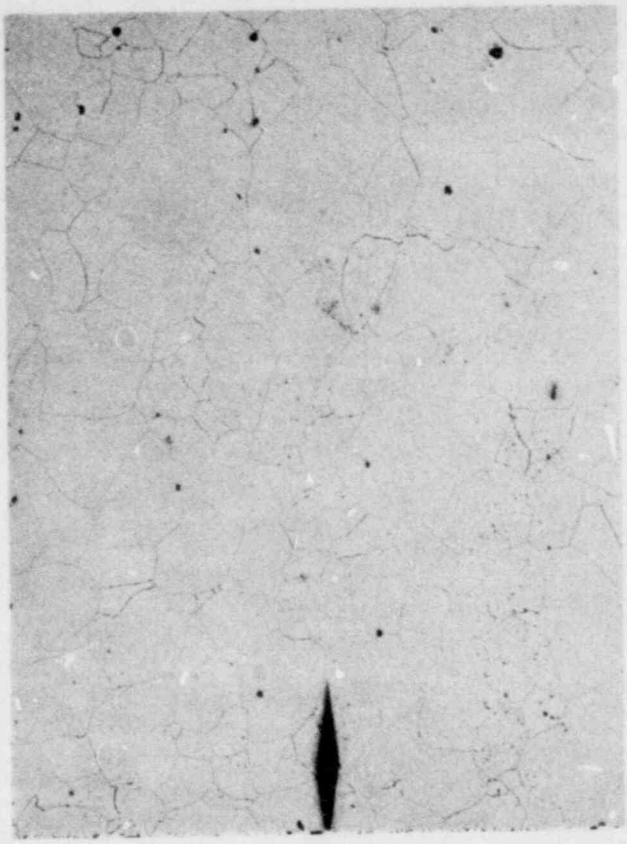

2-34400 1000X

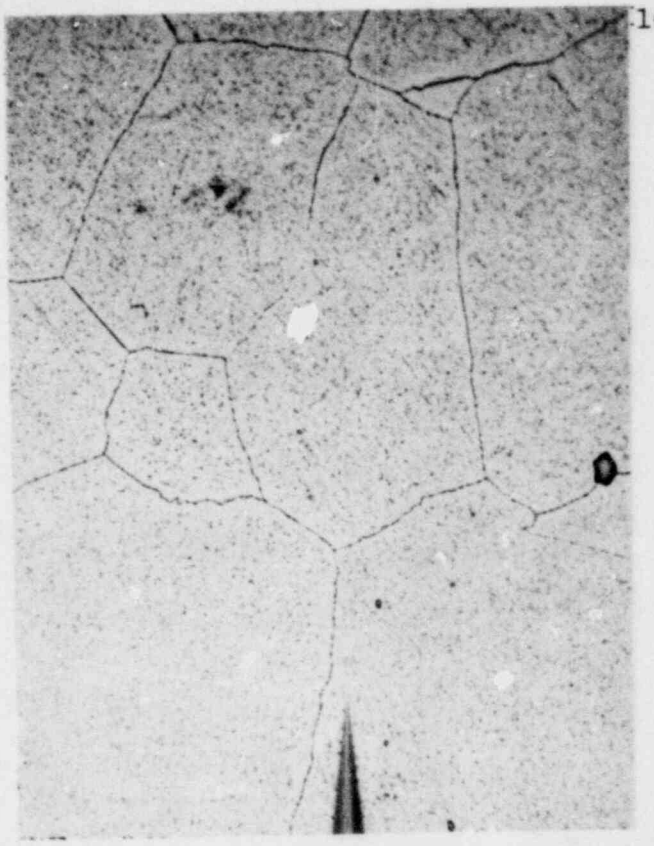

2-34401 1000X

(a) 10% Nital electrolytic etch

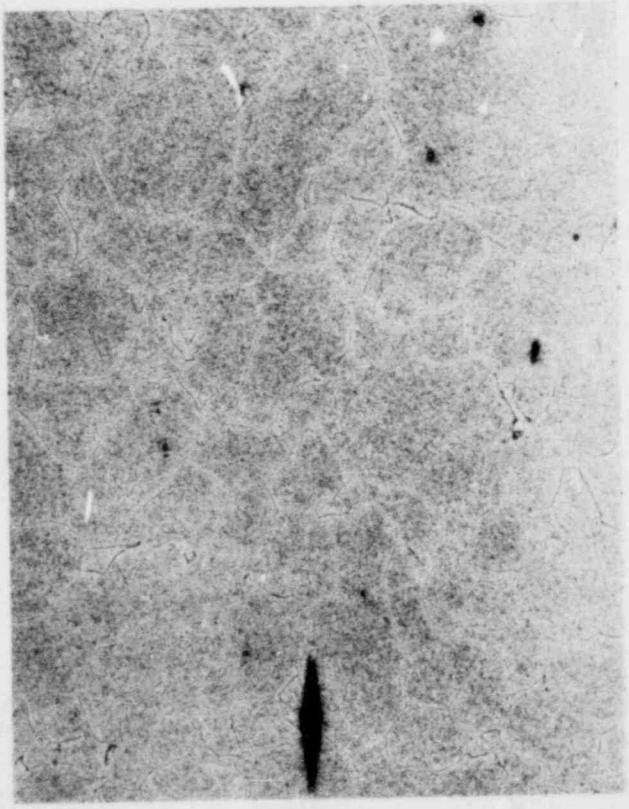

2-34432 100X

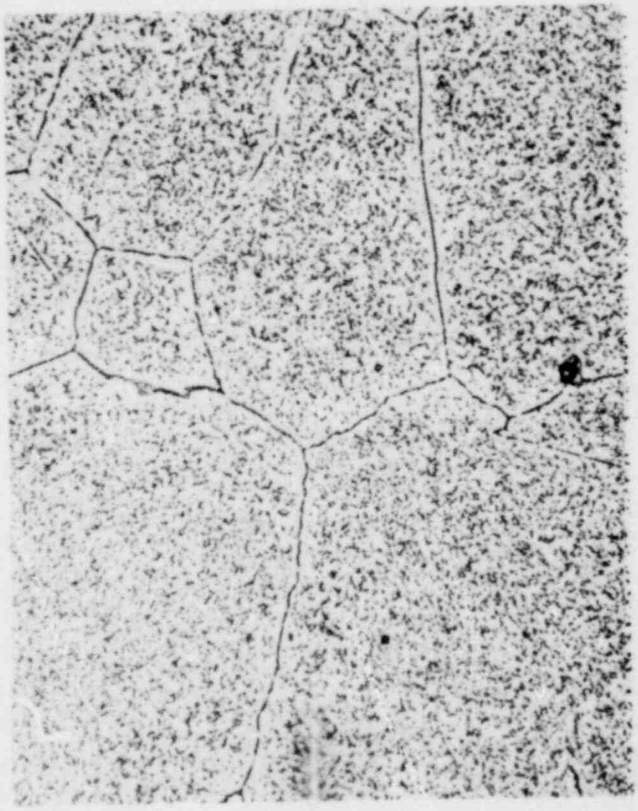

2-34433 1000X

(b) 8:1 phosphoric acid electrolytic etch

FIGURE 3-1. MICROSTRUCTURE OF SAFE-END.
Location 1, Figure 3-3.

The safe-end material exhibits clearly delineated grain boundaries after the phosphoric etch, (See Figure 3-1). At some grain boundary locations, relatively large, discrete carbide particles are evident. Extensive matrix carbides are also resolved after the phosphoric acid etch. This observed condition is consistent with the fact that the safe-end was subjected to two 1100°-1175° stress relieving operations with a total time at temperature of approximately 16 hours.

The microstructure of the thermal sleeve is shown in Figure 3-2. It is evident from the features shown in these micrographs that the thermal sleeve is sensitized (carbides precipitated at grain boundaries). Apparently the material was furnished in a sensitized condition since no stress relief treatments were performed after installation of the thermal sleeve [Figure 3-2(b)]. The more extensive grain boundary carbide precipitation evident at locations near the weld is attributed to the thermal cycle experienced during the welding operation.

The grain size for the two components was determined to be:

Safe-end: ASTM 4.0-4.5

Thermal sleeve: ASTM 6.7

ASME SB 166 does not specify any limits for the grain size of wrought Inconel 600 material. However, the CB&I specification for nickel-chromium-iron forgings (MS-16) states that the grain size shall be as small as practical, with the objective of producing material with an ASTM grain size of 5.

CB&I specification MS-16 states that the Inconel forgings be furnished in the annealed condition in accordance with ASME SB 166. The ASME specification does not specify the particular heat treating parameters for the annealed condition, thus it is possible for material furnished to these specifications to be in a sensitized condition.

Micrographs illustrating the microstructure of the heat-affected zones (HAZ) associated with the repair weld are shown in Figures 3-4 and 3-5. In each case, a zone of more pronounced grain boundary sensitization is apparent immediately adjacent to the fusion line. This feature is normal for the fabrication sequence employed, since sensitization in the HAZ is inherent

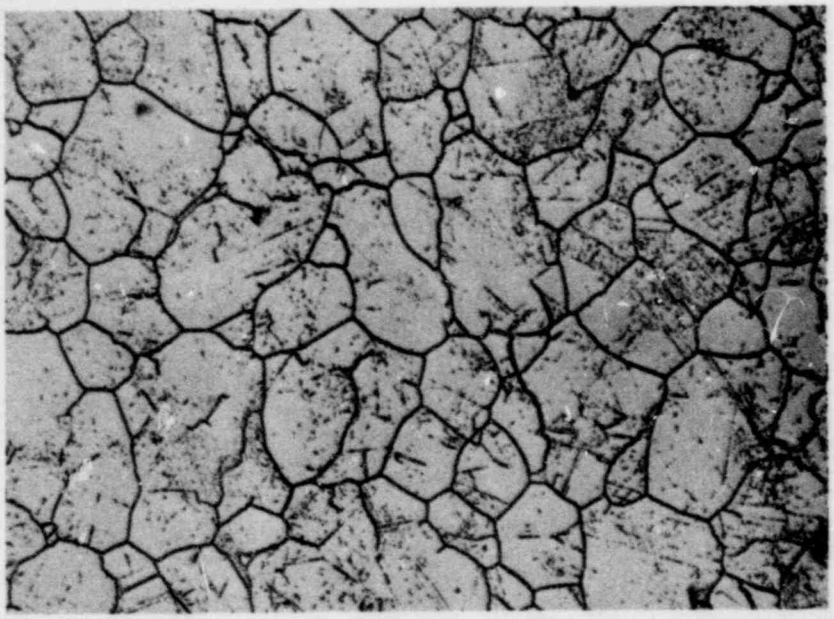

2-34423 (a) Near attachment weld. 200X

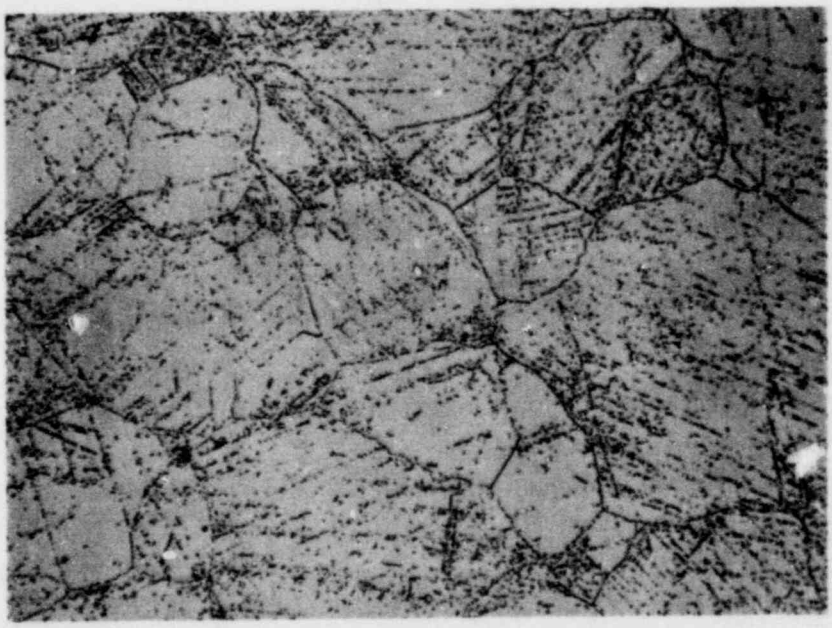

2-34486 (b) Remote from attachment weld. 500X

FIGURE 3-2. MICROSTRUCTURE OF THERMAL SLEEVE.
Location 2, Figure 3-3.

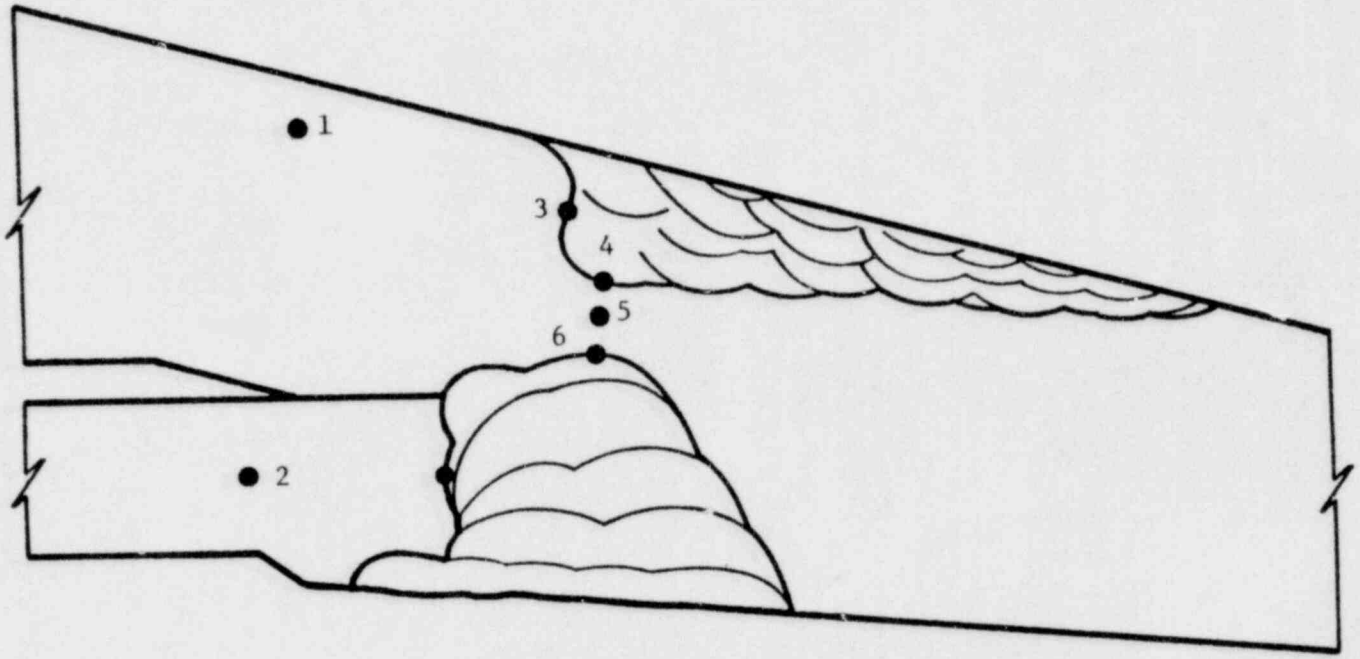

FIGURE 3-3. DIAGRAM OF REPRESENTATIVE SECTION THROUGH THERMAL SLEEVE ATTACHMENT AREA. 5X

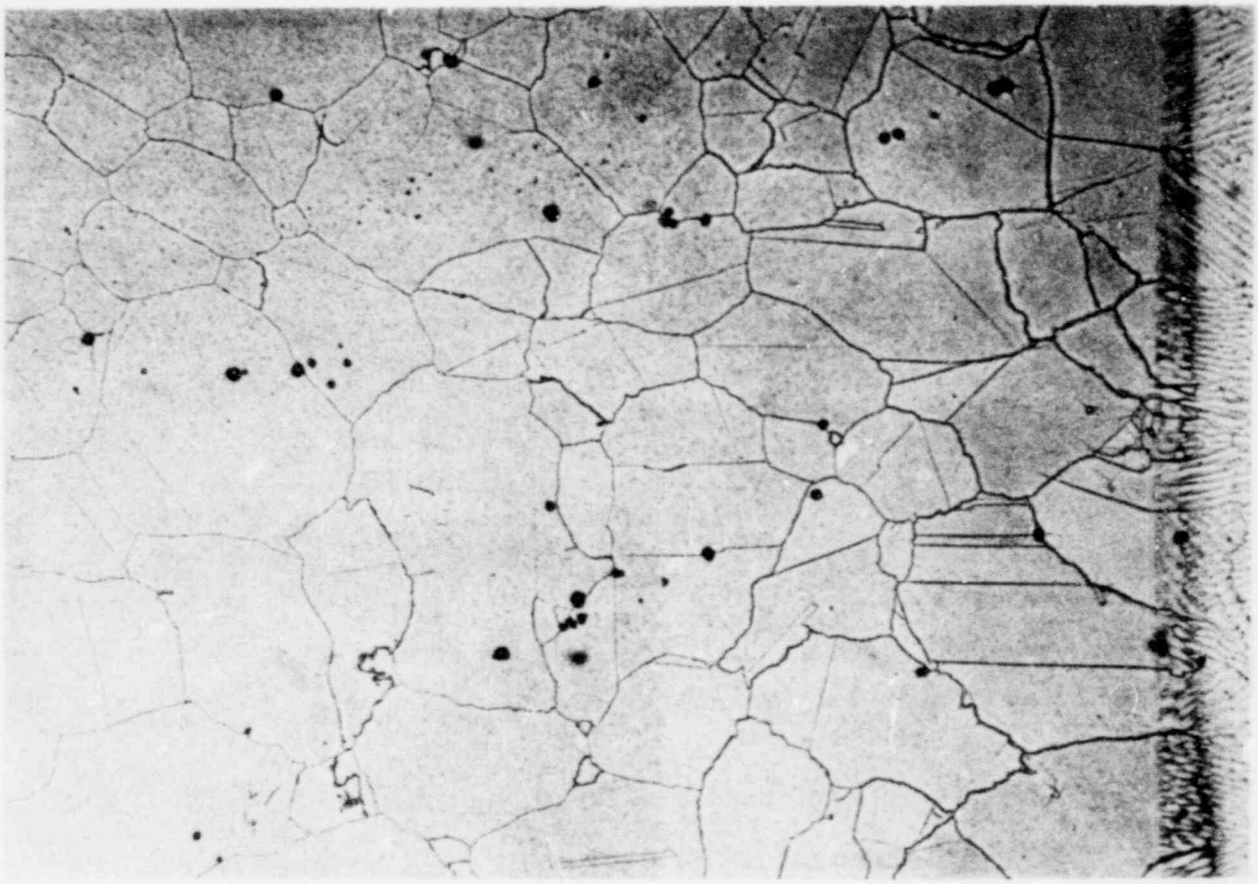

2-34398-399

FIGURE 3-4. MICROSTRUCTURE OF HAZ AT REPAIR WELD.
Location 3, Figure 3-3.
Etchant: 10% Nital, electrolytic. 200X

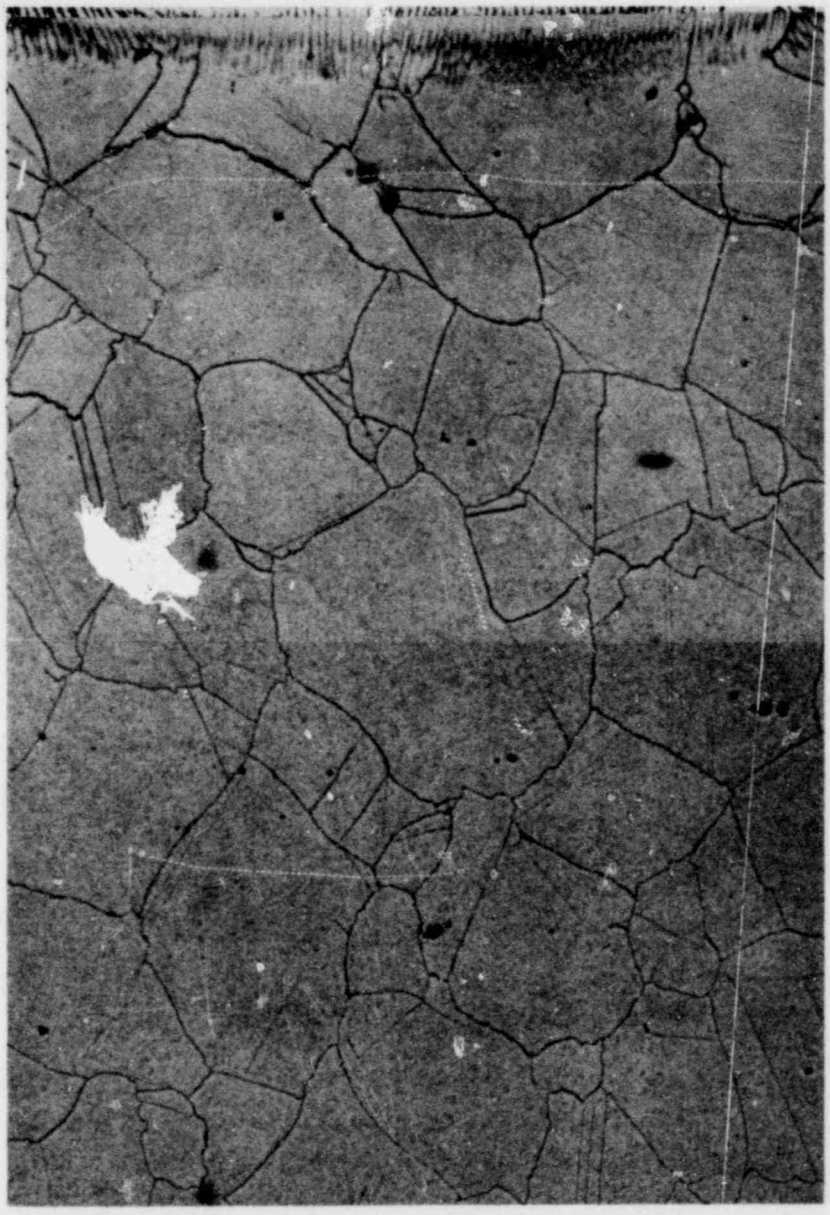

2-34396-397

FIGURE 3-5. MICROSTRUCTURE OF HAZ AT REPAIR WELD. Location 4, Figure 3-3. Etchant: 10% Nital, electrolytic. 200X

in any welding of Inconel 600 and subsequent stress relieving would serve to enhance any earlier sensitization. The microstructure at locations 0.03 in. from the fusion line and beyond is comparable to that observed at locations remote from the weld [compare Figures 3-1(b) and 3-4]. The microstructural features within the HAZ are consistent with normal welding procedures and techniques.

The microstructure midway along the line of closest approach of the repair weld and the thermal sleeve attachment weld is shown in Figure 3-6(a). This structure is comparable to that at remote locations [compare with Figure 3-1(b)] indicating that the repair welding operation did not alter the microstructure in the vicinity of the thermal sleeve attachment.

The HAZ at the thermal sleeve attachment weld is shown in Figure 3-6(b). The microstructural features are similar to those of the repair weld HAZ and are normal for this situation. This zone was not involved in the cracking but the normal microstructure serves to indicate normal welding practice.

Microhardness measurements were made within the safe-end base metal, thermal sleeve base metal, welds and heat affected zones on Section 5-5. The particular locations of the traverses are indicated in Appendix C, Figure C-1. All measurements were made employing a Knoop elongated pyramid indentor with a 200 g load. The results of these measurements are plotted as Knoop Hardness Number (KHN) vs distance in Figures C-2 through C-6. The zones marked "HAZ" in these figures represent the heat-affected-zones that are visually evident in photomicrographs of the metallographic section.

In general, the hardness values measured near the weld fusion lines were noticeably higher than those for base metal (KHN 240-280 vs KHN 184-191). At each weld, the hardness in the HAZ decreased fairly uniformly with distance from the fusion line. The range of hardness beyond the visible HAZ for all traverses was KHN 200-240. This range of hardness is somewhat higher than that measured for safe-end base metal at points remote from the weld.

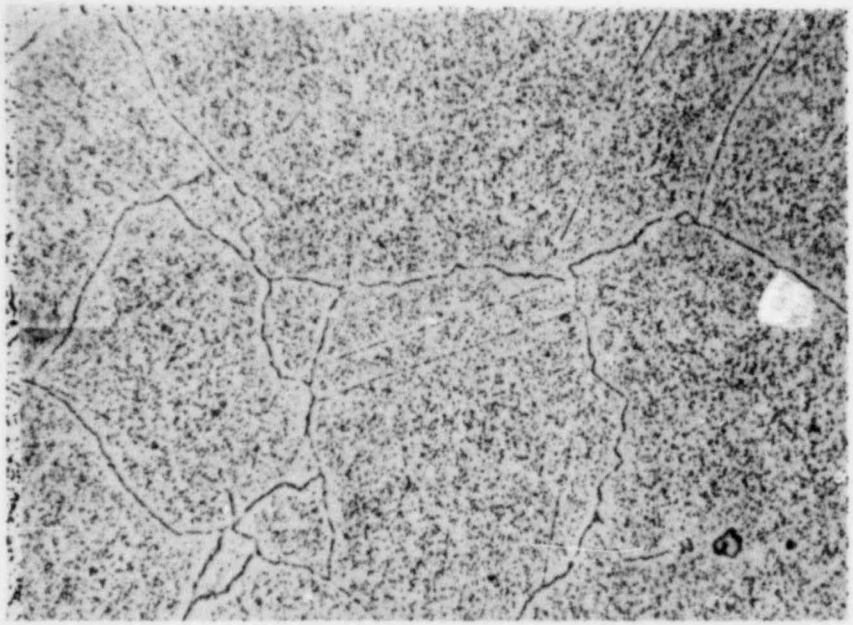

2-34431 500X

(a) Location 5. Phosphoric acid etch.

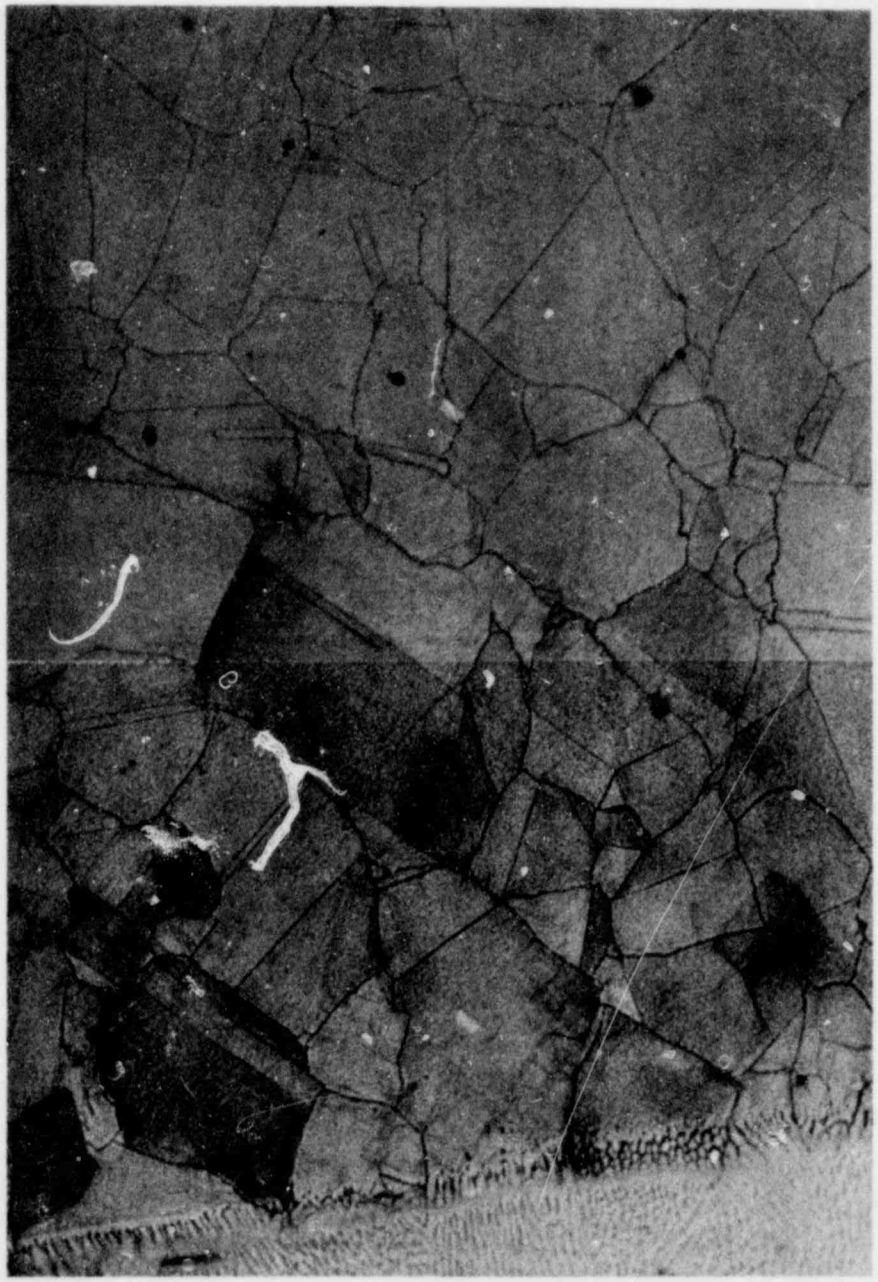

2-34394-395 200X

(b) Location 6. 10% Nital etch.

FIGURE 3-6. MICROSTRUCTURE OF HAZ AND BASE METAL AT THERMAL SLEEVE ATTACHMENT WELD. See Figure 3-3 for locations.

These hardness traverses indicate that the welding operations have resulted in a general hardening effect in the vicinity of the thermal sleeve attachment. However, the indicated increase is not considered sufficient to markedly influence the toughness or crack susceptibility of the safe-end material.

4.0 CHARACTERIZATION OF CRACKING

4.1 Microstructural Features

Metallographic examinations of selected sections through the thermal sleeve attachment area were performed to establish the microstructural features of the zone in which cracking occurred. Micrographs illustrating the features observed are shown in Figures 4-1 through 4-7 and in Appendix D.

The heat-affected zone of the root-pass weld bead is evident in each section as a zone with noticeably fewer matrix carbide precipitates than the unaffected base metal and with a different grain boundary etching response. At most locations the material immediately adjacent to the fusion line is essentially devoid of matrix carbides, and the amount of these precipitates increases with distance from the fusion line (Figures 4-2, 4-3 and 4-6). A varying degree of grain boundary carbide precipitation is also evident within the HAZ. In general, the grain boundaries of the wrought material immediately adjacent to the fusion line are lightly etched indicating limited carbide precipitation. In each section a narrow region of heavily-etched grain boundaries is evident. The grain boundaries within this region generally exhibit more extensive carbide precipitation than the furnace-sensitized base metal. All of these features are the result of re-solution of pre-existing carbides during welding and subsequent carbide precipitation within the HAZ during cooling. The extent and distribution of the precipitated carbides vary with distance from the fusion line depending on the peak temperature reached and the particular cooling rate. Minor differences in the nature of the HAZ noted among the sections are attributed to normal variations in heat input and cooling rates over the circumference of the weld.

In all sections examined the crack path is completely intergranular with extensive branching. The intersection of the crack with the inside surface of the safe-end (surface of tight crevice) occurred at a point within the HAZ some distance away from the tip of the tight crevice. The fact that this condition exists completely around the circumference indicates that crack initiation occurred within the HAZ. The early stages of crack propagation generally followed a path parallel to the root pass fusion line. In the

2-34434,-435

FIGURE 4-1. SECTION THROUGH THERMAL SLEEVE ATTACHMENT AREA. Section 1-1, Figure 1-4, Etchant: 8:1 Phosphoric acid. 100X

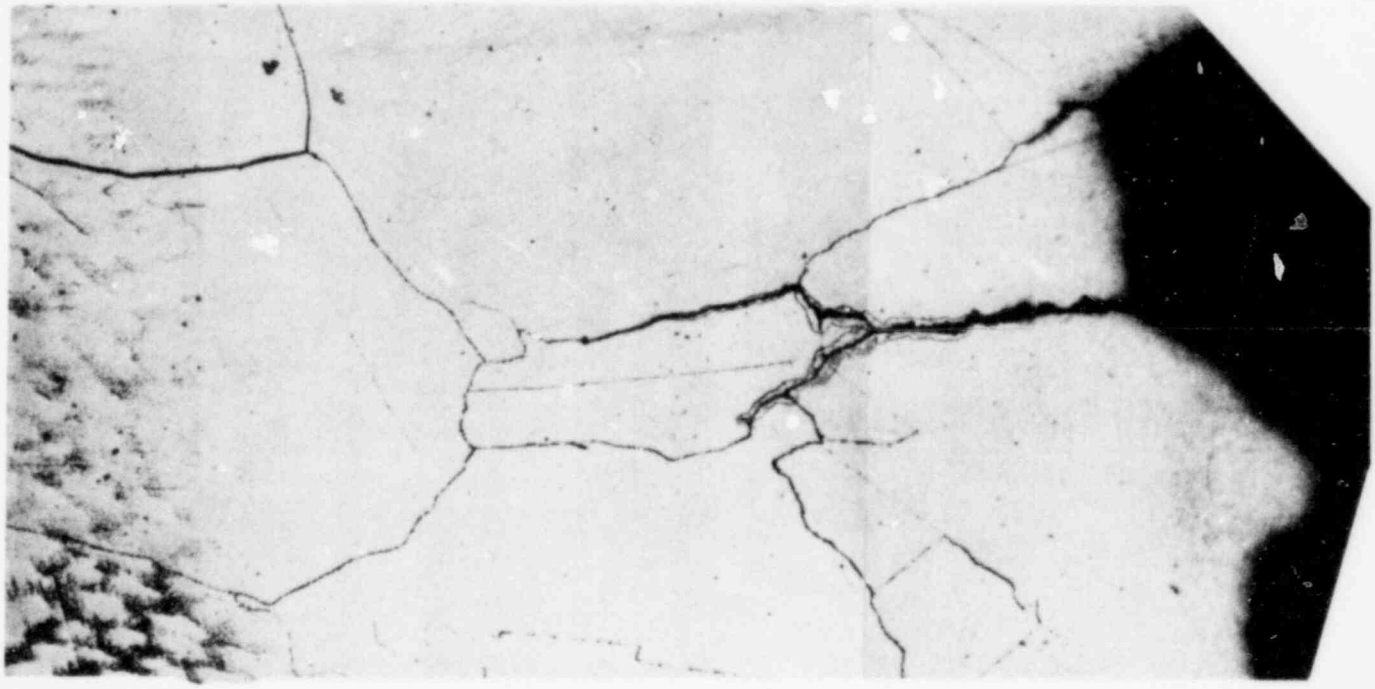

2-34440,-441

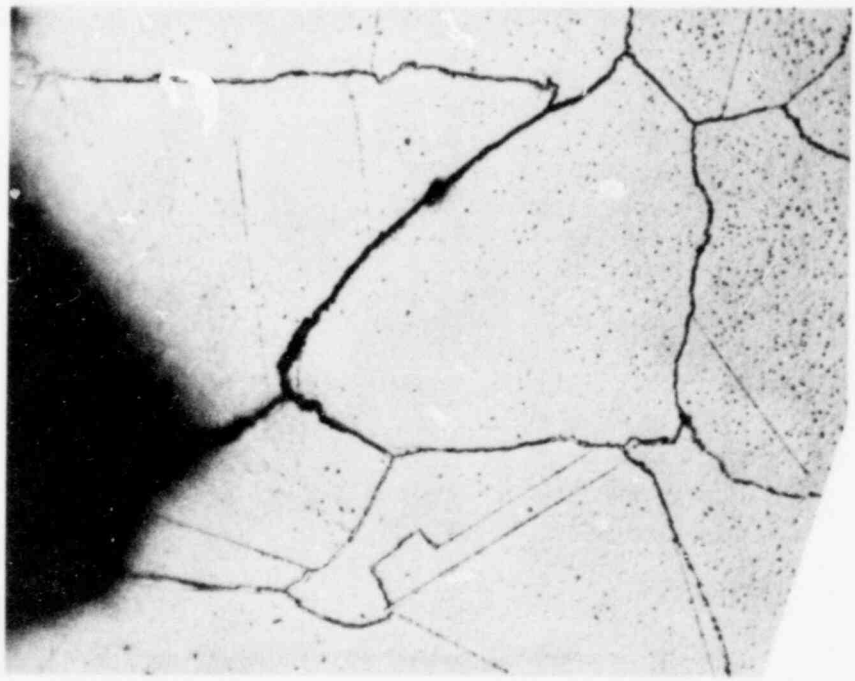

2-34442

FIGURE 4-2. MICROSTRUCTURE AT POINTS ON OPPOSITE SIDES OF CRACK. Section 1-1, Location 1, Figure 4-1. Etchant: 8:1 Phosphoric acid. 500X

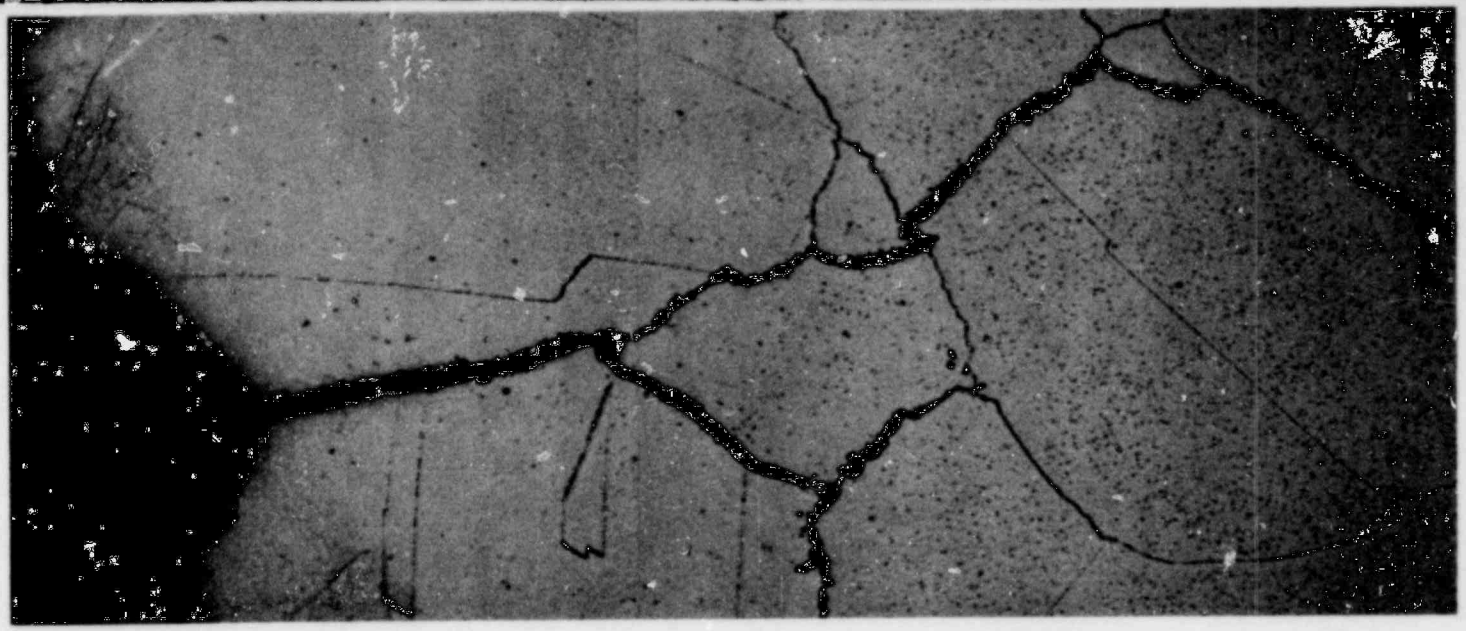

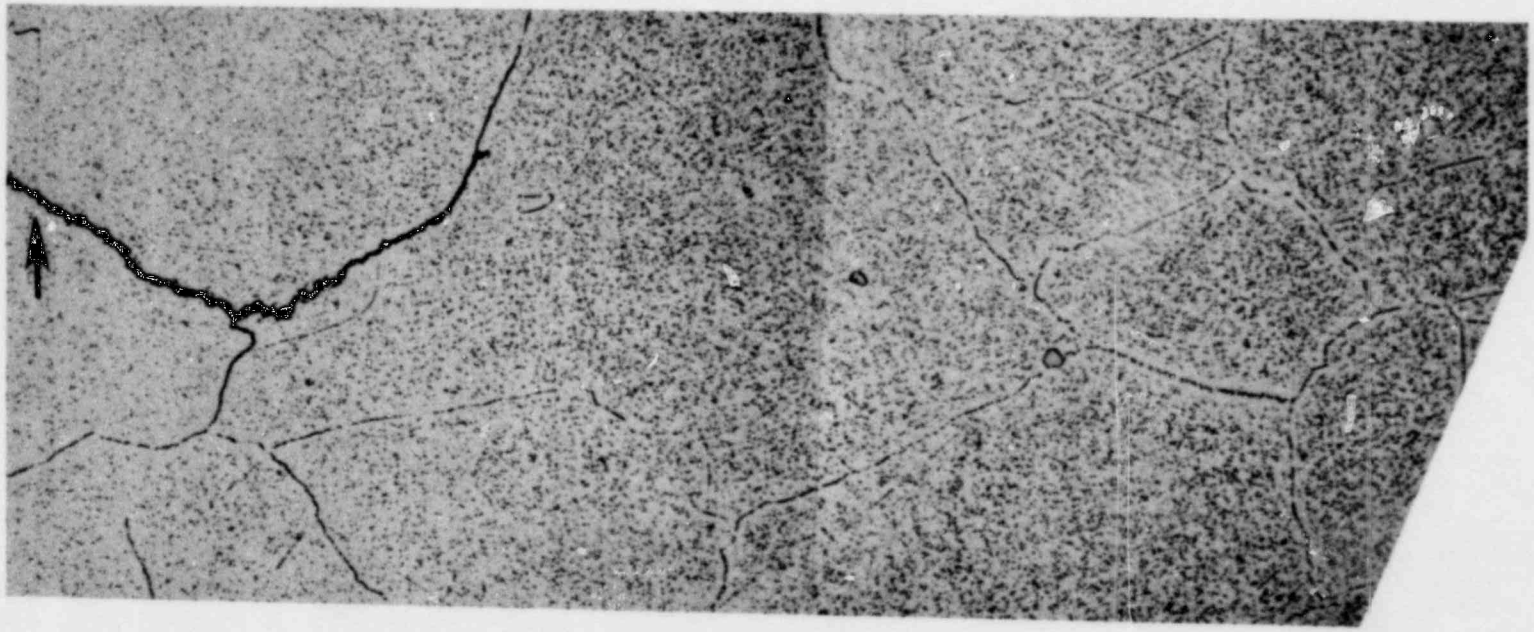

FIGURE 4-3. MICROSTRUCTURE AT MAIN CRACK. Section 1-1, Location 2, Figure 4-1. Arrows indicate match points. Etchant: 8:1 Phosphoric acid. 500X

2-34443,-446

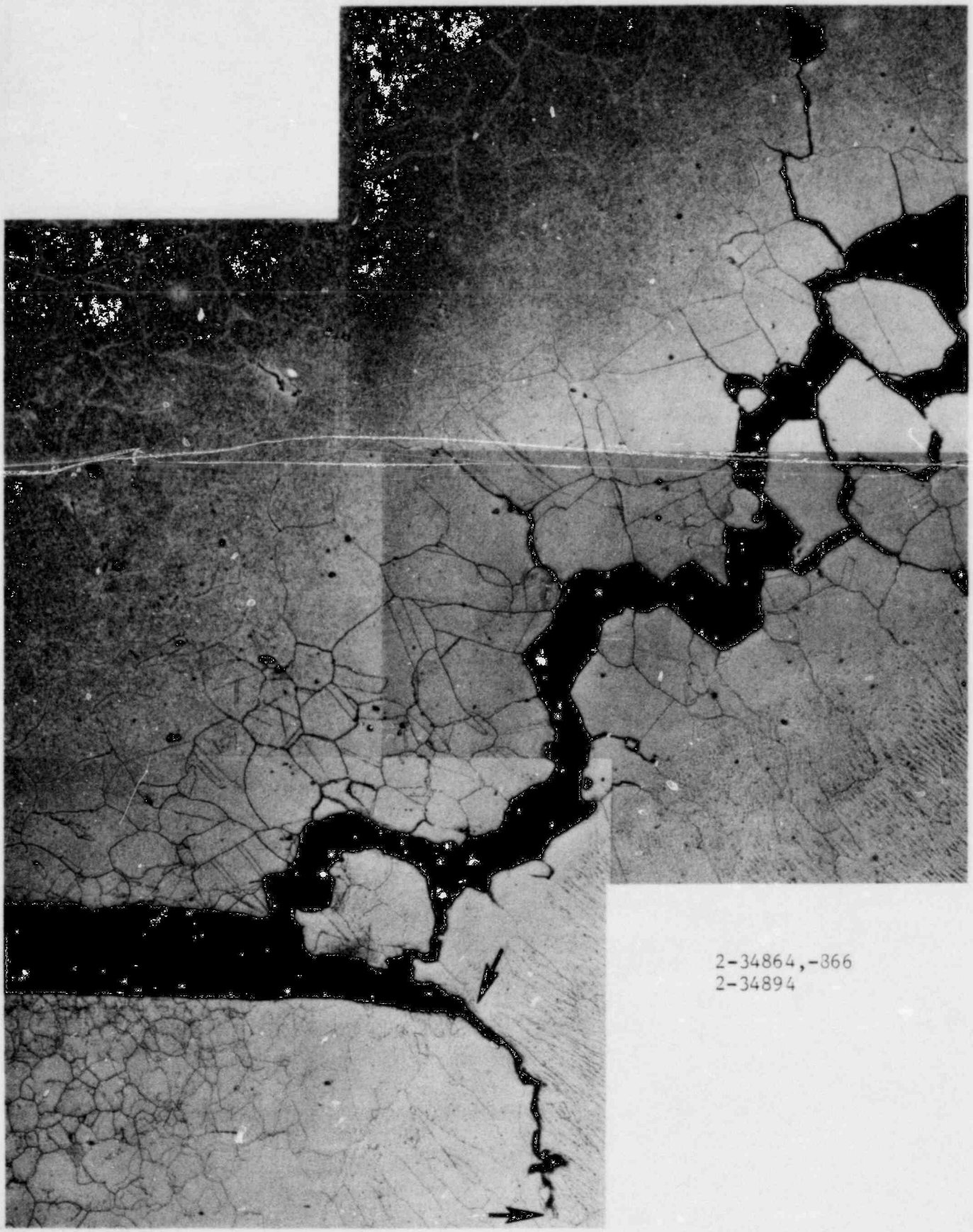

2-34864,-366
2-34894

FIGURE 4-4. SECTION THROUGH THERMAL SLEEVE ATTACHMENT AREA. Section 2-2, Figure 1-4. Etchant: 8:1 Phosphoric acid. 100X

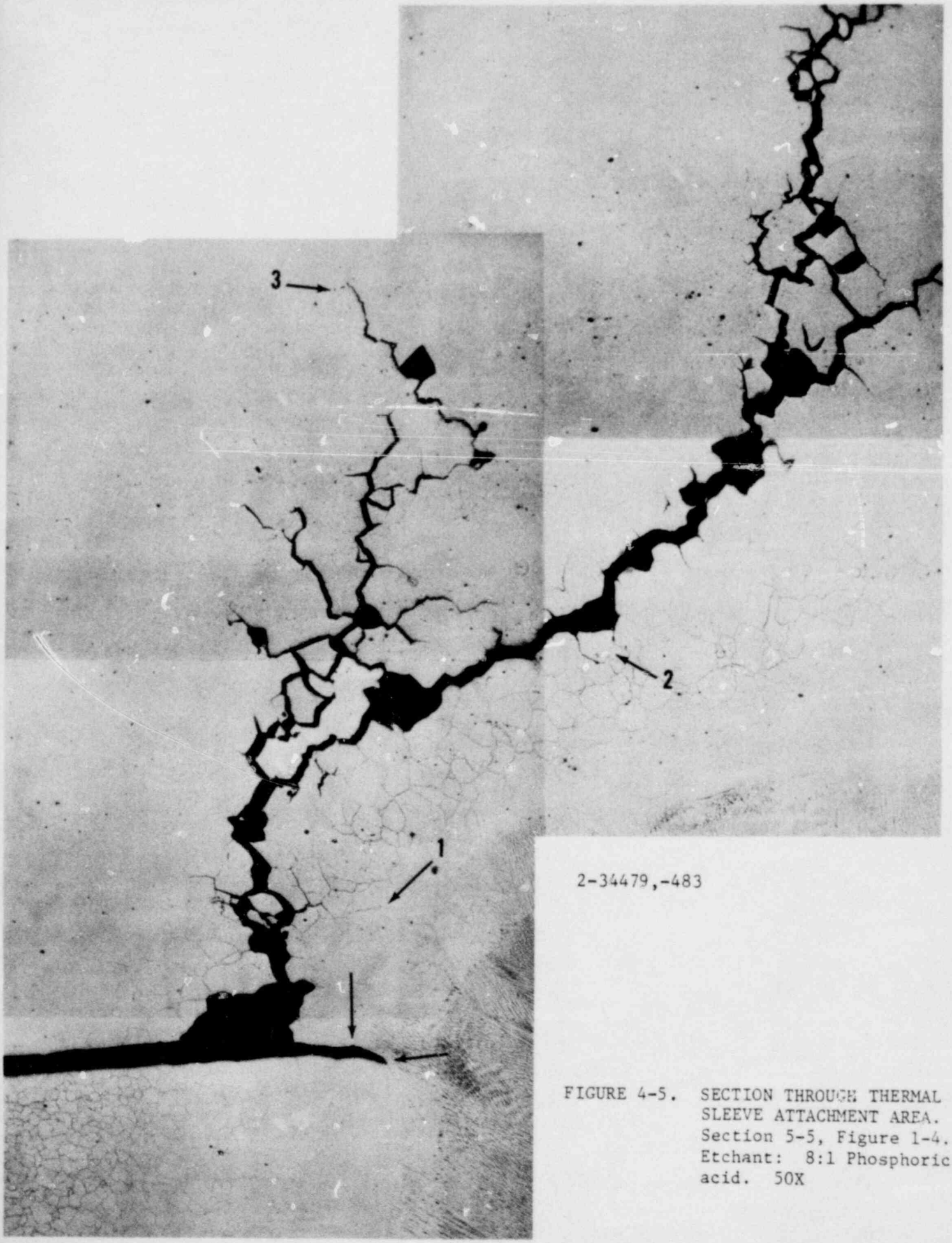

2-34479,-483

FIGURE 4-5. SECTION THROUGH THERMAL SLEEVE ATTACHMENT AREA. Section 5-5, Figure 1-4. Etchant: 8:1 Phosphoric acid. 50X

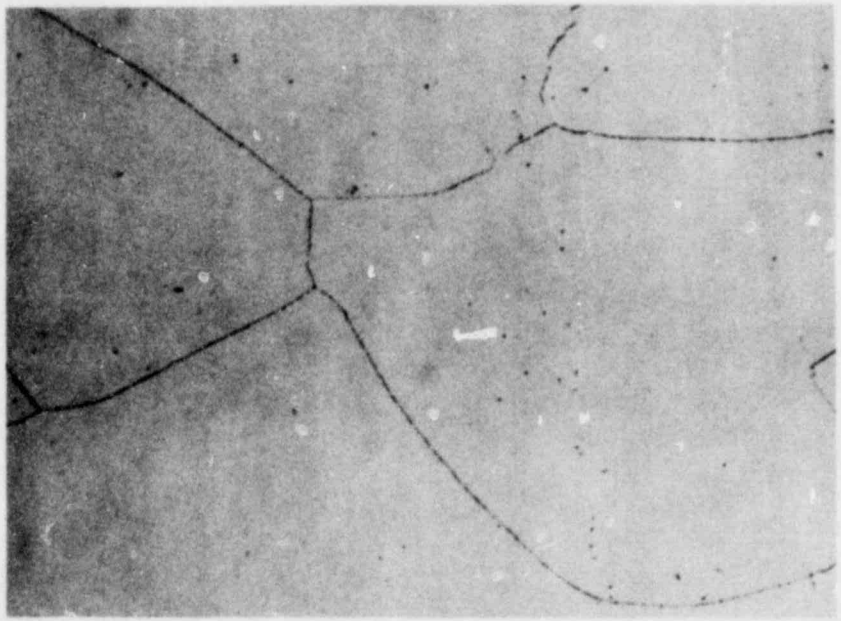

2-34488 (a) Location 1.

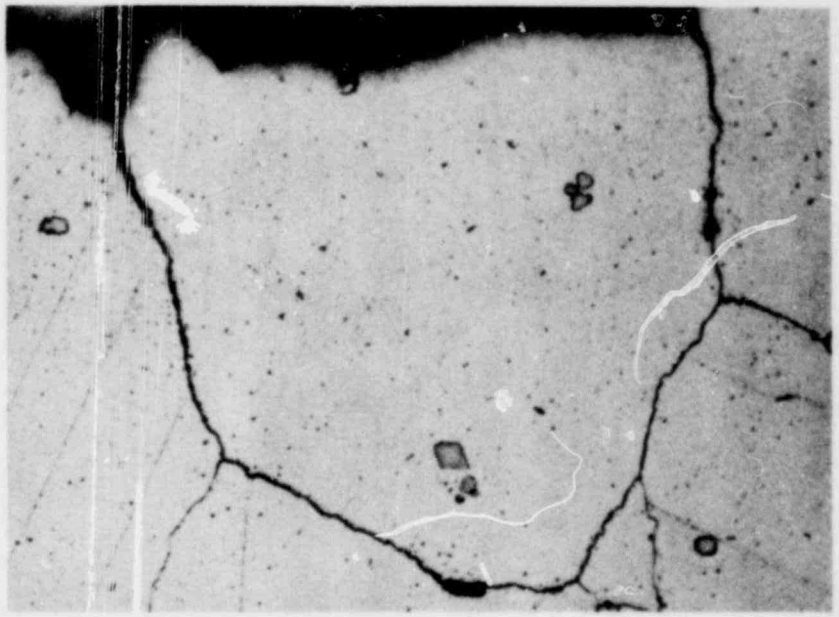

2-34484 (b) At main crack. Location 2.

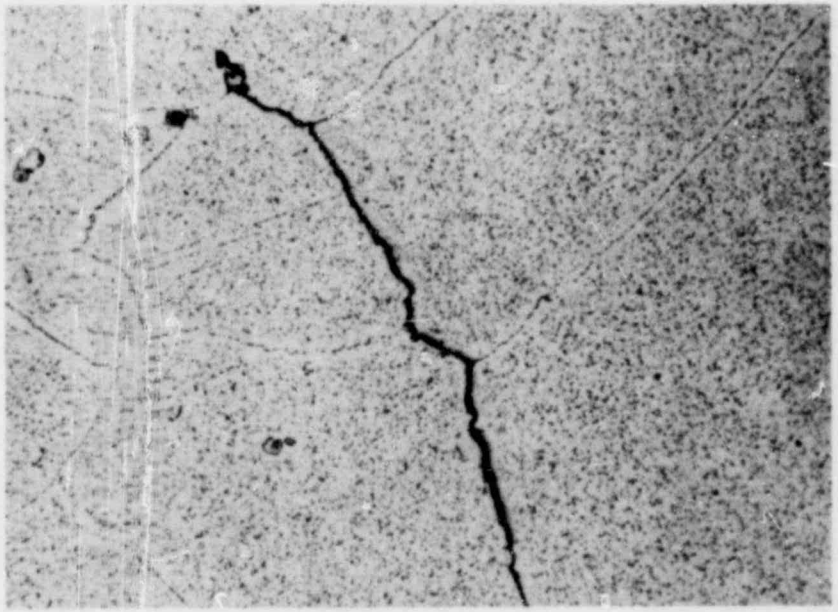

2-34485 (c) At crack tip. Location 3.

FIGURE 4-6. MICROSTRUCTURE IN VICINITY OF MAIN CRACK. Section 5-5, See Figure 4-6 for locations. Etchant: 8:1 Phosphoric acid. 500X

FIGURE 4-7. SECTION THROUGH THERMAL SLEEVE ATTACHMENT AREA. Section 11-11, Figure 1-4. Etchant: 8:1 Phosphoric acid. 75X

later stages of propagation the crack diverts from the thermal sleeve attachment weld into unaffected base metal, see Figures 4-5, D-3 and D-5.

The location of the initial portion of the crack path within the heat-affected zone varied around the circumference. At Section 1-1 crack initiation and early propagation occurred within the carbide free zone between the fusion line and the zone of heaviest grain boundary carbide precipitation, see Figure 4-1. At other sections crack initiation occurred within the region of heaviest grain boundary precipitation, and in some cases the initial stage of cracking extended across this region into unaffected base metal, Figures 4-4 and 4-5.

The configuration of the safe-end and thermal sleeve is such that the attachment weld forms the closure of the tight crevice. At Section 1-1, Figure 4-1, fusion of both components is complete, forming a relatively blunt crevice tip. Fusion was also essentially complete at Sections 4-4 and 5-5 (Figures 4-5 and D-1). At the other sections, lack of fusion was evident, forming a tight, irregular extension of the crevice into the attachment weld, see Figures 4-4, 4-7, D-3 and D-4. This lack of fusion extended approximately 0.02 to 0.04 in. from the fusion line. Such a feature is not uncommon for the joint configuration employed in this case. The significance of the lack-of-fusion defect depends on the type of weld intended in the initial design. If a full-penetration weld was not specified, this lack of fusion cannot be considered as significant. In any case, the feature is not related to the cracking problem, since it was observed that crack initiation occurred in the HAZ away from the crevice tip.

The entire length of the tight crevice was examined in each metallographic section. In each case, cracking was observed only at a single location, (intersecting the inside surface within the attachment weld HAZ), and there was no evidence of any other intergranular attack or incipient cracking along the crevice.

Micrographs at the tip of the crack in Section 4-4 where the crack approaches the repair weld are shown in Appendix D, Figure D-2. At this location, crack propagation has continued within unaffected base metal in spite of the proximity of the more heavily sensitized HAZ.

4.2 Fractographic Features

Three specimens were cut from the thermal sleeve attachment area of the safe-end sample and broken open to expose the crack surfaces. These specimens are designated as Nos. 1, 2 and 4 in Figure 1-4. The specimens were decontaminated by washing and brushing or by ultrasonic cleaning in a detergent solution, and examined in the scanning electron microscope (SEM) to establish the topographic features of the crack surface. Macrographs of the crack surfaces are shown in Figure 4-8 and SEM fractographs illustrating the fine-scale topographic features observed are shown in Figures 4-9 through 4-12 and in Appendix E.

The crack surfaces of all three specimens were characterized by distinct intergranular facets at all locations examined. Figures 4-9, E-1 and E-4 are representative of the fractographic features observed at the intersection of the crack surface with the inside surface of the safe-end. The crack surface was completely intergranular along this edge and there were no features to identify any discrete initiation sites. The features of the crack front, at locations where partial penetration occurred are shown in Figures E-3 and E-5. The transition from the service-induced crack to the laboratory overload fracture is apparent and in each case, intergranular features are evident at the extremities of the crack.

Specimen No. 1 was taken from a location where the final stages of cracking passed through the repair weld. A transition in surface topography, marking the line of intersection of the crack with the repair weld is apparent in Figure 4-8(a). The fine-scale features at this transition are shown in Figure 4-11 and fractographs from the crack surface within the repair weld are shown in Figure 4-12. Distinct intergranular features are evident in the portion of the surface corresponding to crack propagation in base metal. The features of that portion of the surface corresponding to the repair weld demonstrate that crack propagation in this zone occurred in an intercolumnar mode. The transition in surface topography at the intersection of the crack with the repair weld is strictly due to the different microstructures characteristic of the weld metal and the base metal.

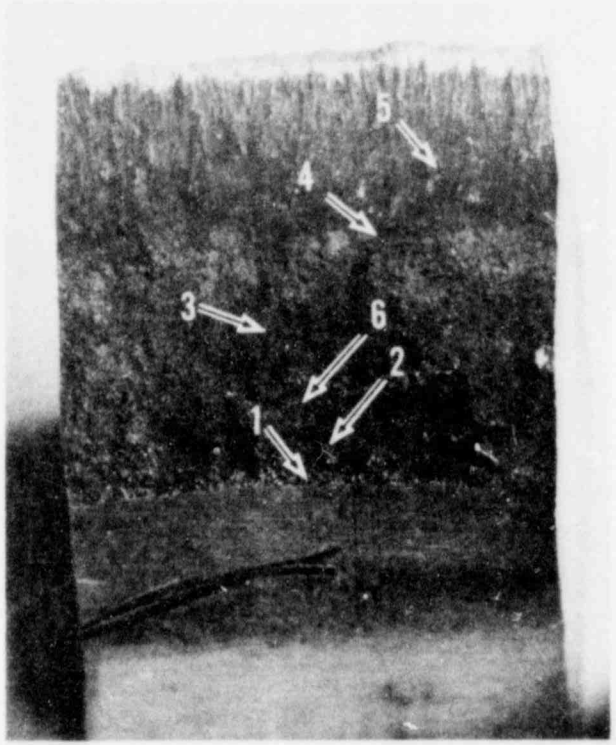

2-34351 (a) Specimen No. 1.

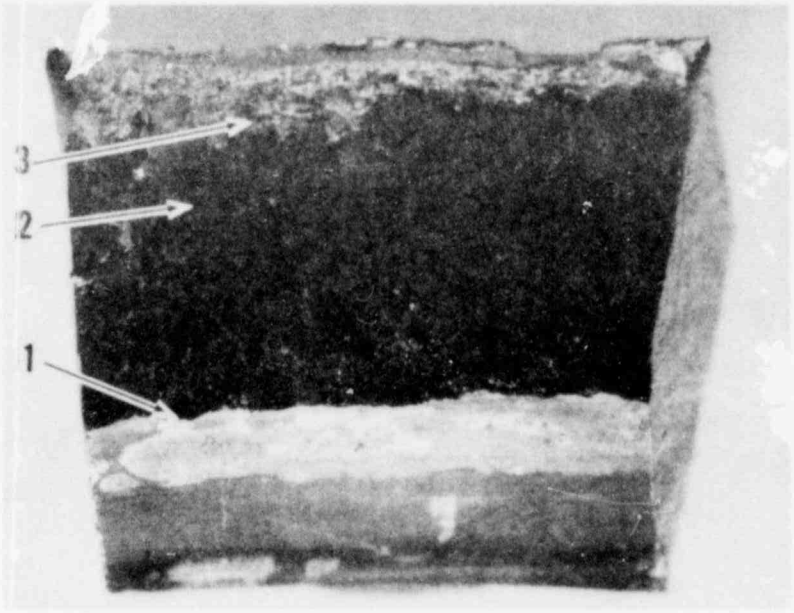

2-35039 (b) Specimen No. 2.

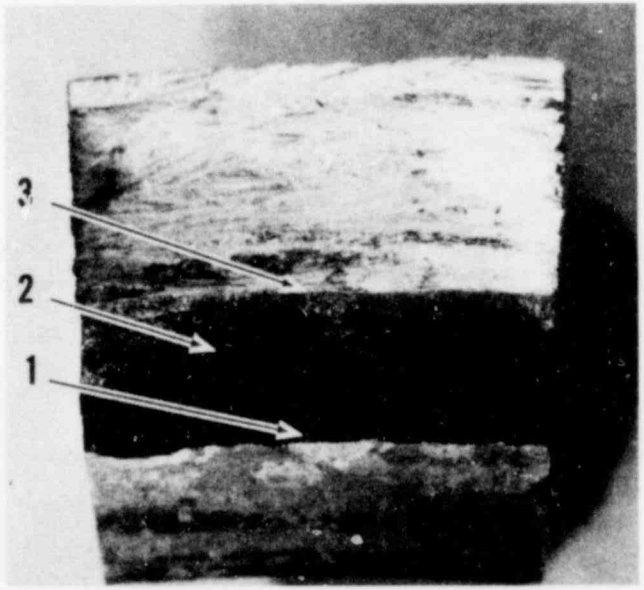

2-35041 (c) Specimen No. 5.

FIGURE 4-8. CRACK SURFACE SPECIMENS. See Figure 1-4 for locations. Crevice surface is at bottom of each photograph. 3X

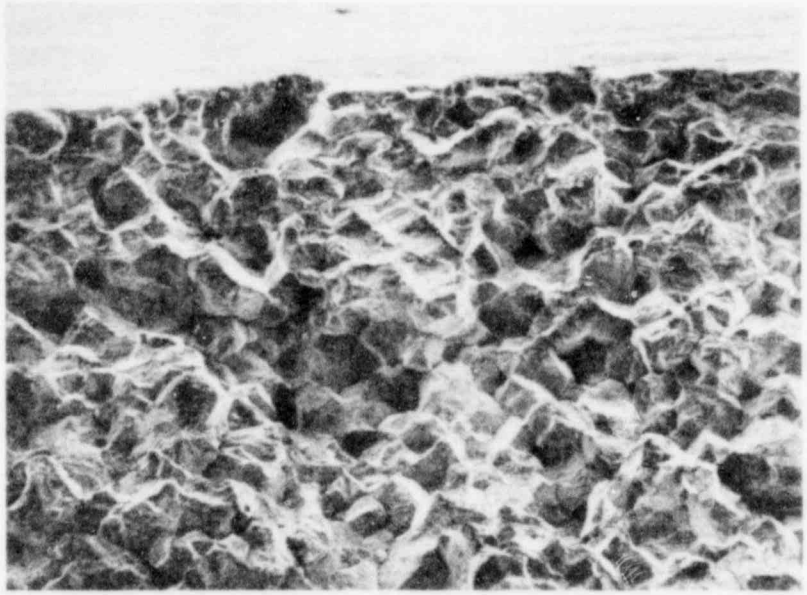

2-114 (a) 50X

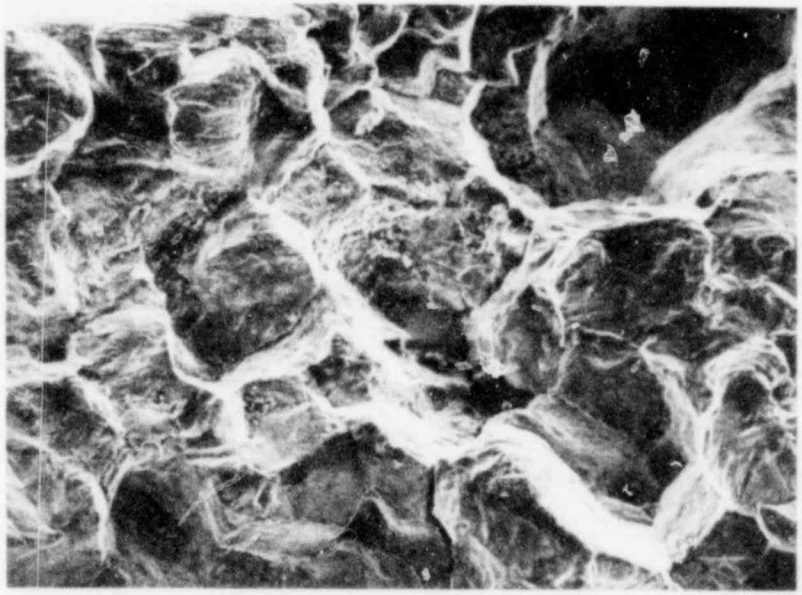

2-115 (b) 150X

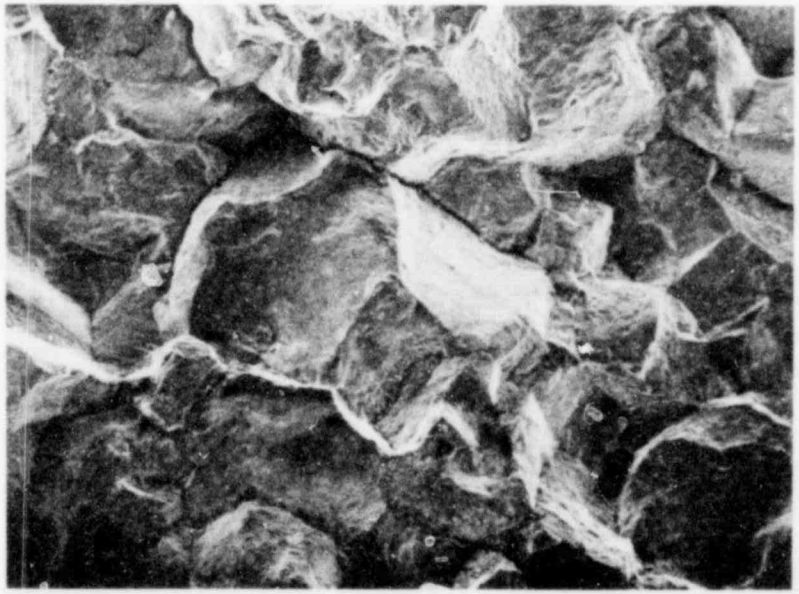

2-113 (c) 150X

FIGURE 4-9. SEM FRACTOGRAPHS FROM CRACK SURFACE. Specimen No. 1, Location 1, Figure 4-8(a).

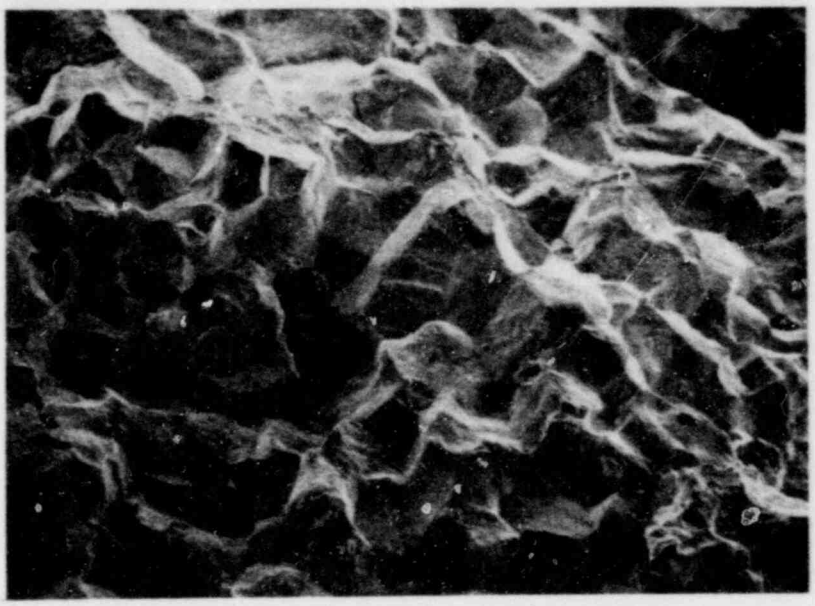

2-174 (a) Location 2. 100X

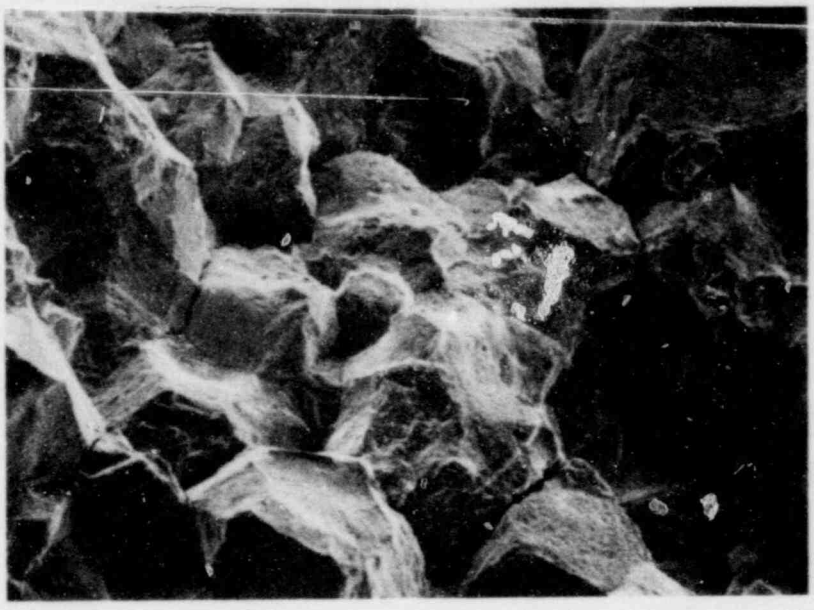

2-117 (b) Location 3. 150X

FIGURE 4-10. SEM FRACTOGRAPHS FROM CRACK SURFACE. Specimen No. 1. See Figure 4-8(a) for locations.

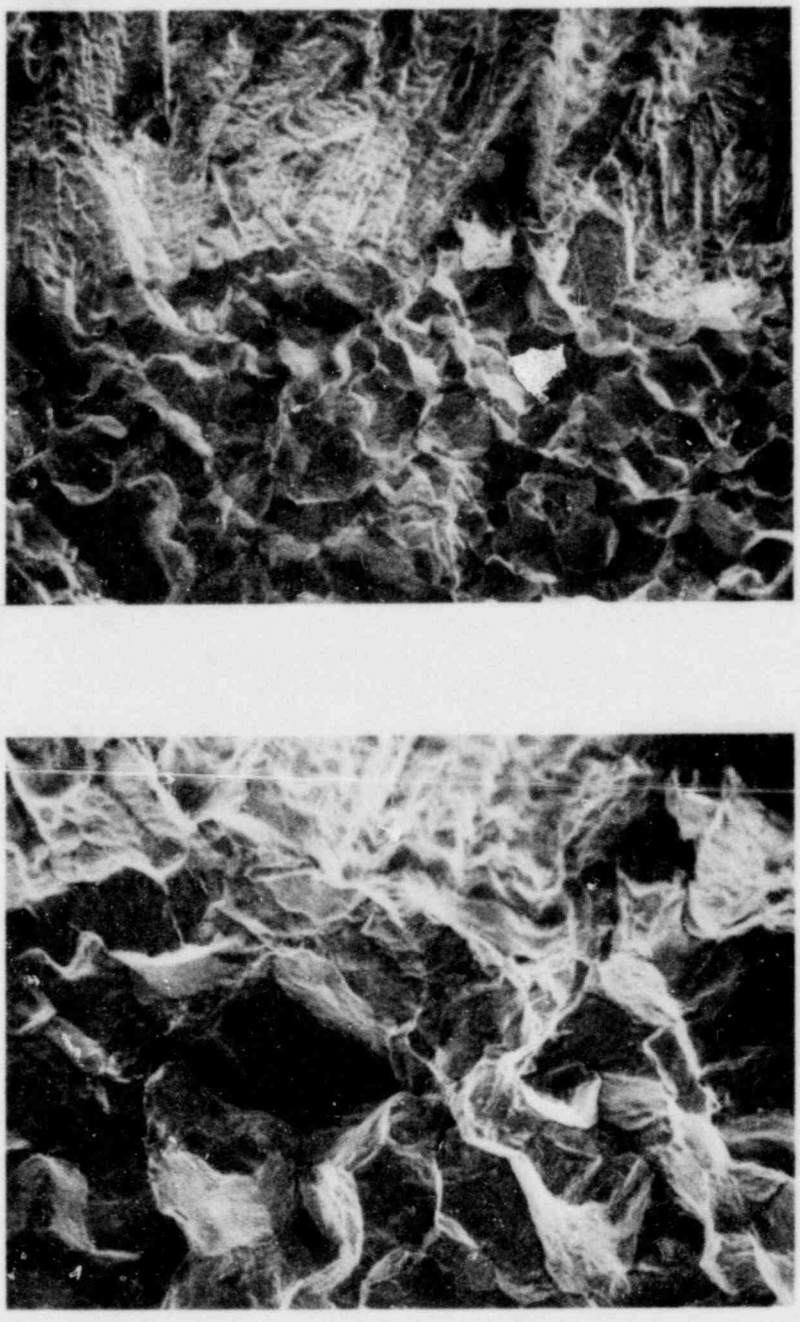

2-120 150X

FIGURE 4-11. SEM FRACTOGRAPHS FROM CRACK SURFACE. Specimen No. 1, Location 4, Figure 4-8(a).

2-191 50X

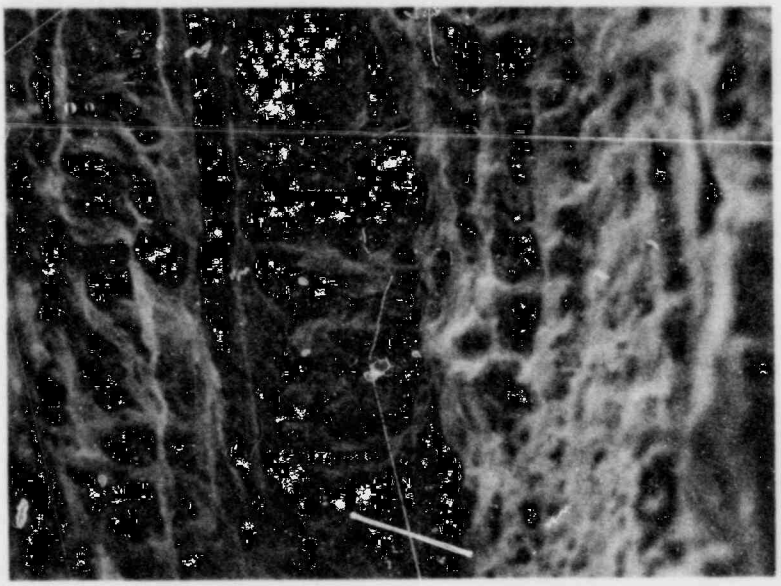

2-192 300X

GURE 4-12. SEM FRACTOGRAPHS FROM CRACK SURFACE. Specimen No. 1, Location 5, Figure 4-8(a).

The fractographic features at the particular points described above, together with those at locations in the central portion of the crack surface (Figures 4-10, 4-11 and E-2) demonstrate that the cracking was completely intergranular. No evidence of any form of step-wise crack propagation was observed in the fractographic examination.

5.0 SURFACE DEPOSIT ANALYSIS

In the examination of the various crack surface specimens, deposits were evident on the intergranular crack surfaces and on the crevice surfaces. Distinctly crystalline deposits, such as shown in Figure 5-1, and a fibrous appearing materials, Figure 5-2, were noted at several locations on the crack surfaces. The particular examples, shown in Figures 5-1 and 5-2, represent small amounts of deposit materials remaining on the crack surface of fractographic Specimen No. 1 after decontamination by gentle washing and brushing. X-ray energy spectra for these particular surface deposits are compared with the spectrum from a clean area in Figure 5-3. Pertinent features of these spectra are as follows:

1. Indicated iron content at location of crystalline deposit is higher than for base metal. [Compare Cr:Fe peak intensity ratios in Figures 5-1(a) and 5-3(c)].

2. Presence of sulfur is indicated at location of fibrous deposit, Figure 5-3(b).

Four crack surface specimens were specifically examined to establish the character of the surface deposits and their distribution. These specimens were cut from the safe-end sample and broken open to expose the crack surface and crevice surface. The exposed surfaces were examined in the SEM both in the original condition and after ultrasonic cleaning. Energy dispersive x-ray spectroscopy was employed to provide in situ, qualitative analysis of the deposit materials*. EDS data and SEM fractographs from Specimen No. 6, representative of all four specimens, are presented in Appendix F. The results of these examinations are summarized as follows:

1. The fibrous type material (Figure 5-2) was the only recognizable deposit evident in examinations of crack surfaces in the original condition. This deposit material was particularly evident at points remote from the crevice and was not present at locations in the immediate vicinity of the crevice.

---

* The EDS analyses of specimens in the original condition (no decontamination) were performed at the Argonne National Laboratory where facilities for SEM examination of radioactively contaminated materials are available.

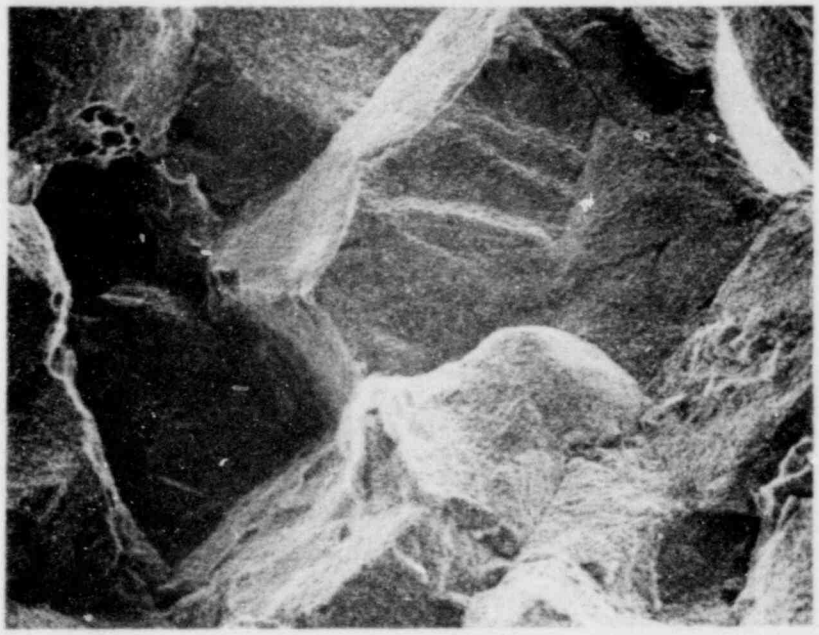

2-175 300X

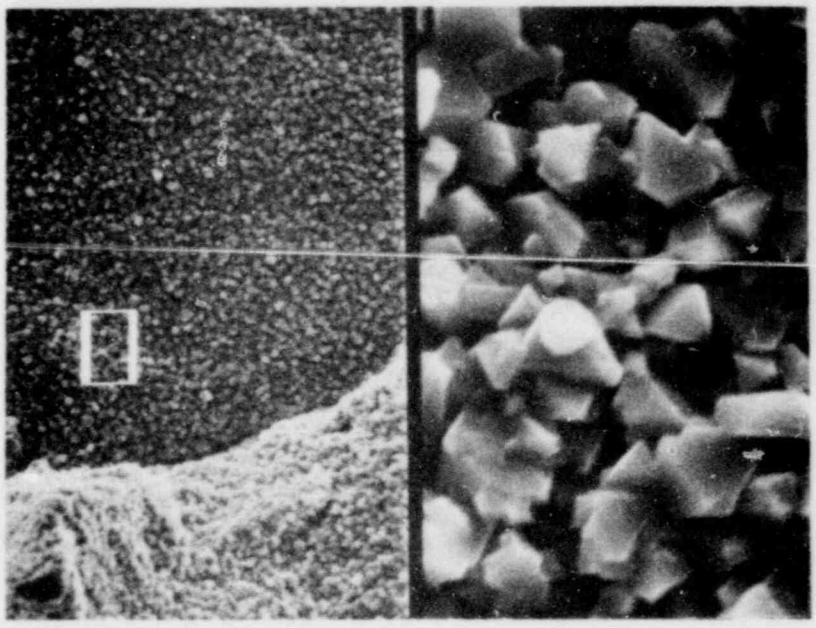

2-178 1000/10,000X

FIGURE 5-1. DEPOSIT ON CRACK SURFACE. SEM fractographs. Specimen No. 1. Location 6, Figure 4-8(a).

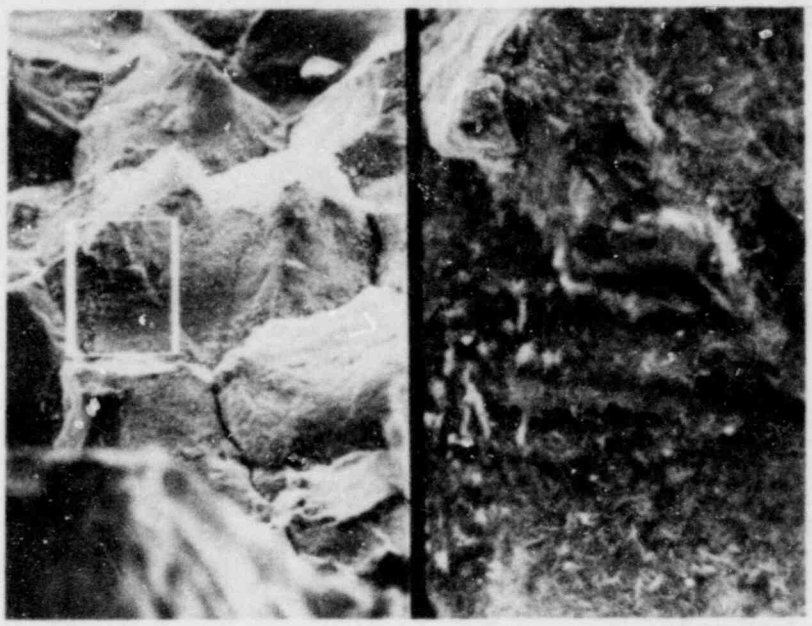

2-187 200/1000X

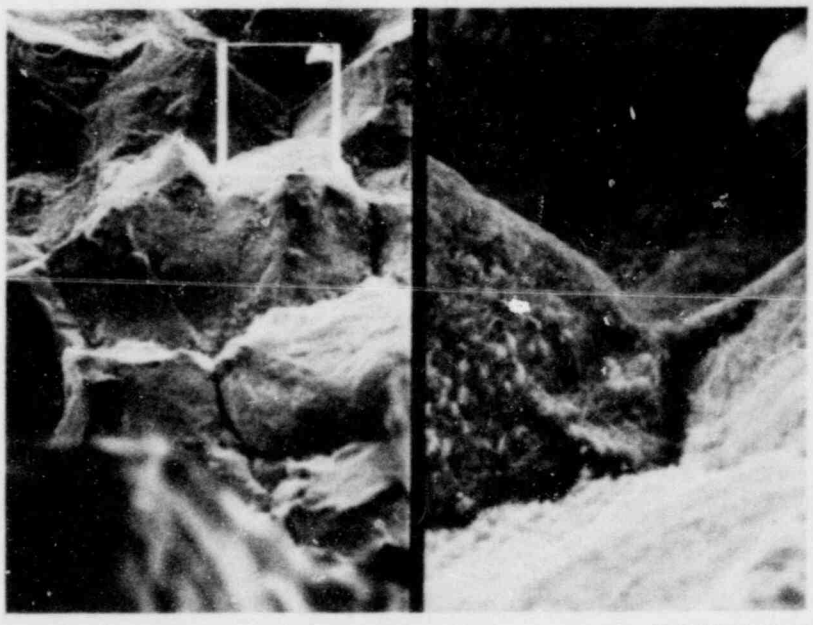

2-189 200/1000X

FIGURE 5-2. DEPOSIT ON CRACK SURFACE. SEM fractographs. Specimen No. 1. Location 4, Figure 4-8(a).

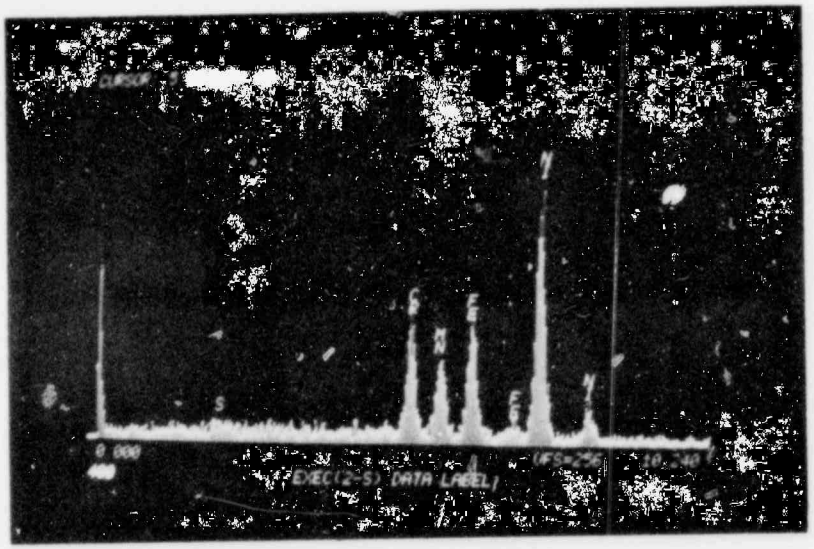

2-233 (a) Crystalline deposit in Figure 5-1

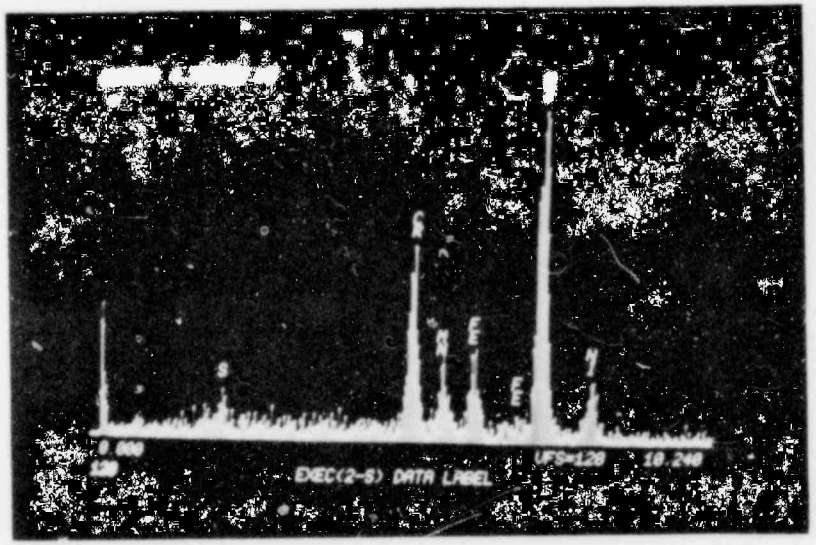

2-237 (b) Fibrous deposit in Figure 5-2

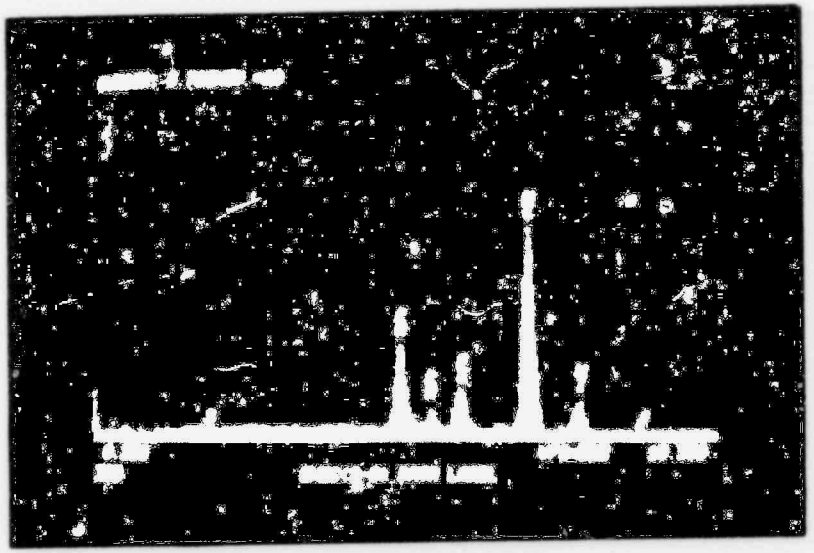

2-263 (c) Clean crack surface

FIGURE 5-3. X-RAY ENERGY SPECTRA. Crack surface, Specimen No. 1.

2. The crystalline deposit material on the crack surfaces was evident only after partial cleaning.

3. The fibrous deposit material on the crack surface contained sulfur.

4. The crystalline deposit material on the crack surface is iron-rich compared to the base metal.

5. Iron was the predominant element detected in the crack surface deposits near the crevice. No sulfur was detected in this material.

6. Deposits on the crevice surface presented a distinctly different appearance from those on the crack surface.

7. Iron was the predominant element detected in the deposit material on the crevice surface. No sulfur was detected in these deposits.

8. The presence of chlorine was indicated at one location on the crevice surface.

SEM examination of the portion of the crevice surface contained in the fractographic specimens, (Specimen Nos. 1, 2, 3 and 4, Figure 1-4) revealed an essentially as-machined condition (original machining marks evident) over the majority of the area. Evidence of limited corrosive attack was noted in a few localized regions. SEM micrographs illustrating the condition of the crevice surface are shown in Figure 5-4.

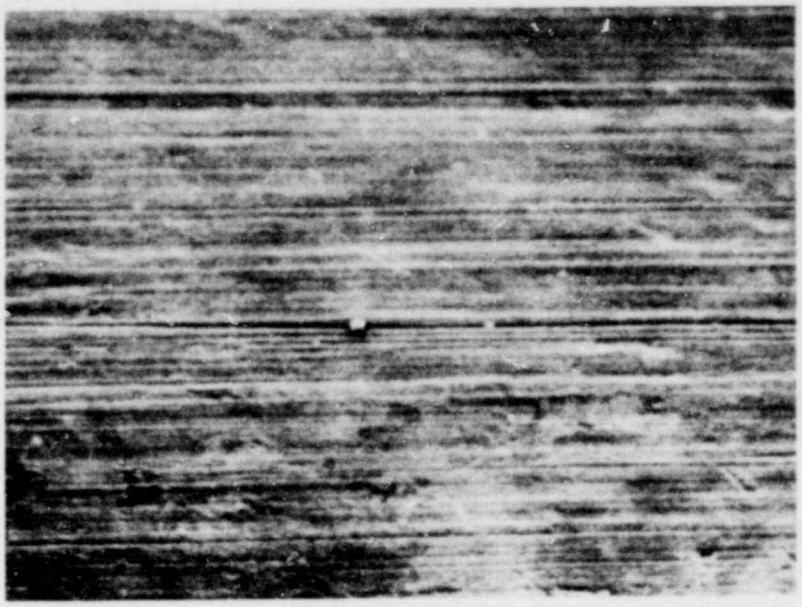

2-243 (a) Typical condition

2-265 (b) Localized region of corrosive attack

FIGURE 5-4. SEM MICROGRAPHS FROM SURFACE OF TIGHT CREVICE. Specimen No. 4, Figure 1-4. 100X

6.0 SUMMARY AND CONCLUSIONS

The observations made to date in this investigation may be summarized as follows.

1. Significant cracking occurred on the inside surface of the safe-end over a full 360° of circumference.

2. All cracking initiated in the immediate vicinity of the tip of the tight crevice between the thermal sleeve and the safe-end.

3. Cracking occurred completely within the safe-end forging, except for the later stages at some locations, where the crack propagated through the repair weld.

4. Crack initiation and the early stages of crack propagation occurred within the heat-affected-zone of the thermal sleeve attachment weld.

5. Cracking occurred at a single location within the HAZ at all sections examined. No multiple cracking along the crevice surface was observed.

6. Minor corrosive attack of the safe-end occurred at some locations on the crevice surface, but no significant intergranular attack or incipient cracking was observed along the crevice surface outside of the HAZ.

7. The cracking was completely intergranular at all locations examined.

8. No evidence of any step-wise crack propagation was observed. Also, there are no fractographic features to indicate discrete initiation sites around the periphery of the crack.

9. The deposits present on the crack surfaces at locations corresponding to the later stages of crack propagation contained significant amounts of sulfur. The specific form of the sulfur, i.e., $SO_4^{=}$, S, $S^{=}$, etc. was not determined. No

evidence of any other extraneous contaminant species on the crack surface was observed. Sulfur was not detected on the surface of the tight crevice. Chlorine was present on the crevice surface at one location.

10. The deposits on the crevice surface and on the crack surface near the crevice consisted of an iron-rich material.

11. Both the safe-end material and the thermal sleeve material are in a sensitized condition. This condition is considered normal for this particular case in view of the post-weld stress-relieving treatment, applicable specifications, and usual mill practice.

12. The chemical compositions of the safe-end material and the thermal sleeve material conform to ASME Specification SB 166.

13. The weld deposit chemistry for both welds conforms to AWS-5.11-76, except for a minor variation in Mn content.

14. The repair welding operation on the outside of the safe-end did not result in any significant modification of the microstructure within the zone of cracking.

The metallographic and fractographic characteristics of the cracking (completely intergranular with no significant direct corrosive attack) serve to identify the cracking mechanism as intergranular stress-corrosion cracking (IGSCC). Laboratory studies have shown Inconel 600 to be susceptible to such cracking in high-purity water environments in certain circumstances. A survey of the literature pertaining to the stress-corrosion cracking susceptibility of Inconel 600 is given in Appendix G.

In general, the published results of laboratory studies indicate that relatively high stresses are necessary for IGSCC in Inconel 600. Stress-corrosion cracking has been observed in uncreviced specimens at stresses as low as the 0.5% offset yield stress, but no cracking has been reported for stress levels below the yield strength. On the basis of reported data, IGSCC of Inconel 600 in BWR environments is not likely unless stresses exceed the yield strength.

One factor indicated by the published data is that the metallurgical condition of Inconel 600, i.e., sensitized vs solution annealed, does not

significantly influence susceptibility to IGSCC. In the case of a weld in Inconel 600, the heat-affected zone will consist of resolution-treated (or lightly sensitized) material adjacent to the fusion line and a heavily sensitized region some distance from the fusion line regardless of the initial condition of the base material. In this investigation cracking was observed to occur in both regions of the HAZ. Also, the crack path diverted from the HAZ into unaffected base metal in the early stages of cracking. In view of these factors, and the fact that no inherent microstructural defects or abnormalities were apparent, the furnace-sensitized condition of the safe-end forging is not considered as a significant contributing factor to the cracking problem.

In many material/environment combinations the presence of a tight crevice can result in severe localized corrosive attack or stress-corrosion cracking. Thus, attention must be directed to the possible role of the tight crevice in IGSCC of Inconel 600 in reactor water environments. It is not likely that the classical differential aeration cell would develop at a crevice in the uniform high-purity water environment, but such regions could entrap air during outages, causing locally high oxygen levels on start-up. Also, if any anionic contaminant is present, acidification of the crevice could develop. Such a condition is known to enhance the susceptibility of Inconel 600 to IGSCC. It has been demonstrated that the presence of a crevice significantly accelerates cracking in low pH and high oxygen content solutions, and GE data indicates that crevices enhance susceptibility to IGSCC in BWR environments. In view of these factors, it is likely that the presence of the crevice is a principal contributing factor to the present cracking problem.

Analysis of deposits on the crack surface identified sulfur as a constituent of one of the deposit materials. The only other elements detected within the crack were the principal base metal constituents (Ni, Cr, Fe). The particular identity of the sulfur-bearing materials and the particular form of the sulfur were not determined. The deposit materials on the surface of the tight crevice were identified as iron-rich, and sulfur was not detected in these deposits.

The presence of sulfur in the crack surface deposits could be associated with the composition of the base metal or result from progressive concentration of a contaminant species within the crack. If significant amounts of sulfur had segregated to grain boundaries during the stress relieving operation, corrosion products formed during IGSCC would contain sulfur*. In the absence of evidence of sulfur on the crevice surface, no definite conclusion can be drawn concerning the source of the sulfur on the basis of the EDS data alone.

The EDS analysis identified chlorine on the crevice surface. A significant quantity was indicated, but evidence of the presence of this element was confined to a single location on one of the specimens examined. In view of this limited evidence, no definite conclusion can be drawn concerning possible chlorine accumulation within the crevice during service.

The results of the EDS analysis performed in this investigation can only be considered as indicating the possibility of sulfur and/or chlorine contamination within the tight crevice. If either species were entrapped from the environment their presence could lead to acidification of the crevice and contribute to cracking as discussed above and in Appendix G. The observation of limited corrosive attack of the crevice surface is an indication that such acidification could have occurred in service. Further investigation of the nature of the deposit materials, employing other techniques such as electron diffraction or Auger spectroscopy, would be necessary to resolve the question of possible contamination in the thermal sleeve attachment area.

Consideration must be given to the source of stresses in the thermal sleeve attachment region which contributed to IGSCC. It is evident that the stresses in the vicinity of the tip of the crevice are the result of applied stresses associated with service loading and residual stresses associated with the attachment weld. The primary stresses (bending + membrane) due to service loading were calculated by GE to be 78% of the yield strength**.

---

* In some laboratory investigations significant amounts of sulfur have been observed on intergranular crack surfaces of a similar Ni-base alloy (Inconel X750) after testing in high-purity water. See Ref. 10, Appendix G.

** Reference 27, Appendix G, pg. G-8.

It is generally recognized that typical butt welds in piping components result in tensile residual stresses on the order of the yield strength of the material. Therefore, residual stresses of this magnitude must be considered to exist at the thermal sleeve attachment weld. Residual stress analyses of the thermal sleeve attachment weld, performed at Battelle-Columbus Laboratories, predict yield-level tensile residual stresses over the entire length of the tight crevice*. Thus, the combined applied and residual stresses result in a net effective stress substantially above the yield strength in the immediate vicinity of the attachment weld.

The fact that multiple cracking did not occur along the crevice is significant. The distribution of the applied and residual stresses in the thermal sleeve attachment area would result in a gradient in the combined tensile stress with the peak stress level at a position on the crevice surface near the fusion line of the attachment weld. The occurrence of cracking only at a single location along the crevice is evidence that the combination of applied and residual stresses to produce an effective peak stress well above the yield strength was a necessary condition for the cracking.

Residual stresses associated with the thermal sleeve attachment weld would be relieved by the occurrence of cracking at that location. As a result, the residual stresses are likely to be involved in crack initiation and in the early stages of crack propagation but would have little or no influence on the later stages of crack propagation. At the inside surface of the safe-end, the cracking was located at an essentially constant distance from the fusion line of the attachment weld. This factor, together with the fact that cracking occurred completely around the inside surface is evidence that residual stresses in the region of the thermal sleeve attachment weld were a significant factor contributing to the cracking problem.

The existence of significant residual stresses in the crack initiation zone due to the repair weld has not been demonstrated. However, consideration of general principles concerning residual stresses developed from welding operations indicates that the repair weld would have resulted in compressive

---

* Reference 27, Appendix G, pg. G-8.

hoop stresses and compressive axial stresses at the thermal sleeve attachment location which would not favor IGSCC. Regardless of the nature of the initial residual stresses associated with the repair weld, such stresses would be altered by subsequent machining and welding. The welding operation performed to attach the thermal sleeve would completely relieve all pre-existing stresses in the vicinity of the crevice tip. Therefore, the final state of stress at the location of eventual crack initiation would be completely controlled by the thermal sleeve attachment weld. In view of these factors, it is not likely that residual stresses from the weld repair contributed to crack initiation or the early stages of propagation.

In view of the factors discussed above, the information and data obtained in this investigation support the following conclusions:

1. The cracking and eventual leakage encountered in the safe-end occurred by intergranular stress-corrosion cracking under the combined influence of stresses in excess of the yield strength (applied + residual) and environmental conditions associated with the tight crevice between the thermal sleeve and the safe-end.

2. There is a possibility that sulfur-bearing and/or chlorine-bearing contaminant species contributed to crack initiation and propagation. This factor was not completely resolved in this investigation, but the presence of a contaminant species is neither a necessary nor a sufficient condition for intergranular stress-corrosion cracking.

3. The furnace-sensitized condition of the safe-end material was not a contributing factor to the cracking problem.

4. The cracking was not associated with any microstructural abnormalities or inherent defects in the safe-end forging or in the thermal sleeve attachment weld.

5. There is no evidence to indicate that the existence of the repair weld on the outside of the safe-end contributed to crack initiation or the early stages of crack propagation.

APPENDIX A

RADIOGRAPHS

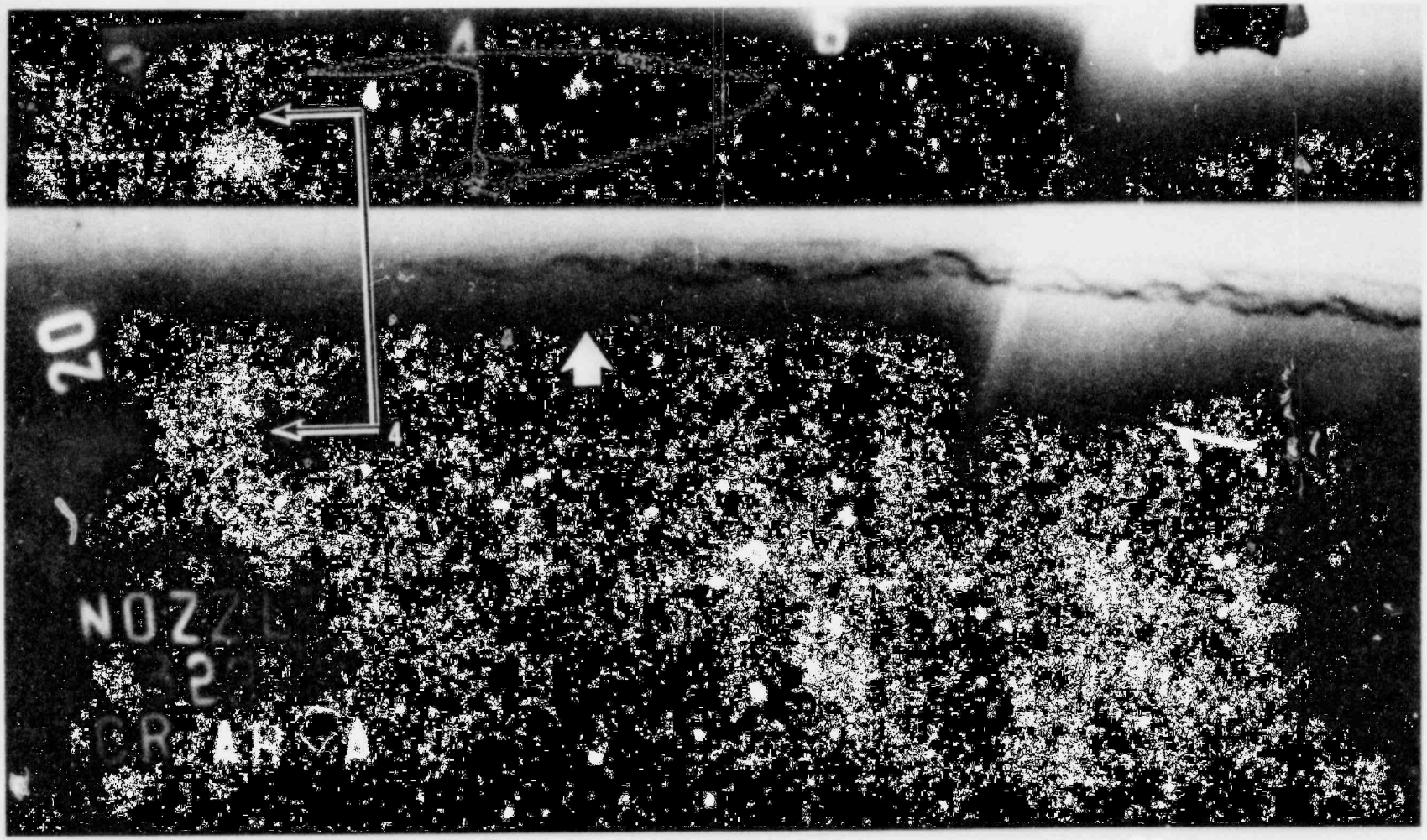

2-34468

FIGURE A-1. SAFE-END RADIOGRAPH. Stations 3 to 6. See Figure 1-4 for location. Section markers indicate location of metallographic sections. Block arrow indicates direction toward vessel.

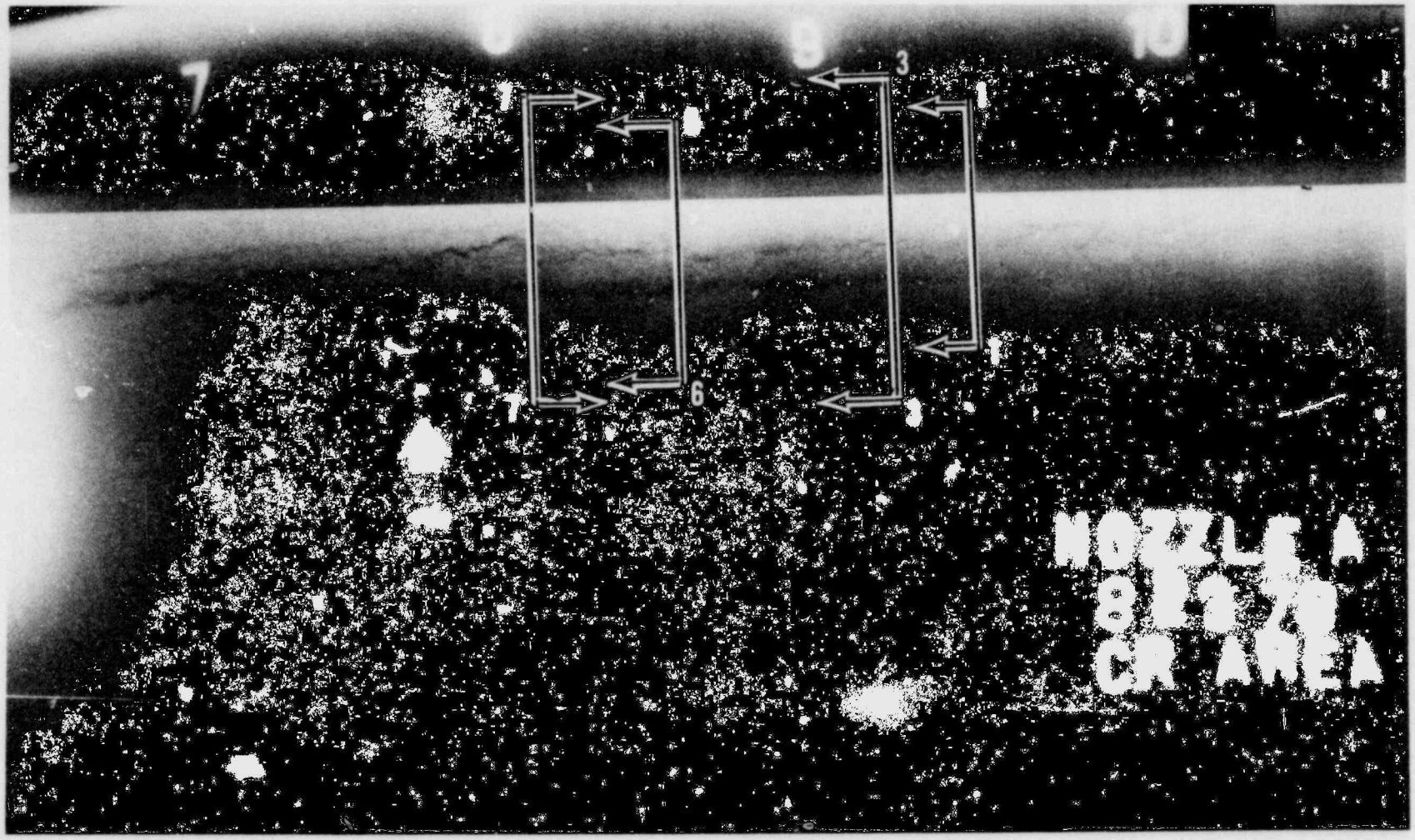

2-34466

FIGURE A-2. SAFE-END RADIOGRAPH. Stations 7 to 10. See Figure 1-4 for location. Section markers indicate location of metallographic sections. Block arrow indicates direction toward vessel.

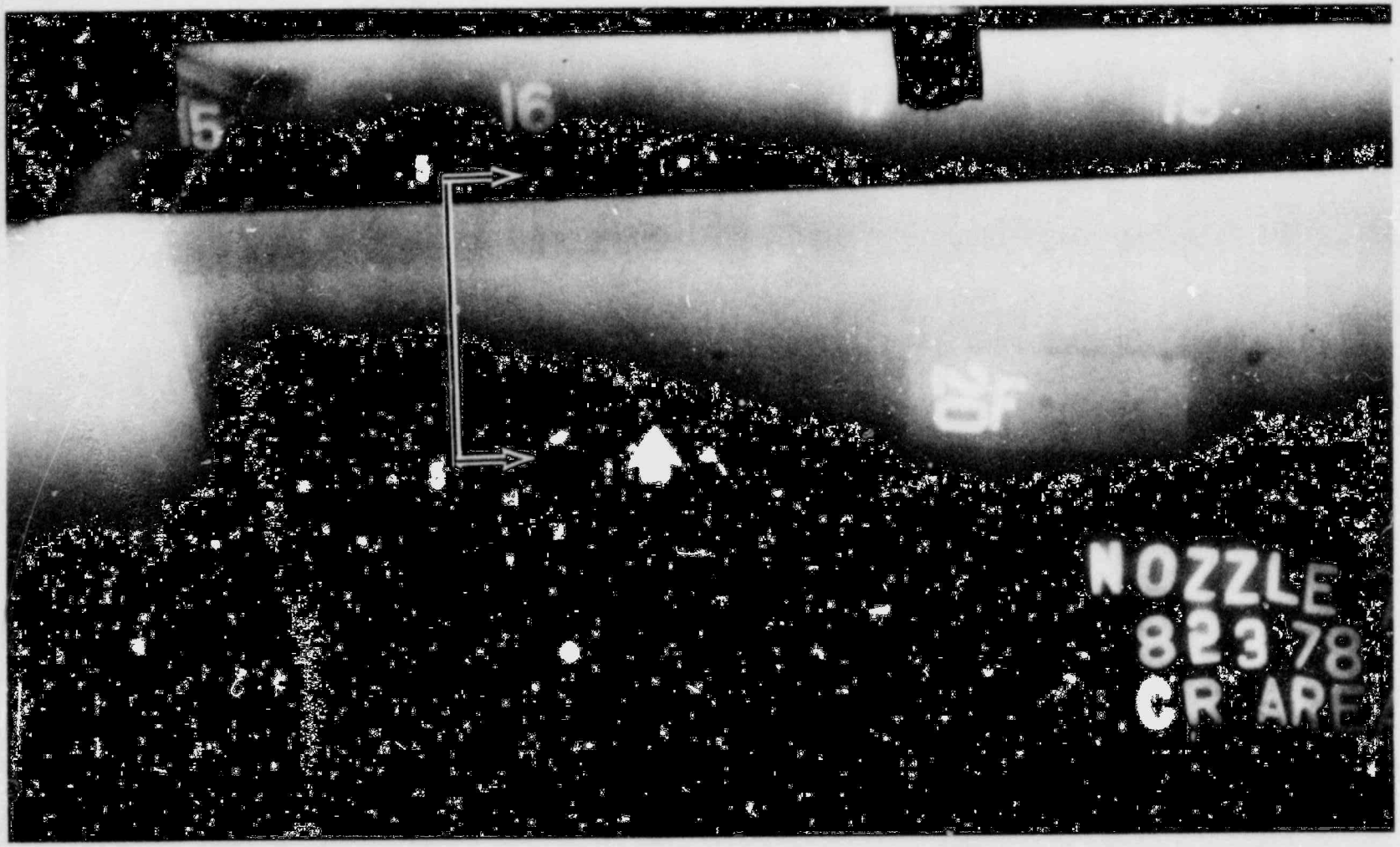

2-34467

FIGURE A-3. SAFE-END RADIOGRAPH. Stations 15 to 18. See Figure 1-4 for location. Section markers indicate location of metallographic sections. Block arrow indicates direction toward vessel.

APPENDIX B

MACROGRAPHS OF METALLOGRAPHIC SECTIONS

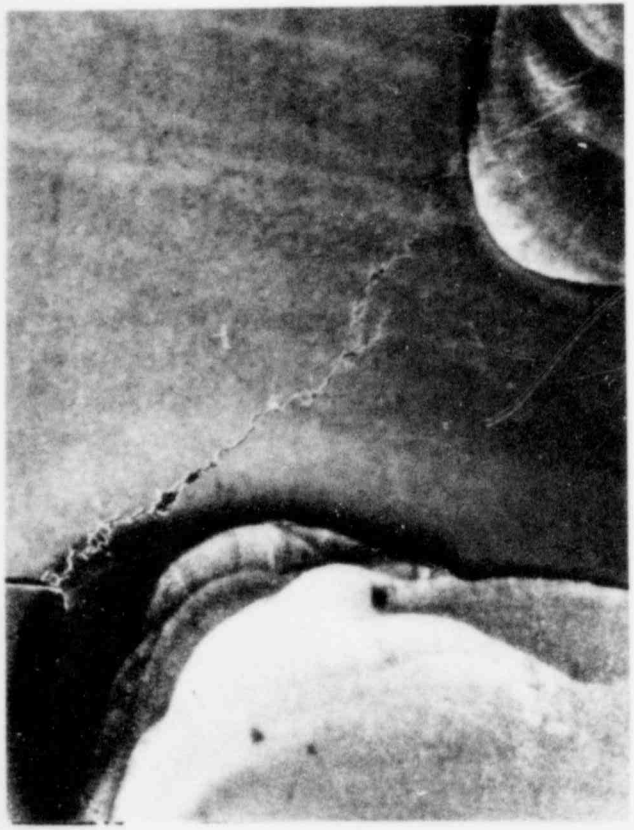

2-34867 7X

(a) Section 2-2. Etchant, 8:1 Phosphoric acid.

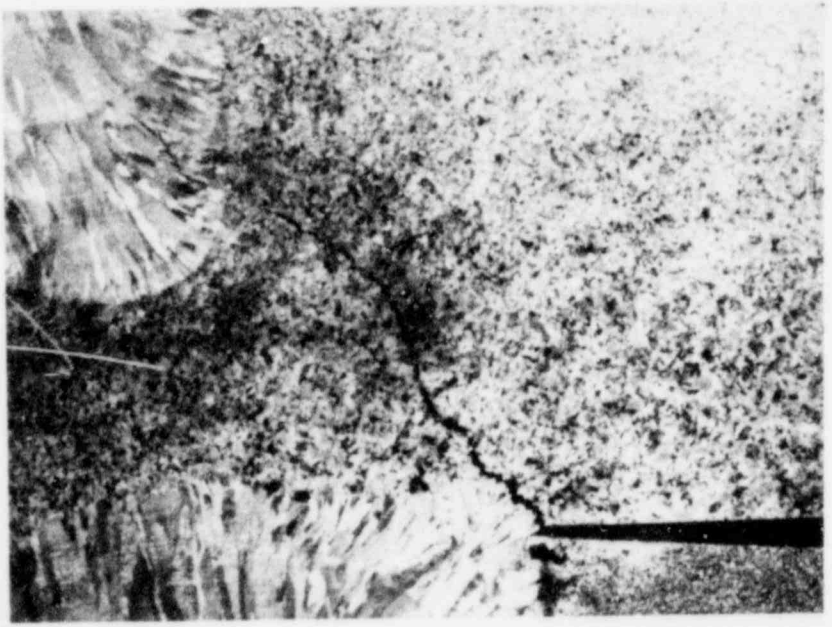

2-34350 5X

(b) Section 3-3. Lapito's etch.

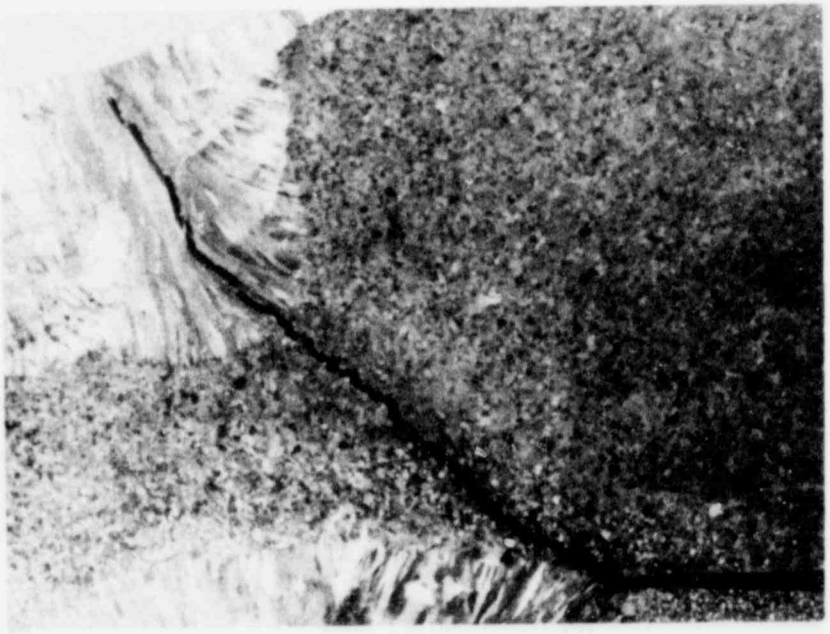

2-34464 5X

(c) Section 6-6. Lapito's etch.

FIGURE B-1. LONGITUDINAL SECTIONS AT THERMAL SLEEVE ATTACHMENT. See Figure 1-4 for locations.

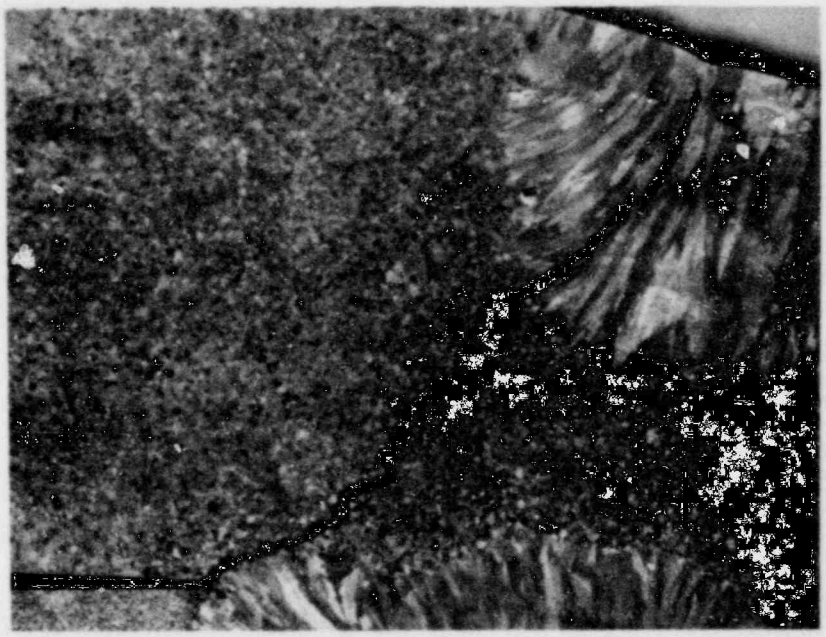

2-34465 (a) Section 7-7. Lapito's etch 5X

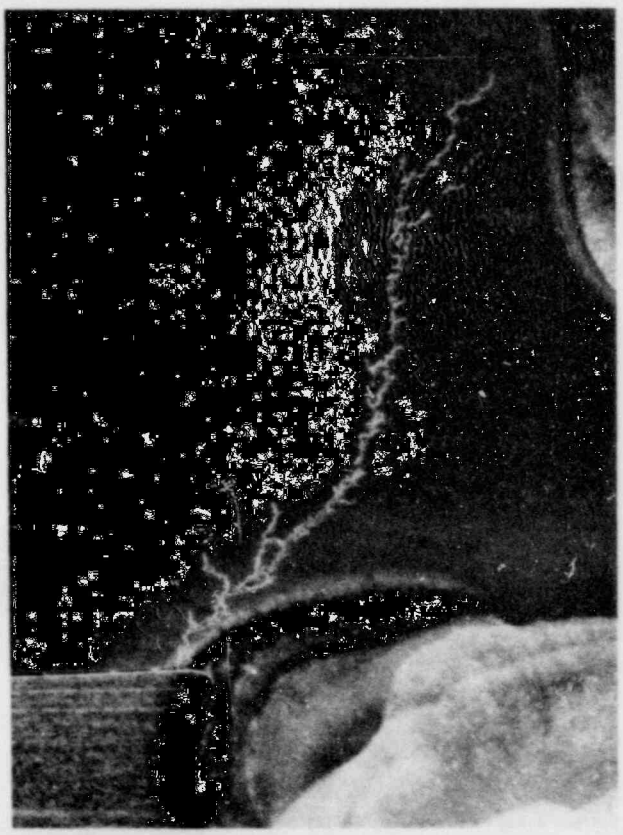

2-34871 (b) Section 10-10. Etchant: 8:1 Phosphoric acid. 7X

2-34880 (c) Section 11-11. Etchant: 8:1 Phosphoric acid. 7X

FIGURE B-2. LONGITUDINAL SECTIONS AT THERMAL SLEEVE ATTACHMENT. See Figure 1-4 for locations.

APPENDIX C

Microhardness Data

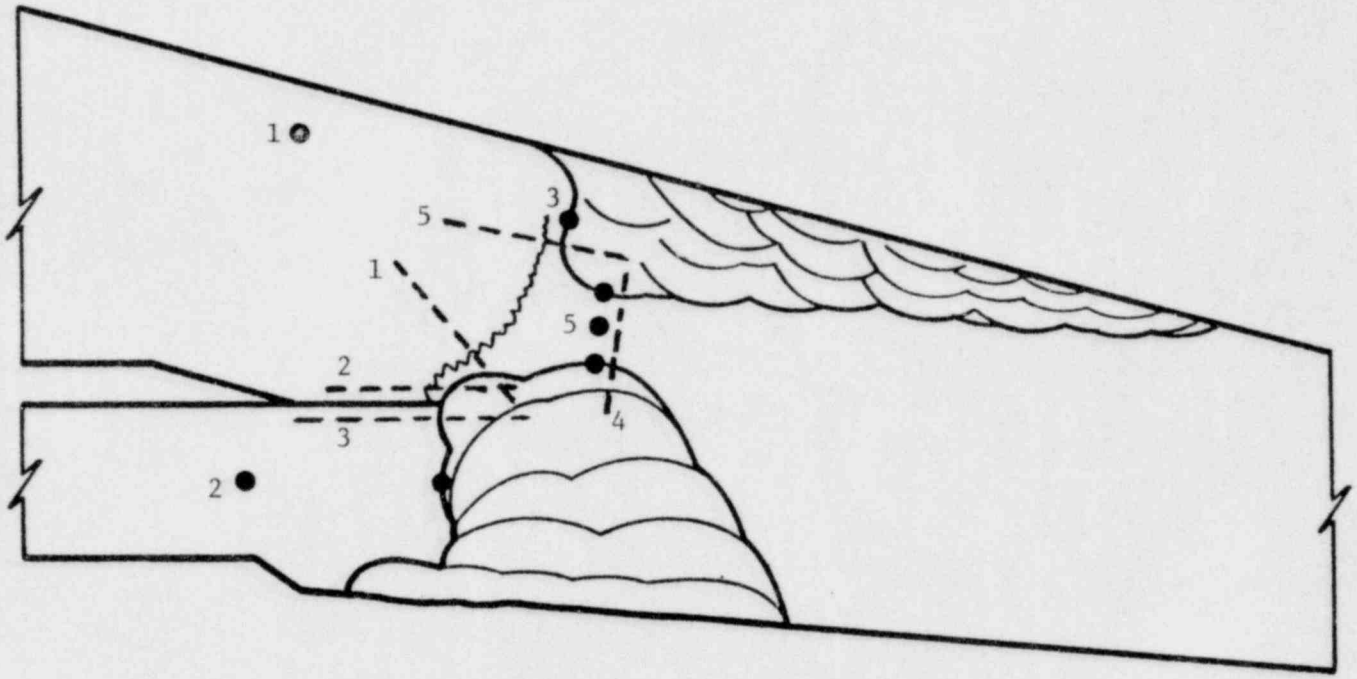

FIGURE C-1. DIAGRAM OF REPRESENTATIVE SECTION THROUGH THERMAL SLEEVE ATTACHMENT AREA. Numbered circles indicate metallographic locations. Dashed lines indicate hardness traverses.

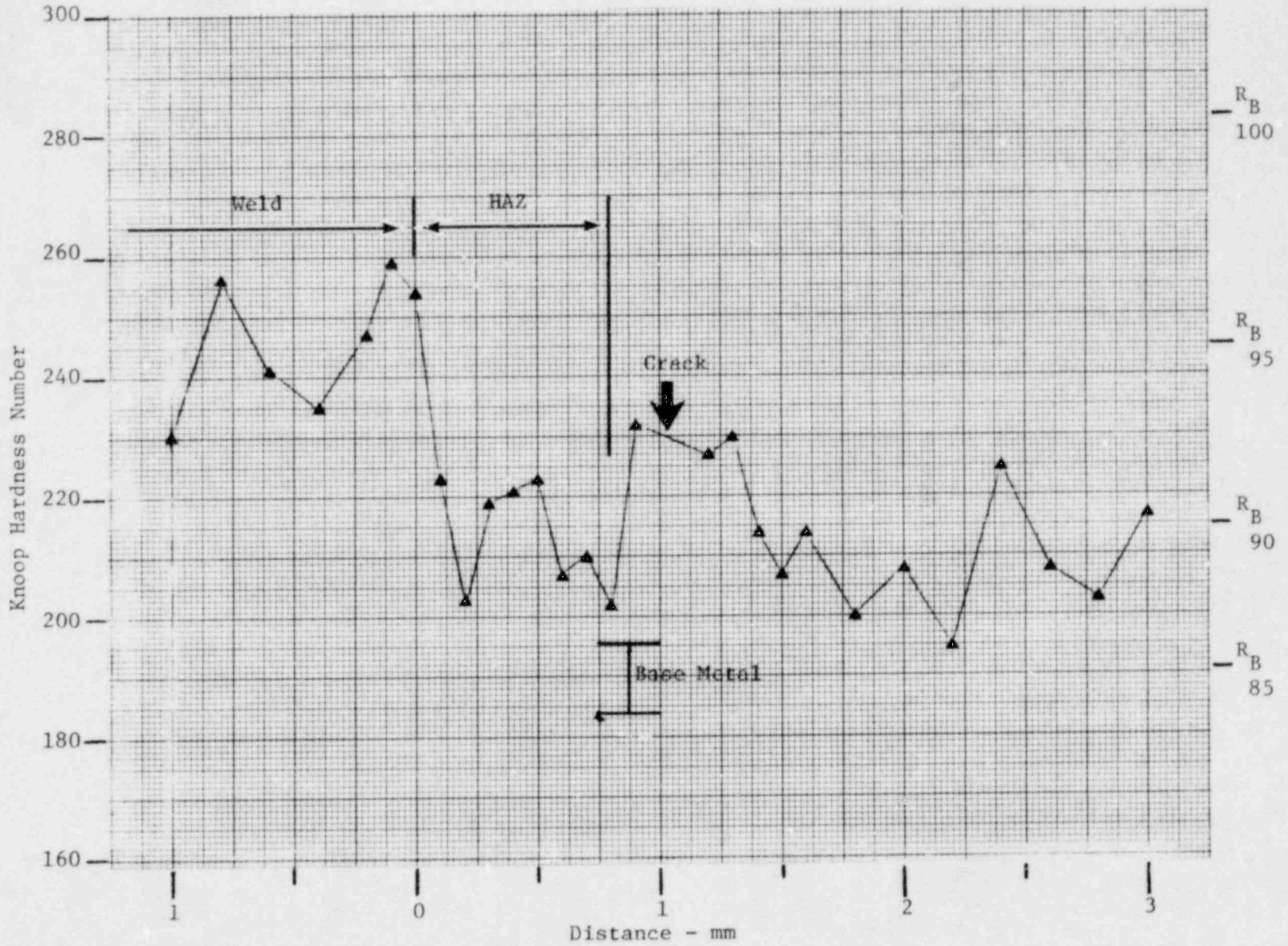

FIGURE C-2. HARDNESS TRAVERSE NO. 1. Section 5-5 Thermal sleeve weld to safe-end base metal across crack path.

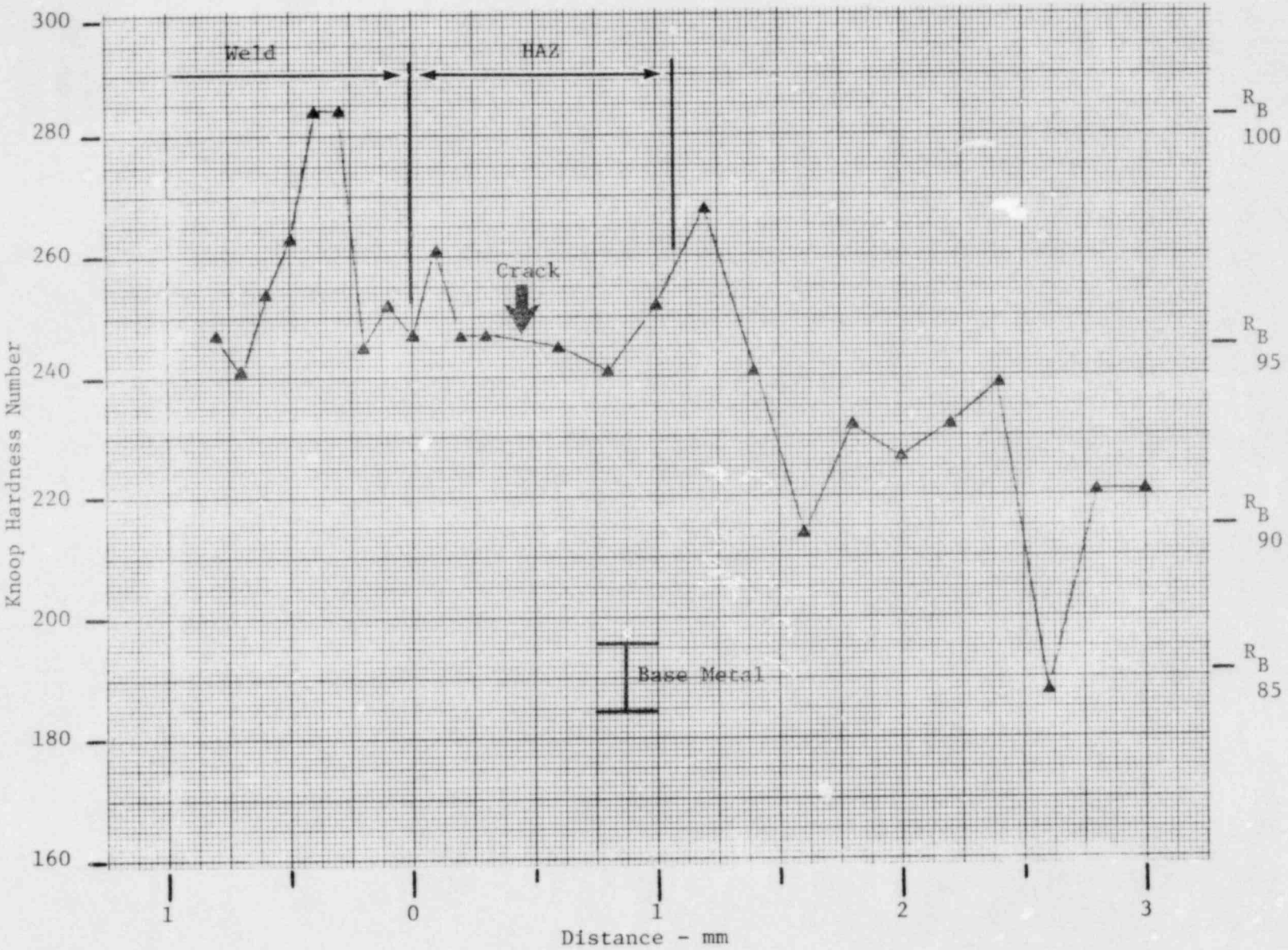

FIGURE C-3. HARDNESS TRAVERSE NO. 2. Section 5-5. Thermal sleeve weld to safe-end base metal along crevice.

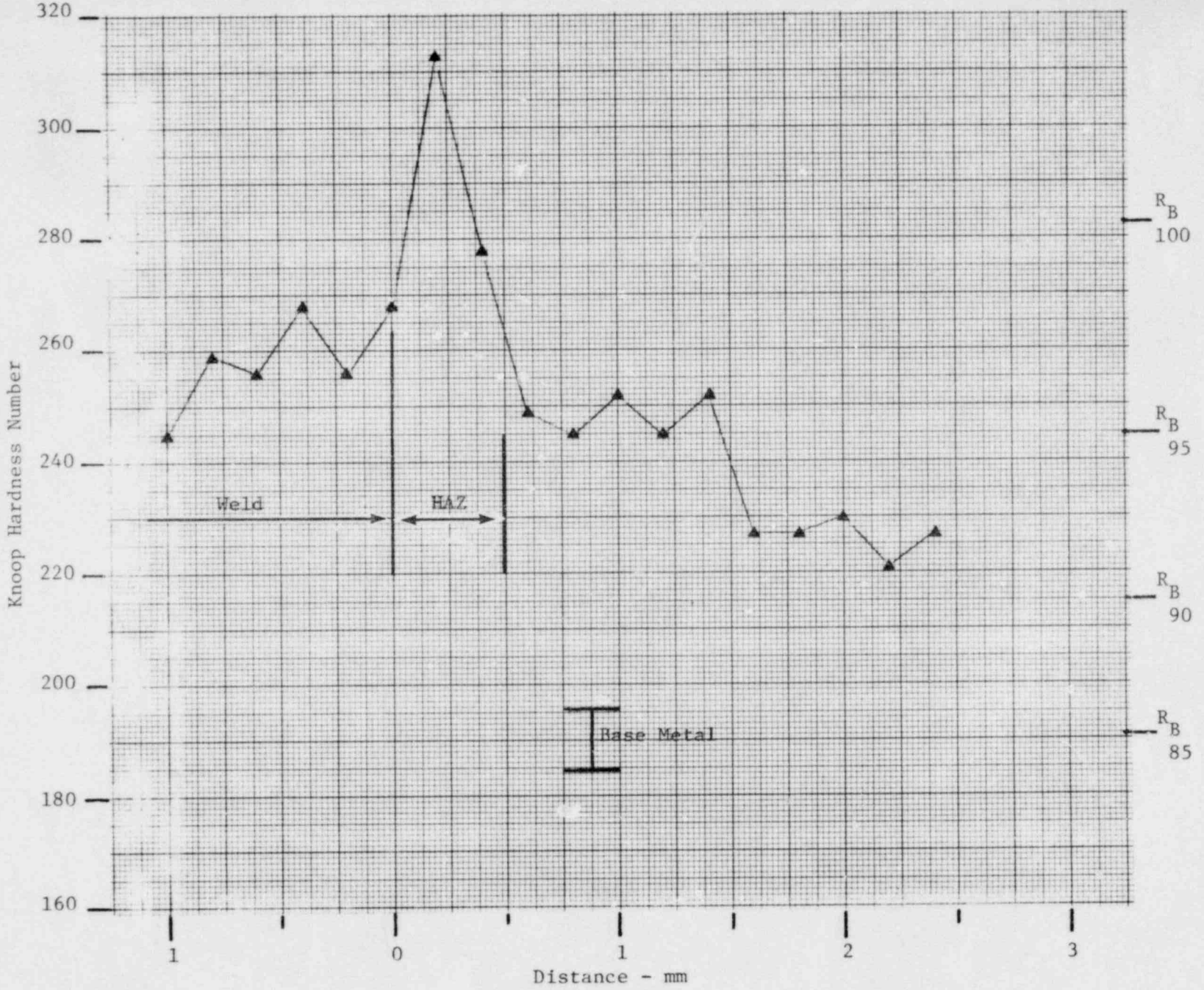

FIGURE C-4. HARDNESS TRAVERSE NO. 3. Section 5-5. Thermal sleeve weld to thermal sleeve base metal.

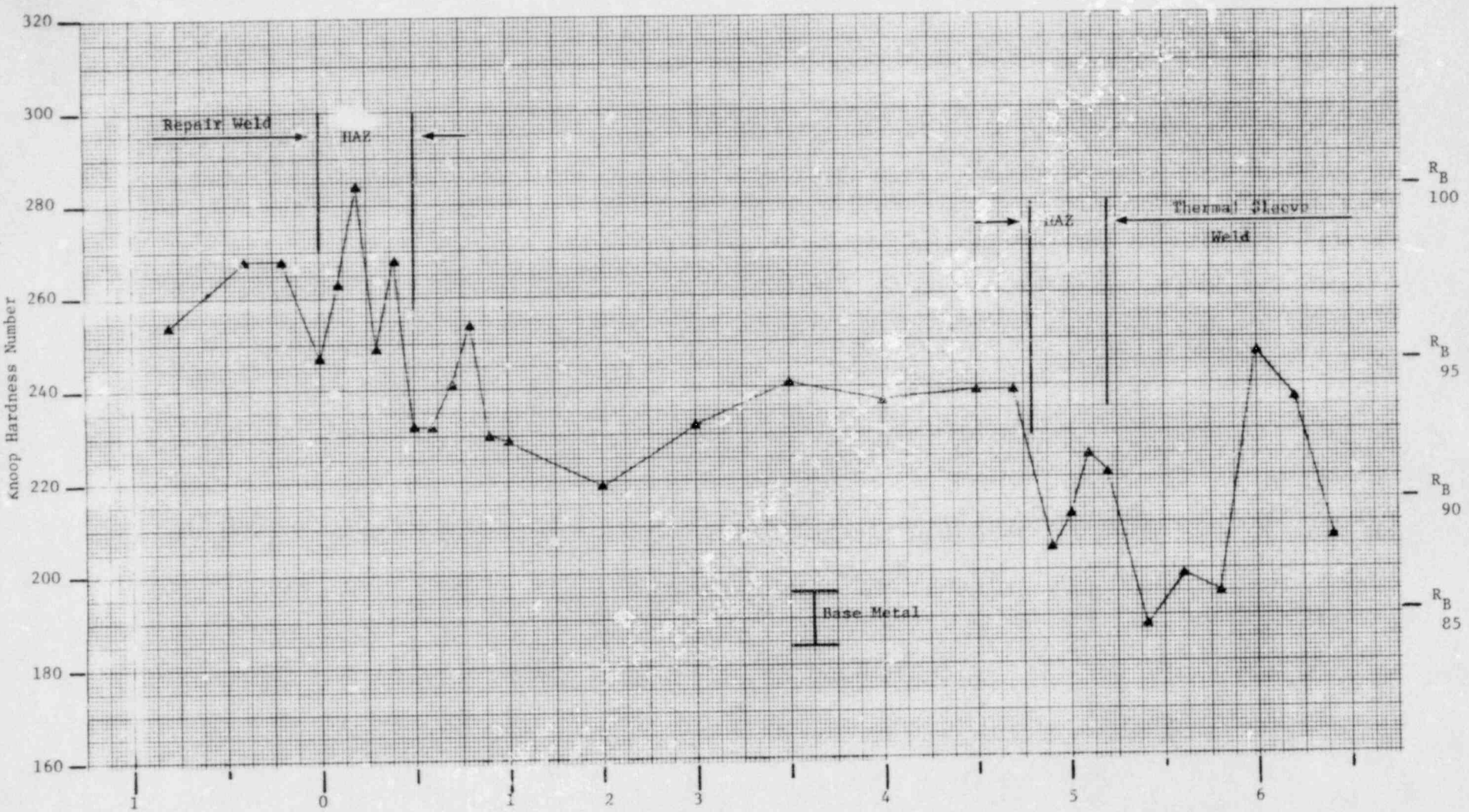

FIGURE C-5. HARDNESS TRAVERSE NO. 4. Section 5-5. Repair weld to thermal sleeve weld.

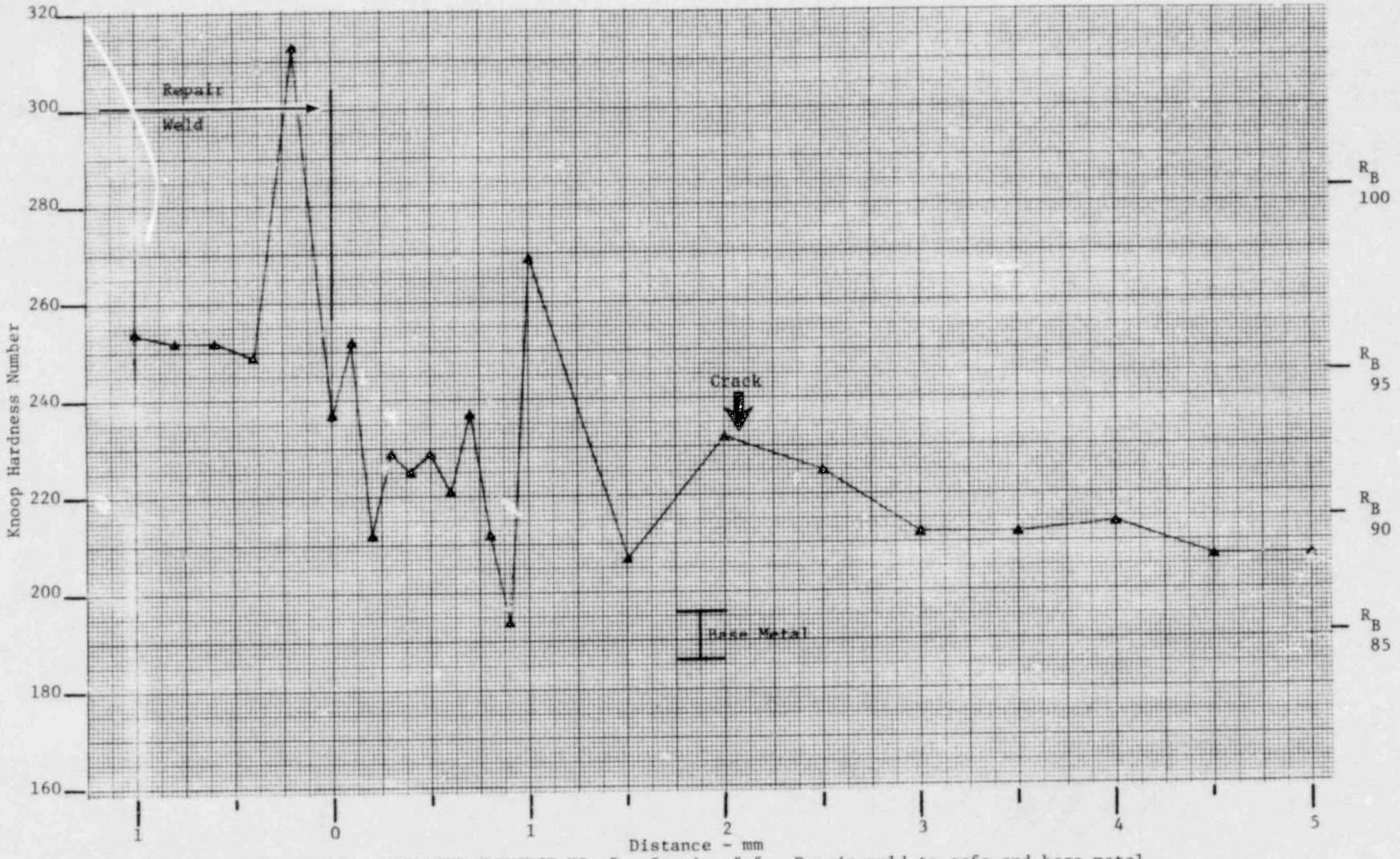

FIGURE C-6. HARDNESS TRAVERSE NO. 5. Section 5-5. Repair weld to safe-end base metal.

APPENDIX D

Micrographs from Sections through Thermal Sleeve Attachment Area

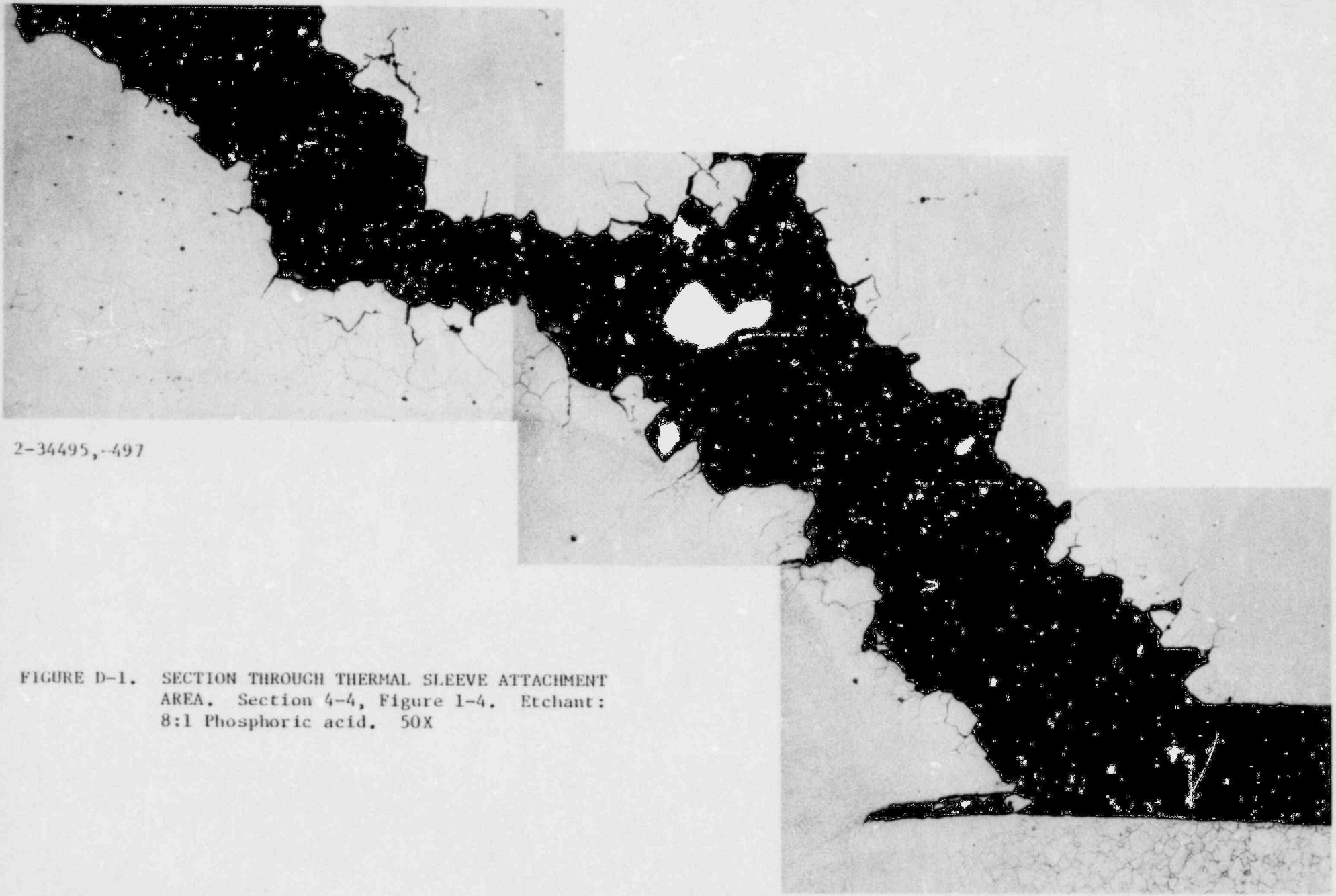

2-34495,-497

FIGURE D-1. SECTION THROUGH THERMAL SLEEVE ATTACHMENT AREA. Section 4-4, Figure 1-4. Etchant: 8:1 Phosphoric acid. 50X

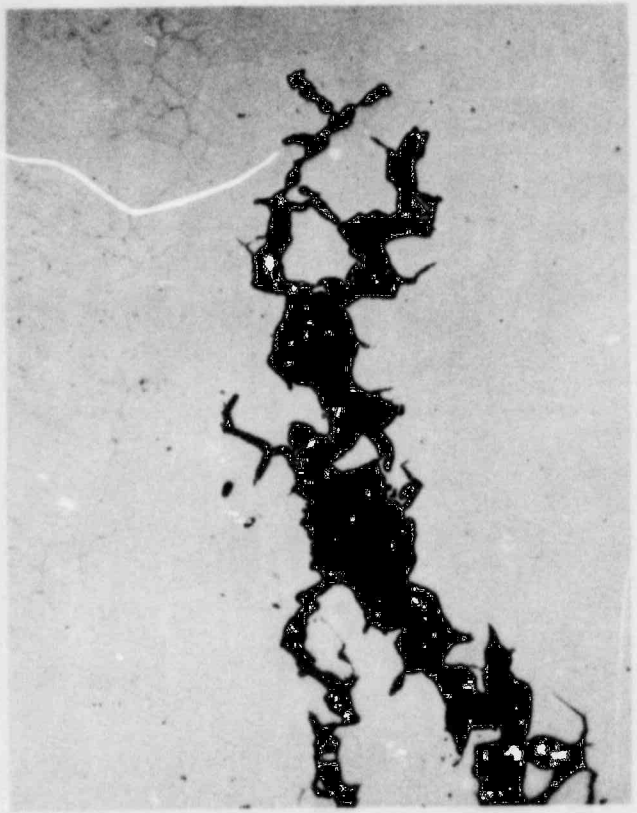

2-34494 (a) 50X

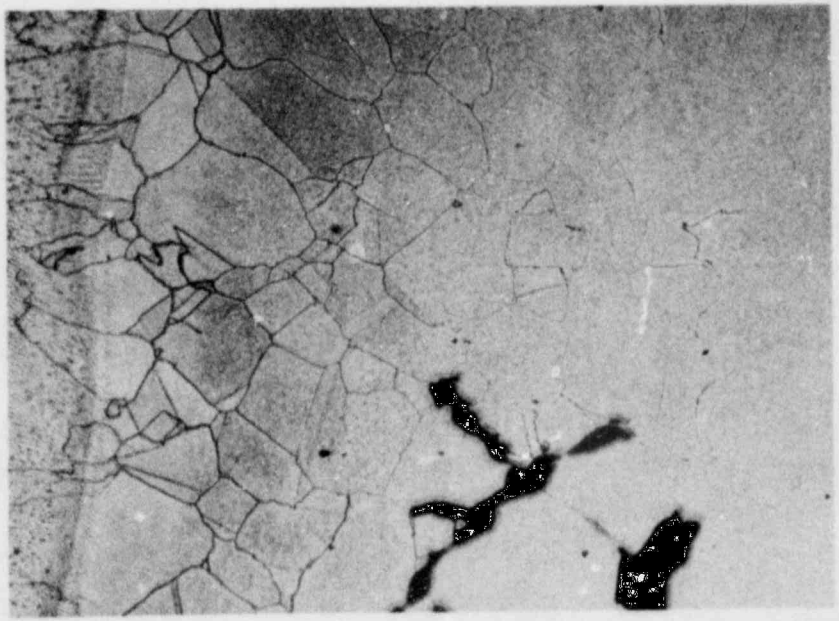

2-34521 (b) 100X

FIGURE D-2. MICROSTRUCTURE AT CRACK TIP. Section 4-4. See Figures 2-3 and 4-4. Etchant: 8:1 Phosphoric acid.

FIGURE D-3. SECTION THROUGH THERMAL SLEEVE ATTACHMENT AREA. Section 9-9, Figure 1-4. Etchant: 8:1 Phosphoric acid. 75X

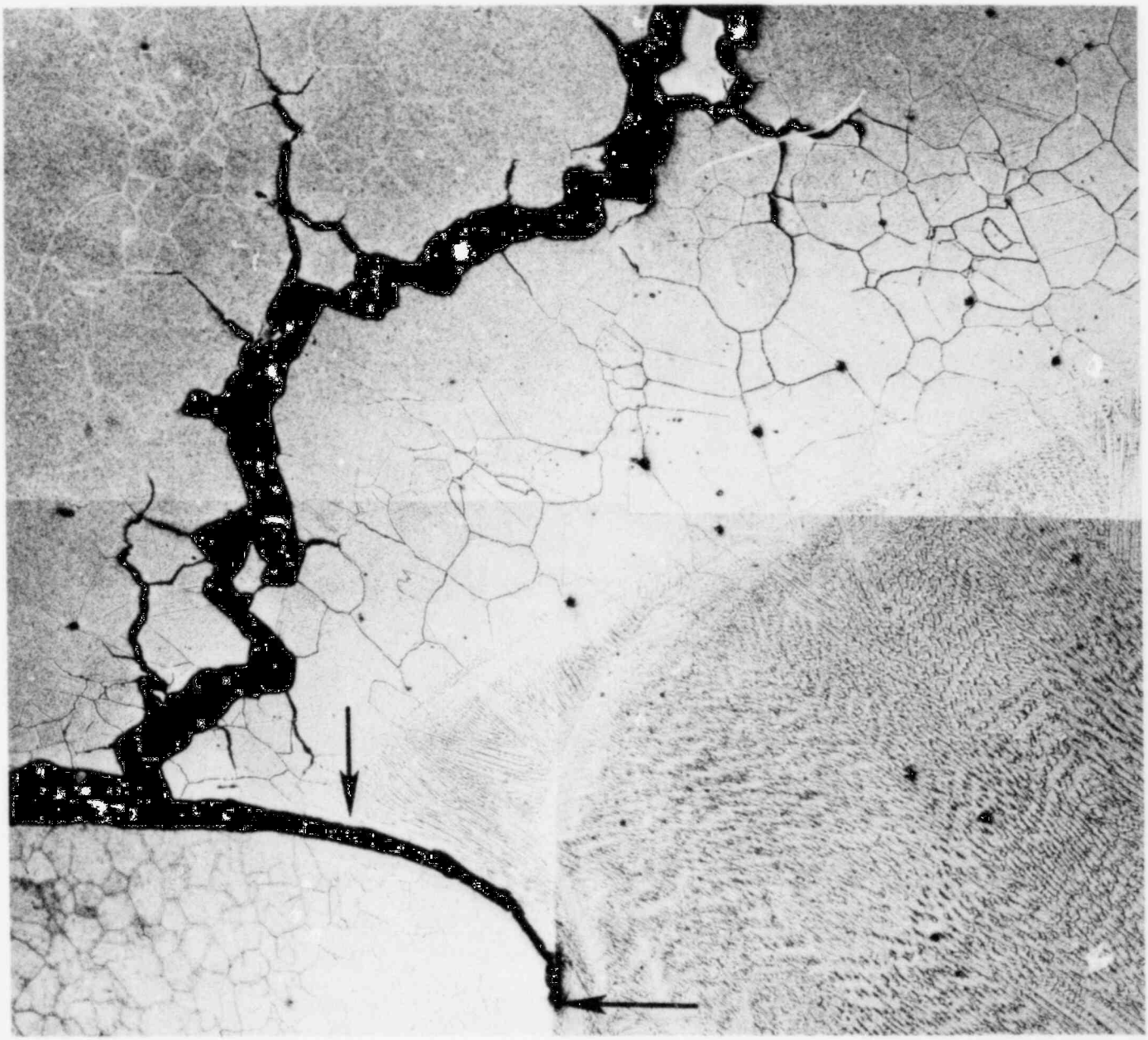

2-34872,-873
2-34889,-890

FIGURE D-4. SECTION THROUGH THERMAL SLEEVE ATTACHMENT AREA. Section 10-10, Figure 1-4. Etchant 8:1 Phosphoric acid. 100X

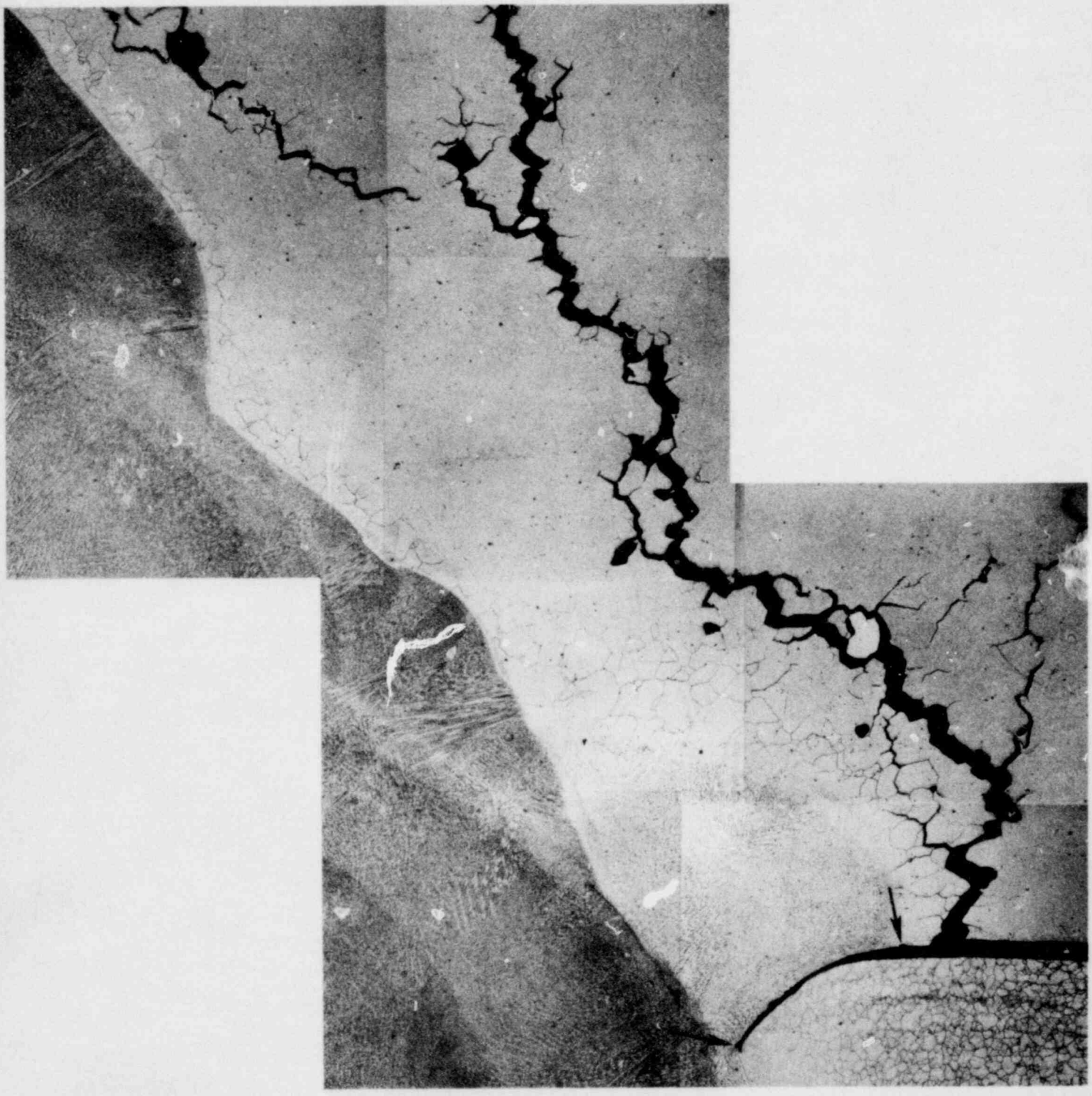

FIGURE D-5. SECTION THROUGH THERMAL SLEEVE ATTACHMENT AREA.
Section 11-11, Figure 1-4. See Figure 4-7.
Etchant: 8:1 Phosphoric acid. 37.5X

APPENDIX E

Selected SEM Fractographs

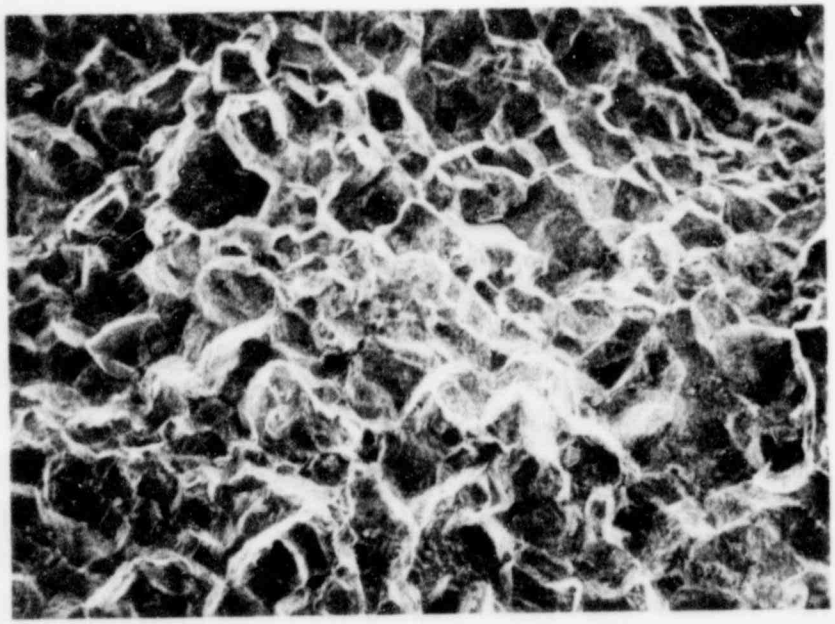

2-238 (a) 100X

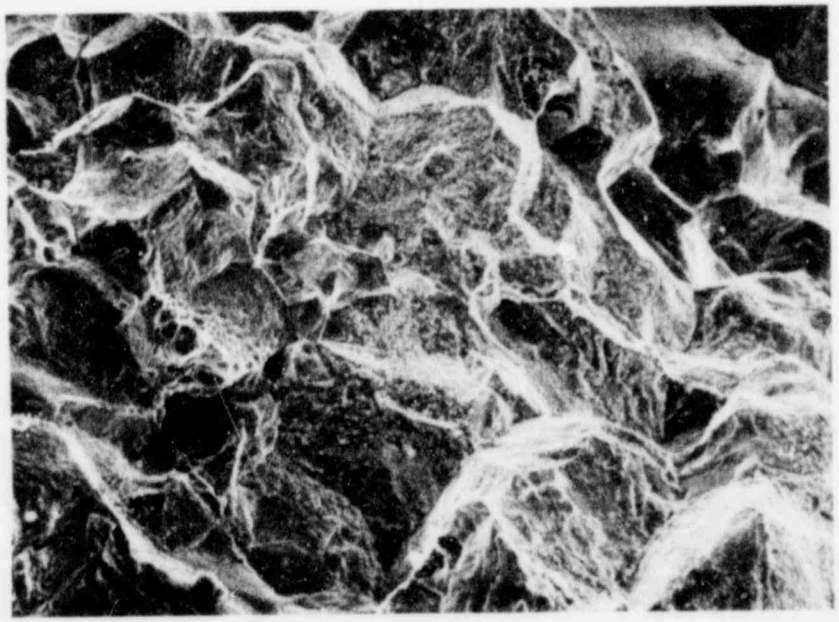

2-239 (b) 300X

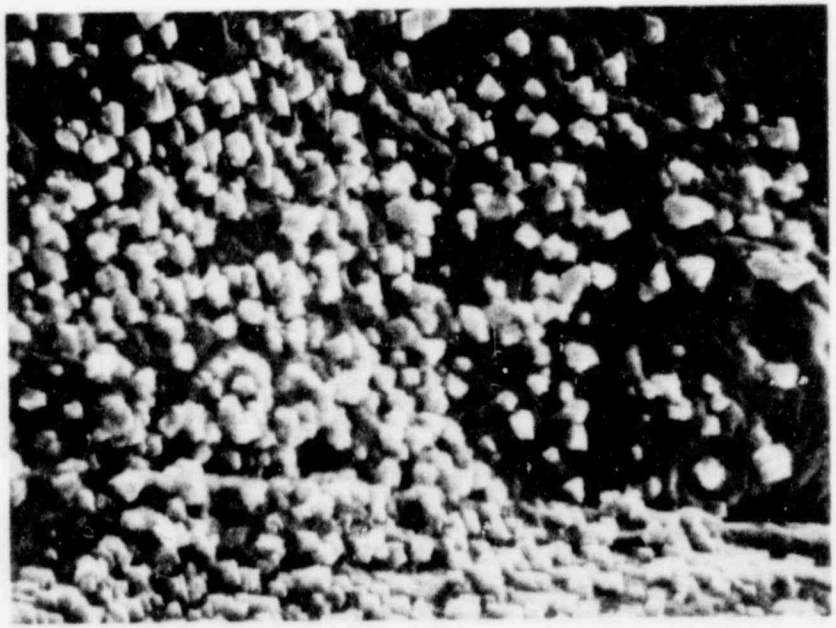

2-241 (c) 3000X

FIGURE E-1. SEM FRACTOGRAPHS FROM CRACK SURFACE. Specimen No. 2, Location 1, Figure 4-9(b).

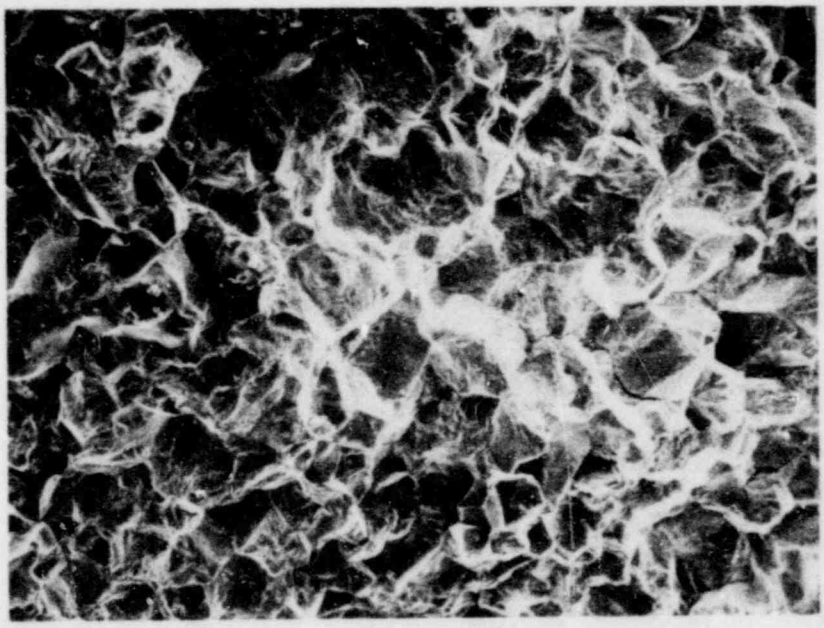

2-247 100X

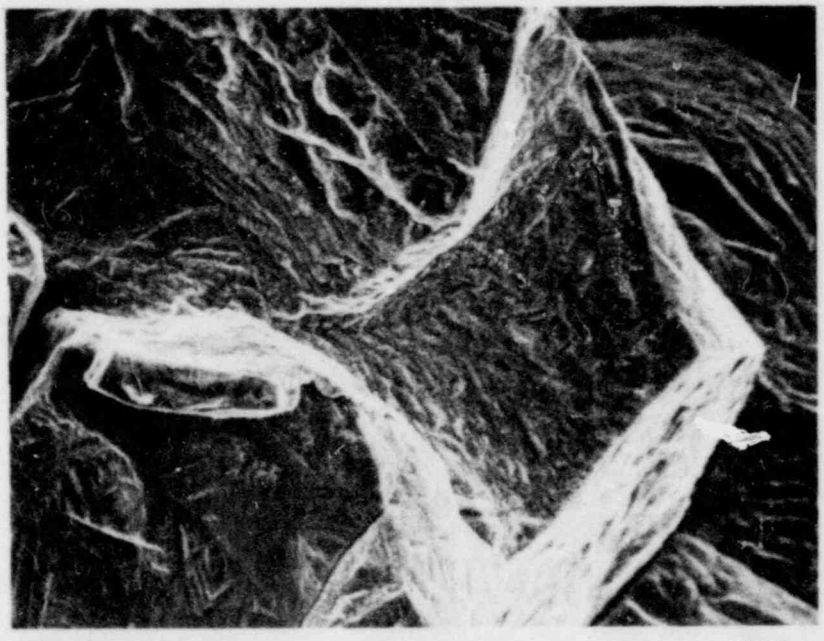

2-210 1000X

FIGURE E-2. SEM FRACTOGRAPHS FROM CRACK SURFACE. Specimen No. 2, Location 2, Figure 4-9(b).

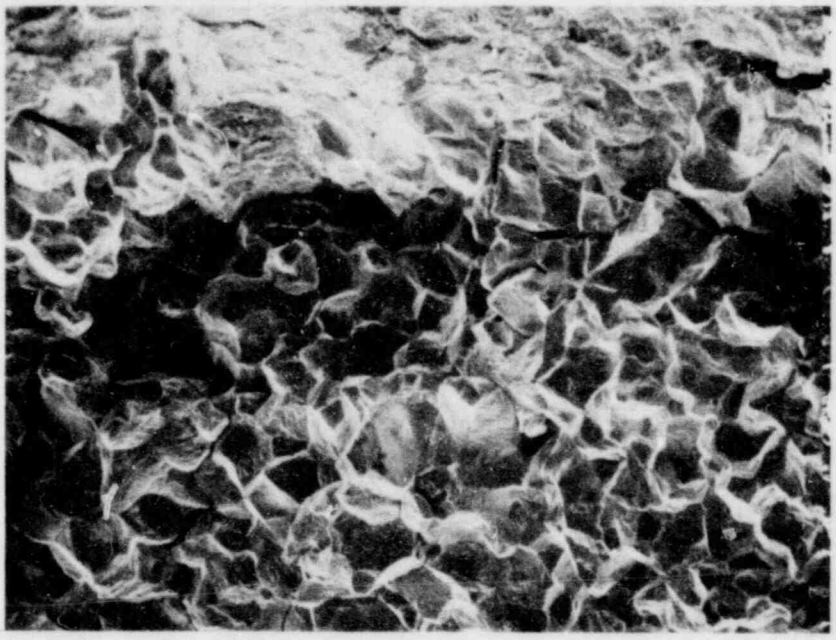

2-253 100X

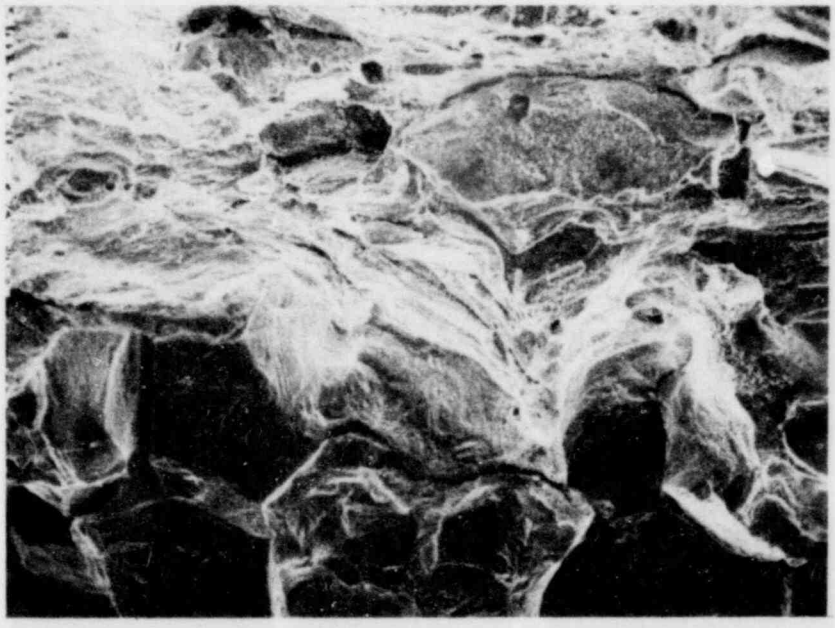

2-254 300X

FIGURE E-3. SEM FRACTOGRAPHS FROM CRACK SURFACE. Specimen No. 2, Location 3, Figure 4-9(b).

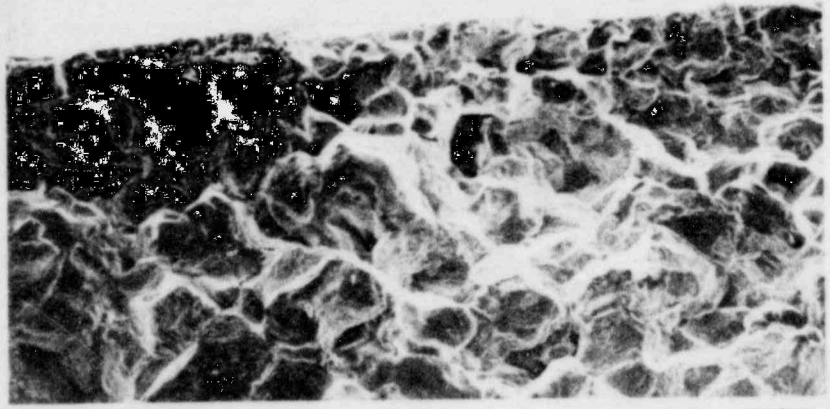

2-269 100X

2-270 (a) Location 1. 500X

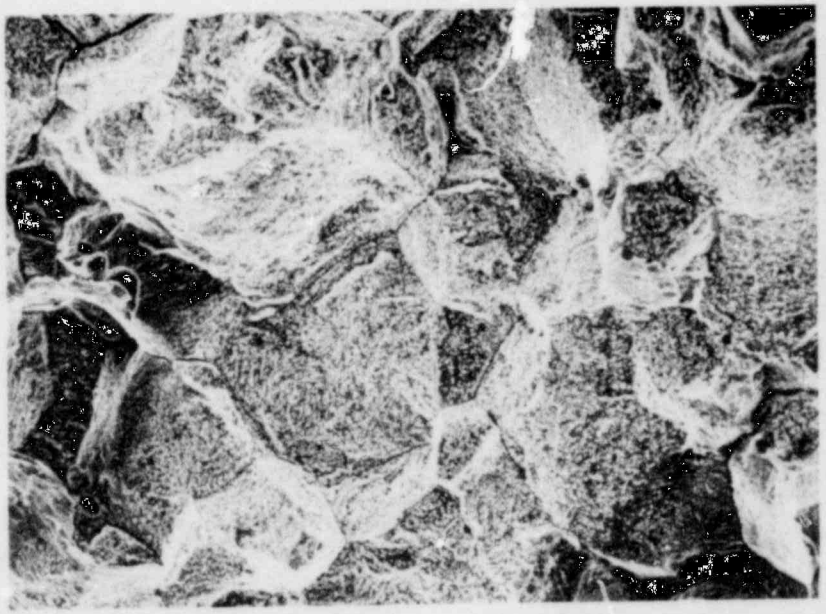

2-258 (b) Location 2. 300X

FIGURE E-4. SEM FRACTOGRAPHS FROM CRACK SURFACE. Specimen No. 5. See Figure 4-9(c) for locations.

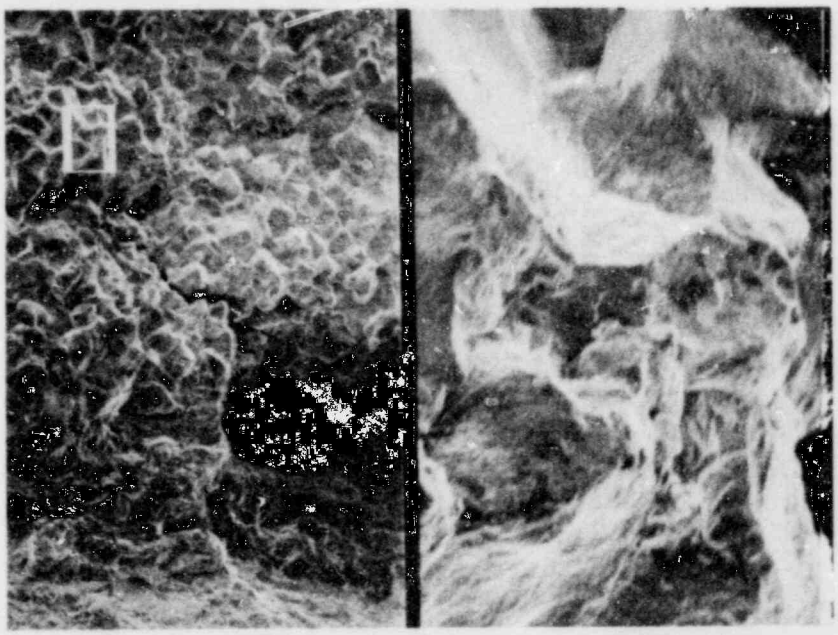

2-216 30/300X

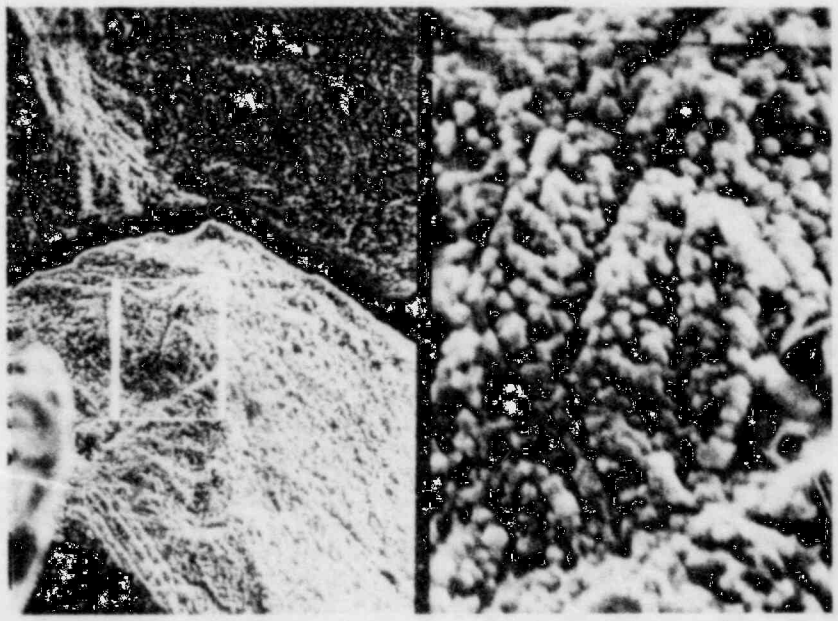

2-218 1000/5000X

FIGURE E-5. SEM FRACTOGRAPHS FROM CRACK SURFACE. Specimen No. 5, Location 3, Figure 4-9(c).

APPENDIX F

SURFACE DEPOSIT ANALYSIS DATA

SUMMARY NOTES ON EDS DATA

Crack Surface

Location E

1. High Fe and small S peak in overall spectrum [F-2(a)].
2. Particle at A is Cr rich [F-2(b)].
3. Deposit cluster at B is Fe rich [F-2(c)].
4. Fe decreased, S peak remains after ultrasonic cleaning [F-3(a)].
5. Small crystalline particles remain after ultrasonic cleaning [F-3(b)].

Location F

1. X-ray spectra for original and cleaned condition same as for Location E.

Location G

1. Fibrous deposit present [F-4(b)].
2. Sulfur present before cleaning [F-4(a)].
3. Deposit removed by ultransonic cleaning [F-4(c)].
4. No sulfur after ultrasonic cleaning [F-4(c)].
5. Fe/Cr ratio unchanged by removal of deposit material [F-4(a) and F-4(c)].

Location H

1. Distinct S peak in overall x-ray spectrum [F-5(a)].
2. Sulfur uniformly distributed [F-5(b)].
3. Fe/Cr ratio comparable to base metal.

Location I

1. Major S indication in overall x-ray spectrum. Highest S/Cr ratio noted [F-6(a)].

2. Sulfur uniformly distributed over intergranular facets [F-6(b), F-7(c)].

3. Fibrous deposit [F-7(a)].

4. Cluster of fibrous deposit material shows high S [F-7(a)].

5. Fe/Cr ratio comparable to base metal.

Location J

1. Major S indication in overall spectrum [F-8(a)].

2. Fibrous deposit on crack surface in repair weld as well as on crack surface in base metal [F-8(c)].

3. Sulfur uniformly distributed on intergranular facets in base metal and repair weld areas [F-8(b)].

Crevice Surface

Location A

1. Fe present in surface deposit [F-9(b)].

Location B

1. Fe/Cr >1, Fe/Ni > 1 in overall spectrum. Cr/Ni ratio higher than for base metal [F-10(a)].

2. Fe/Cr >> 1, Fe/Ni >> 1 in cluster of deposit material. Cr/Ni ≈ 1 [F-10(b)].

3. Fe is predominant element in deposit material. Deposit material contains Cr.

Location C

1. Fe/Cr ≈1 in overall spectrum [F-11(a)].

2. Fe/Cr and Fe/Ni >> 1 in area of heavier deposit [F-11(b)].

3. Fe is predominant element in deposit material.

Location D

1. Fe/Cr ≈ 1 in overall spectrum [F-12(a)].

2. Major Cl peak in overall spectrum. Note only indication of Cl among all locations examined.

FRACTURE

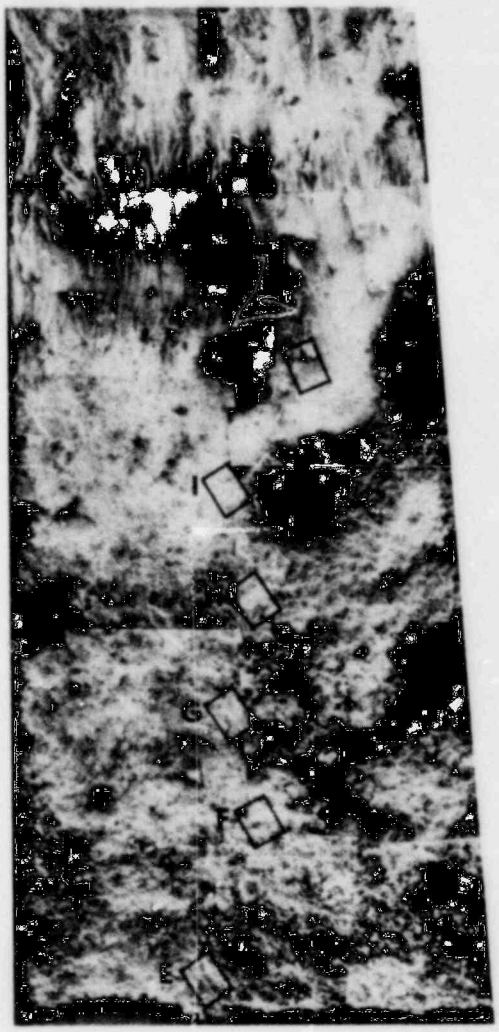

CREVICE

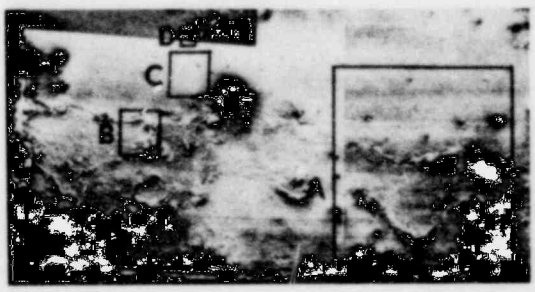

3 mm

FIGURE F-1. CRACK SURFACE AND CREVICE SURFACE - SPECIMEN NO. 6.
See Figure 1-4 for location.

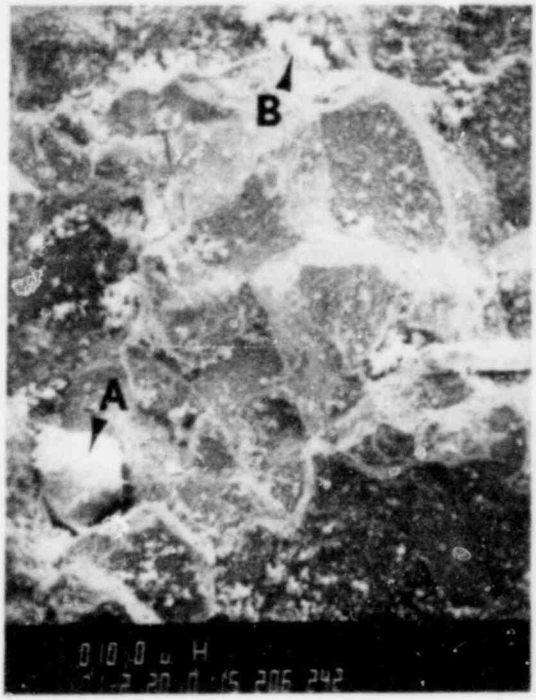

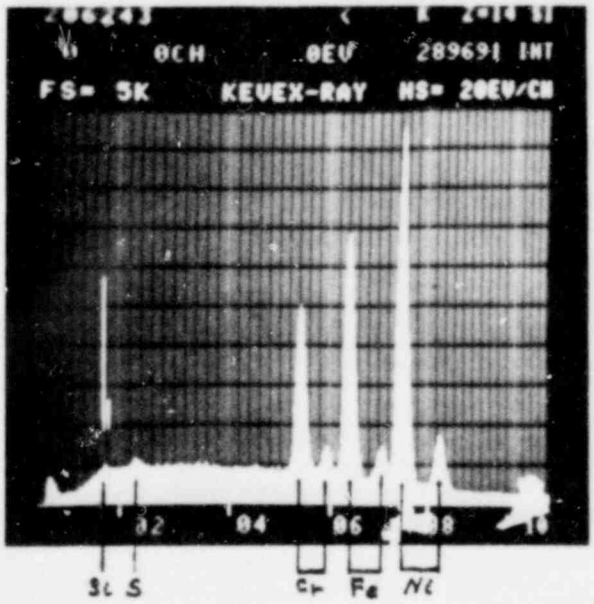

(a) 120X

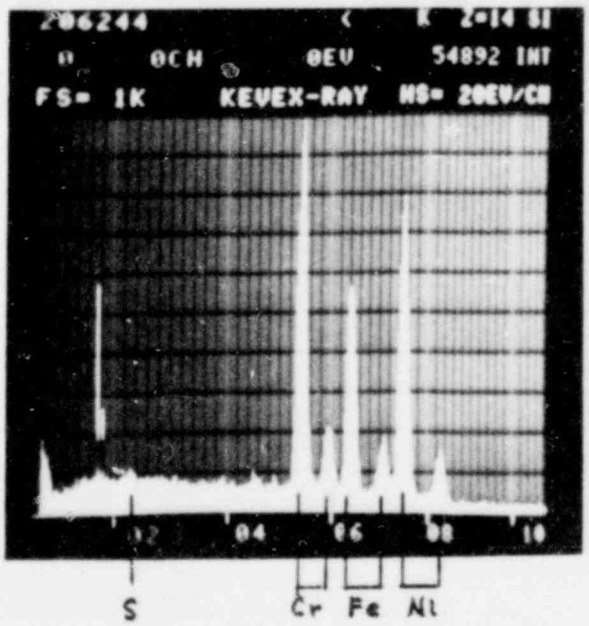

(b) Point A in (a)

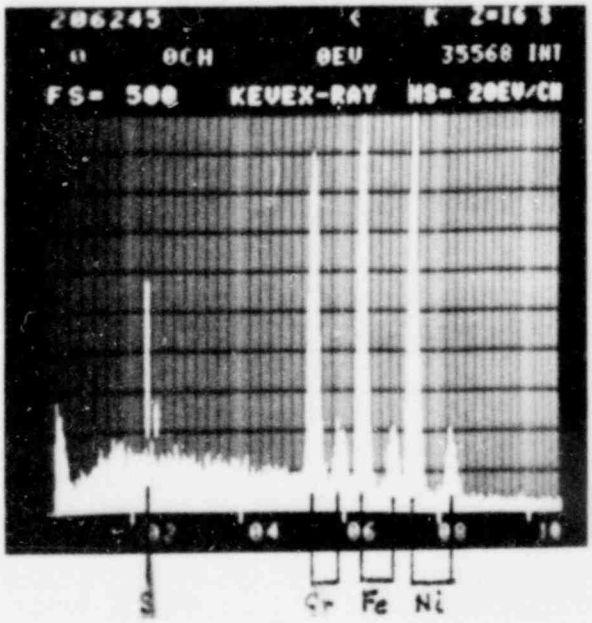

(c) Point B in (a)

FIGURE F-2. LOCATION E.

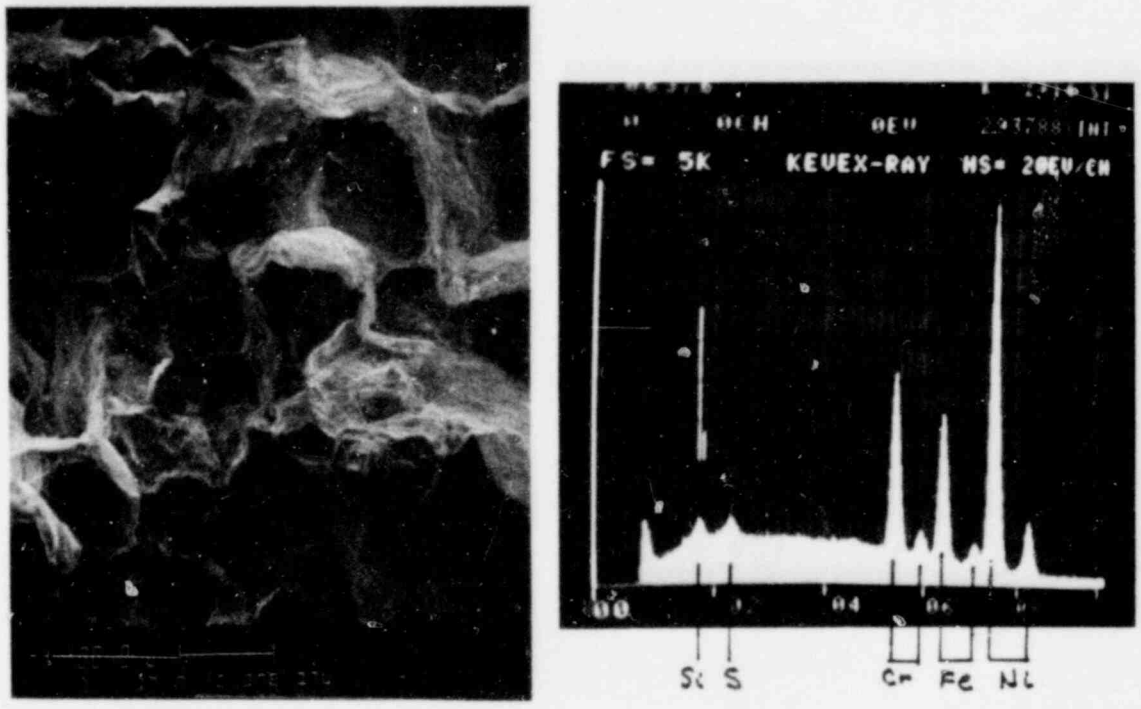

(a) Location E. Same area as F-2(a). 120X

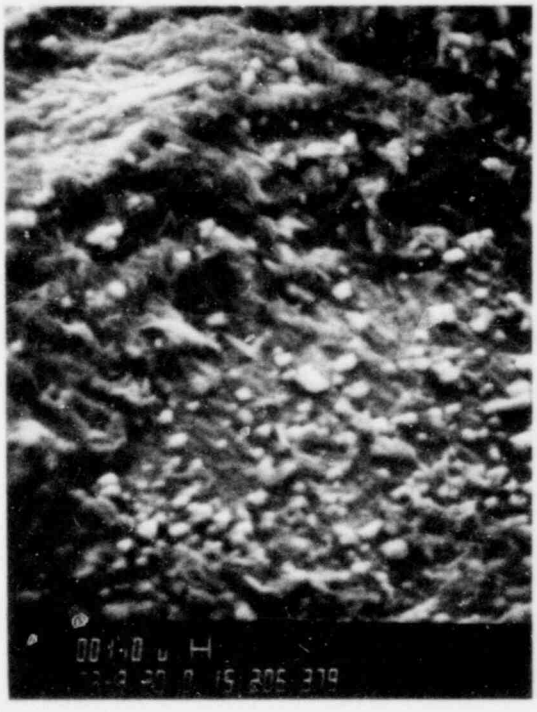

(b) Location F. 2000X

FIGURE F-3. LOCATIONS E AND F.
After ultrasonic cleaning.

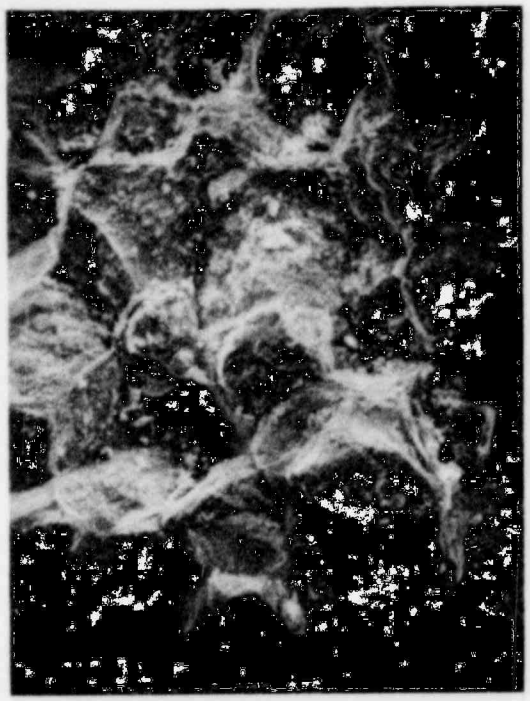

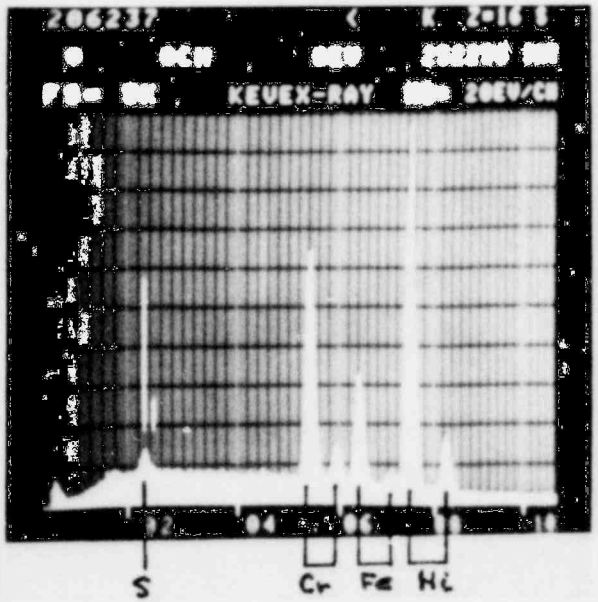

(a) 150X

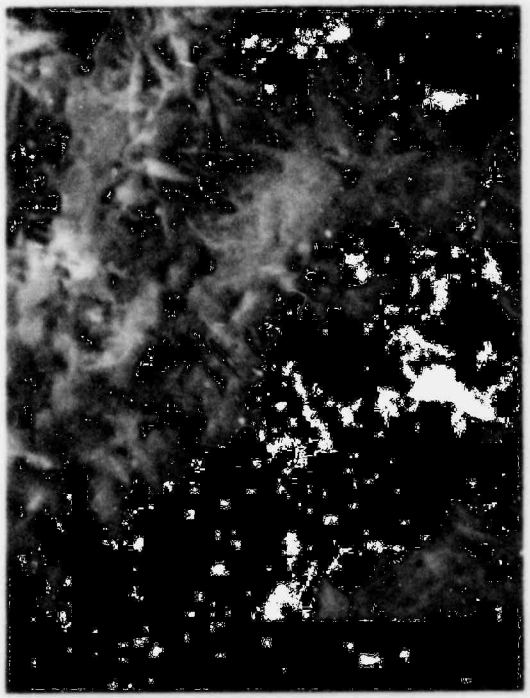

(b) 1500X

FIGURE F-4. LOCATION G.

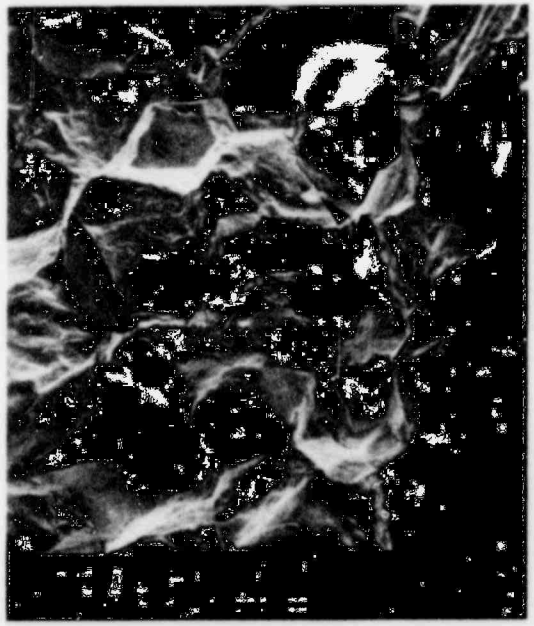

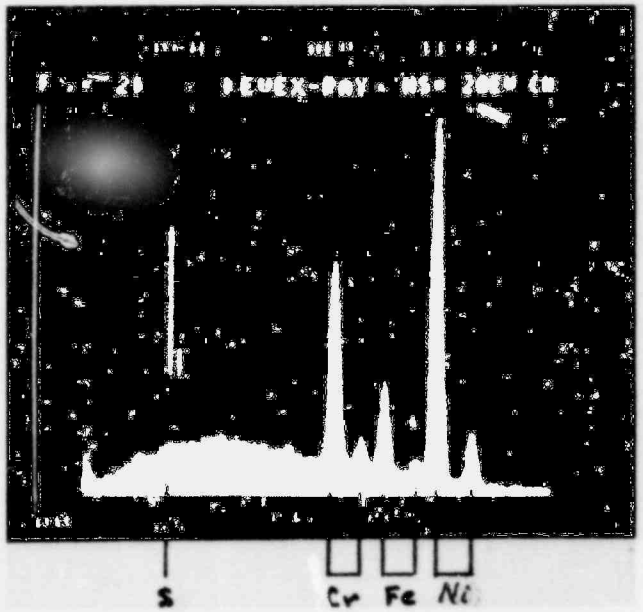

(c) After ultrasonic cleaning. 150X

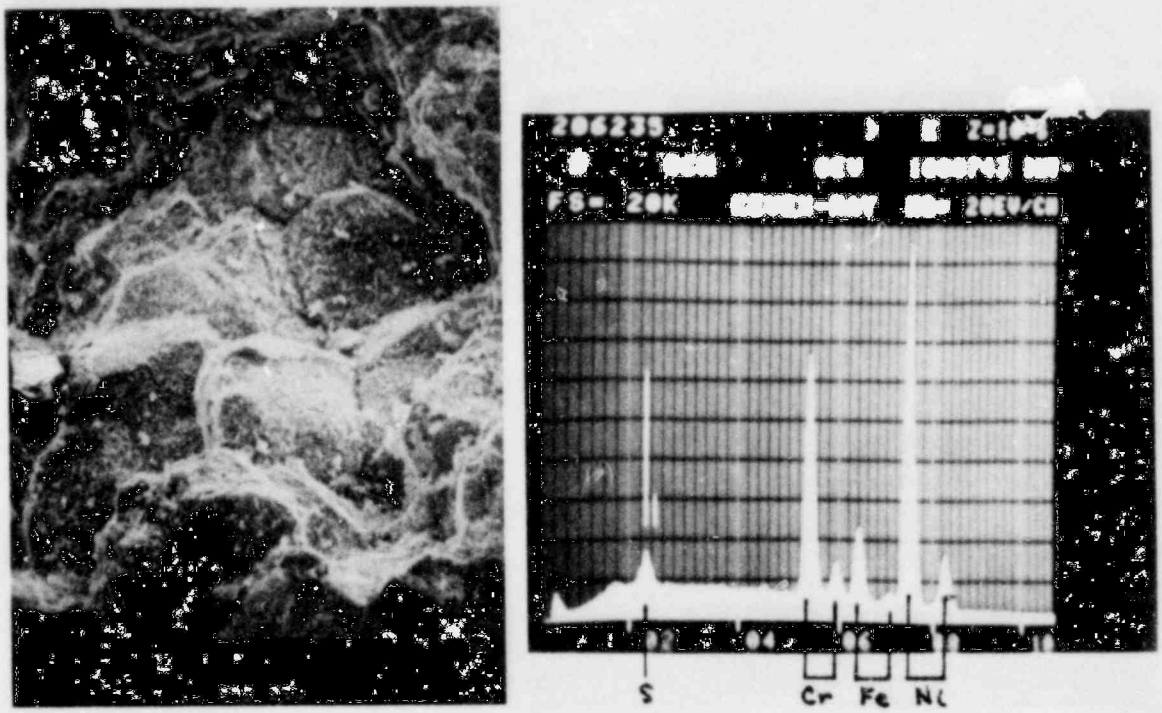

(a) 150X

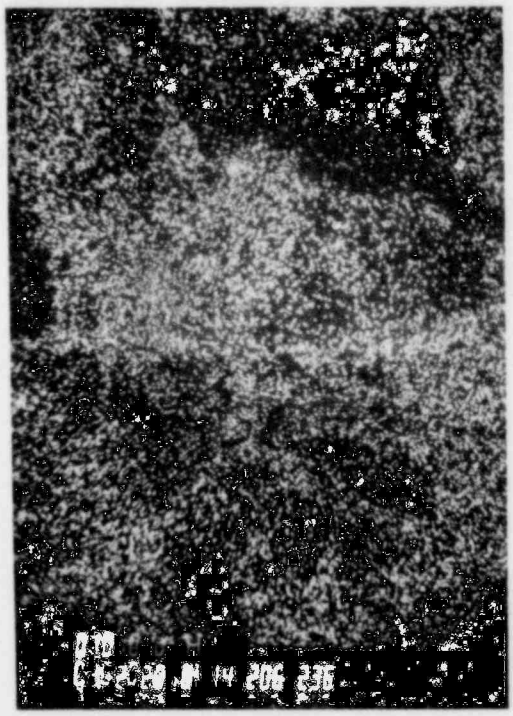

(b) Element distribution map for S. 150X

FIGURE F-5. LOCATION H.

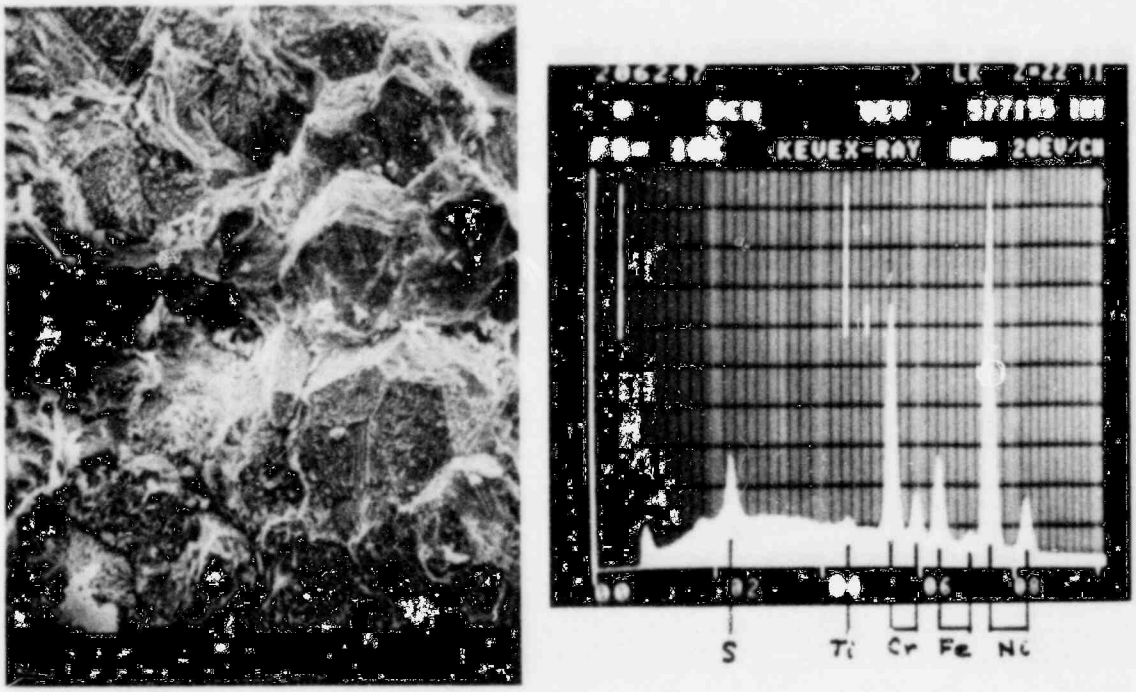

(a) 150X

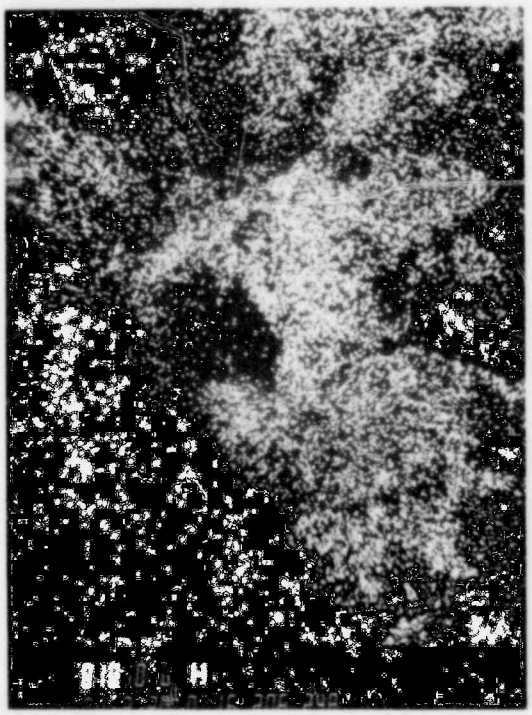

(b) Element distribution map for S. 150X

FIGURE F-6. LOCATION I.

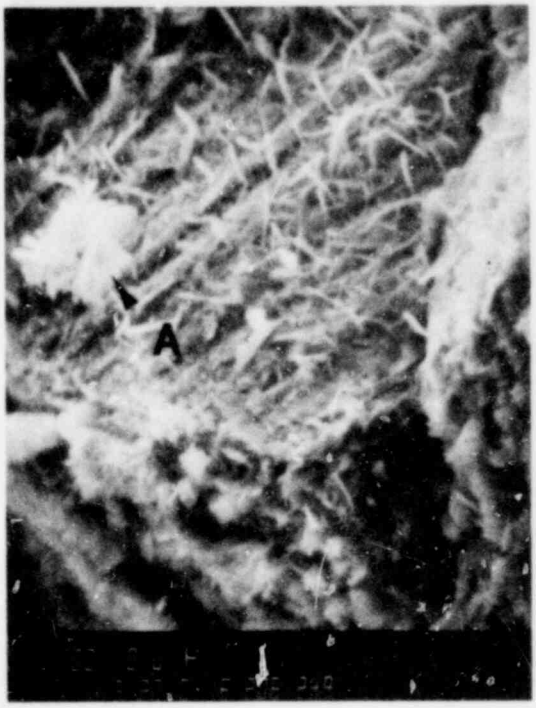

(a) 1500X

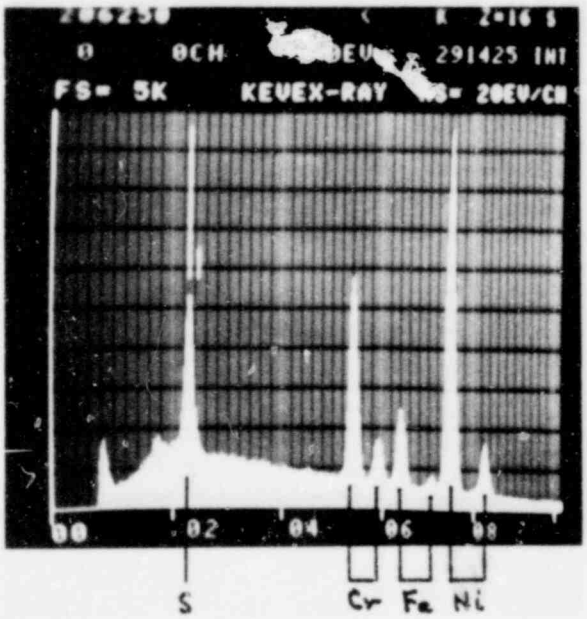

(b) Point A in (a)

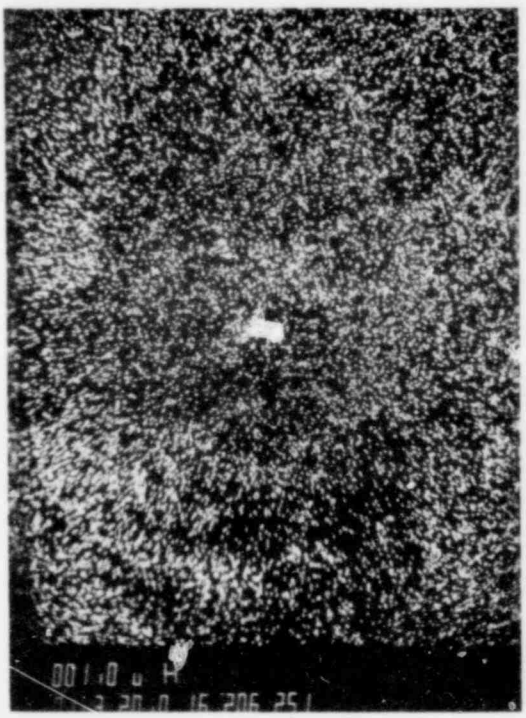

(c) Element distribution map for S. 1500X

FIGURE F-7. LOCATION I.

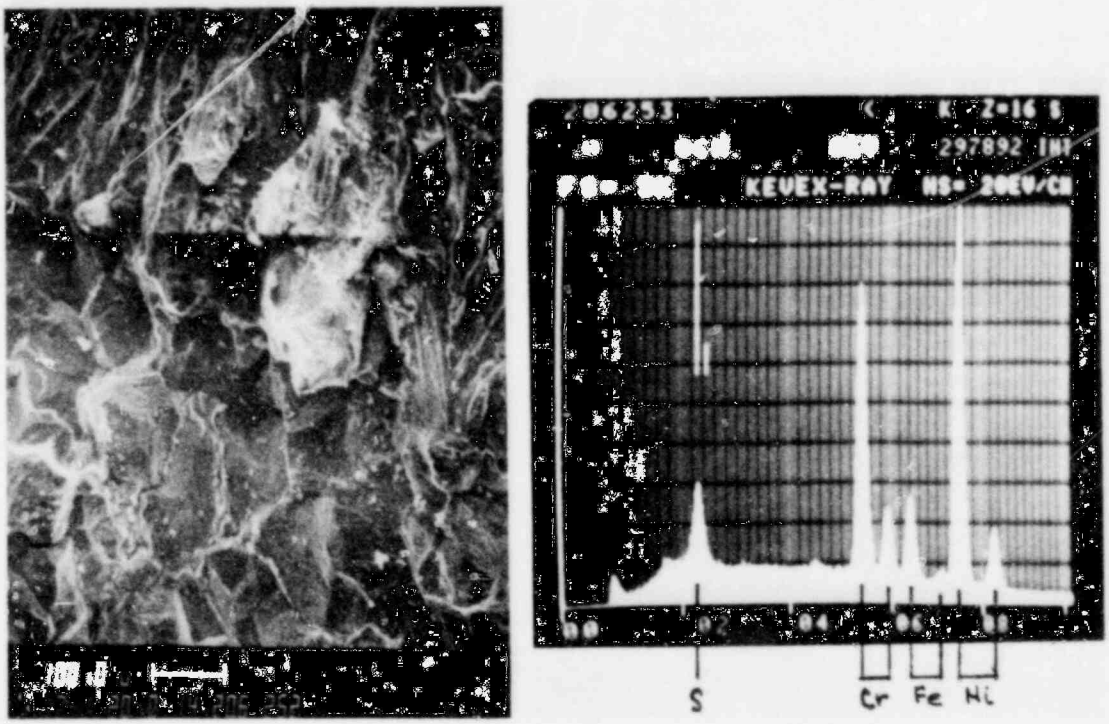

(a) 100X

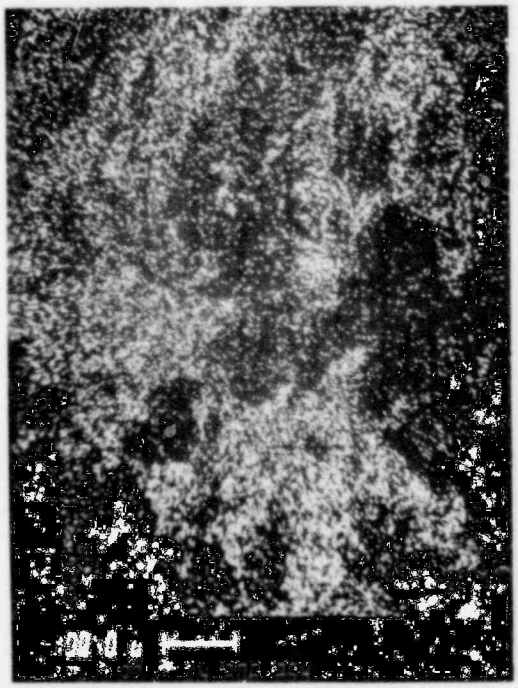

(b) Element distribution map for S. 100X

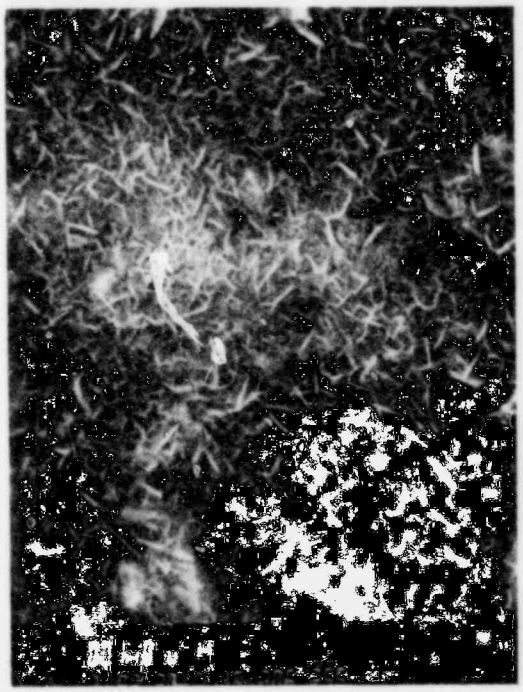

(c) Point A in (a). 1000X

FIGURE F-8. LOCATION J.

(a) 25X

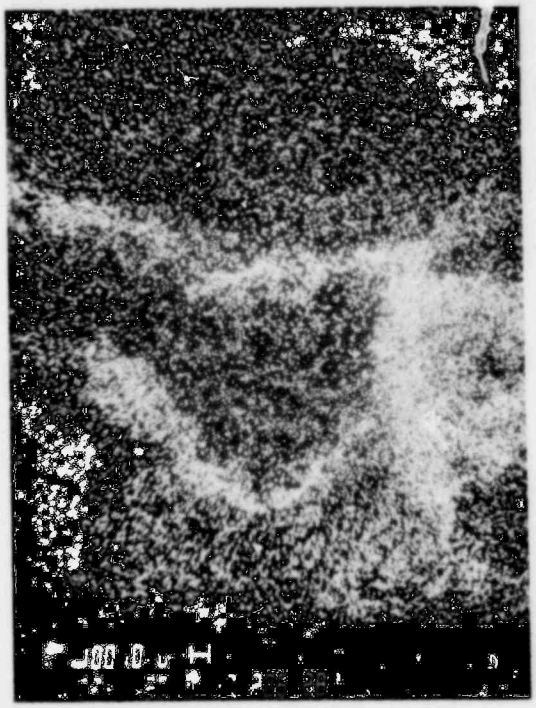

(b) Element distribution map for Fe. 25X

FIGURE F-9. LOCATION A. Crevice surface.

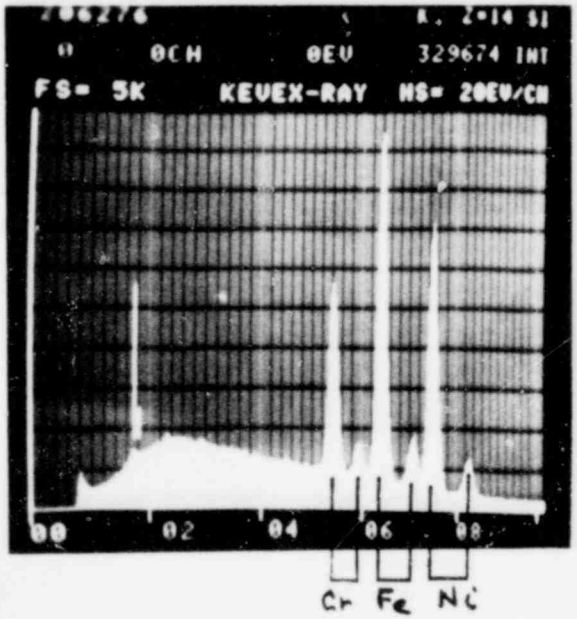

(a) 150X

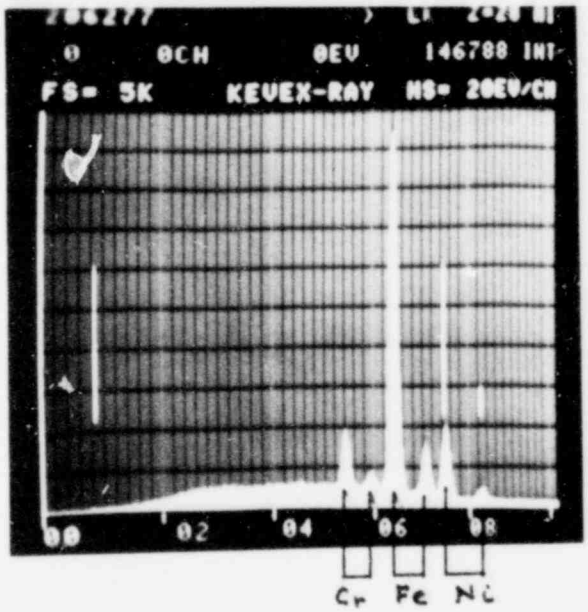

(b) Point A in (a)

FIGURE F-10. LOCATION B. Crevice surface.

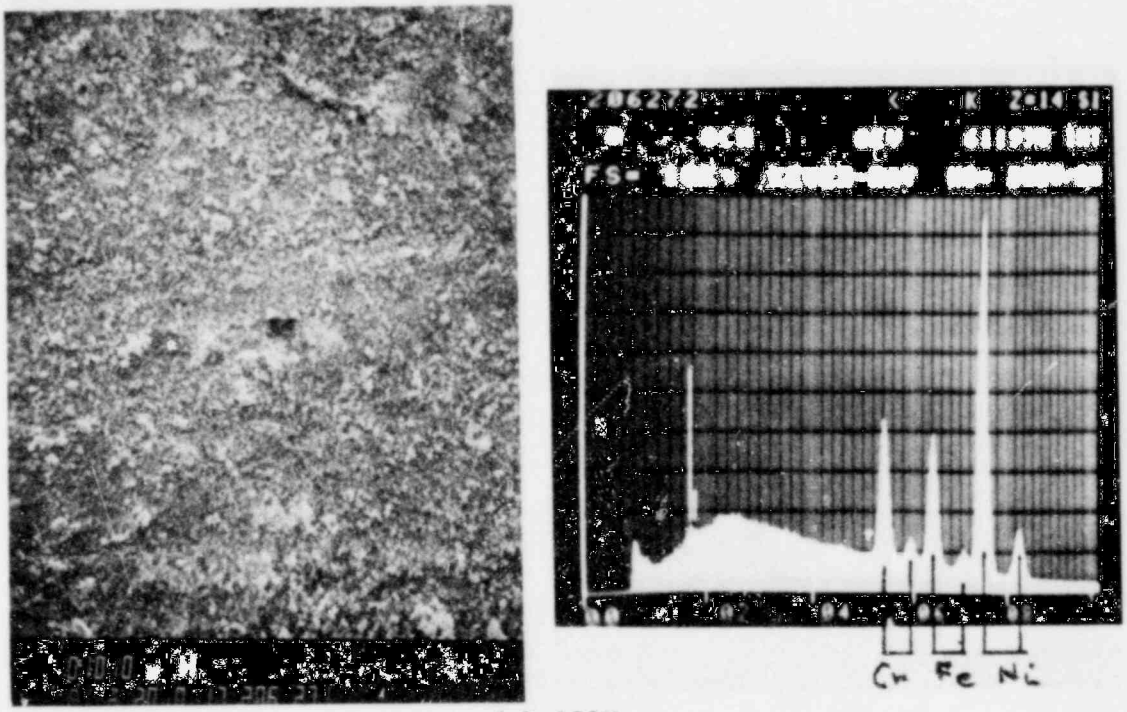

(a) 150X

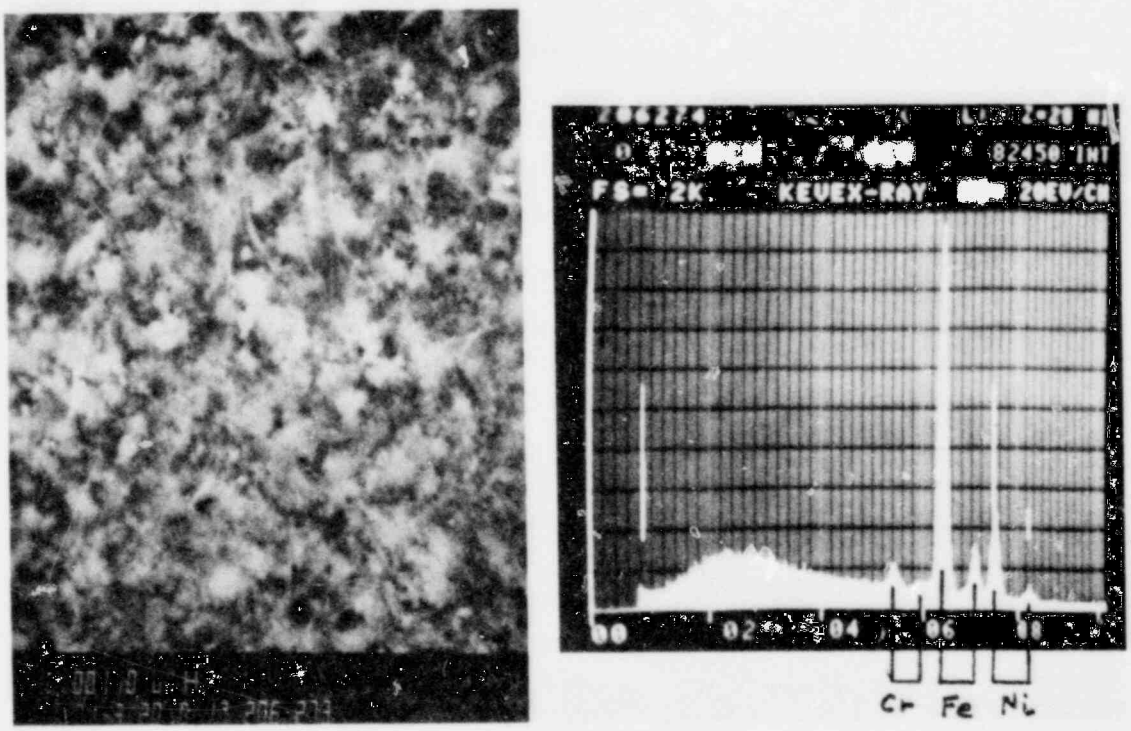

(b) 1500X

FIGURE F-11. LOCATION C. Crevice surface.

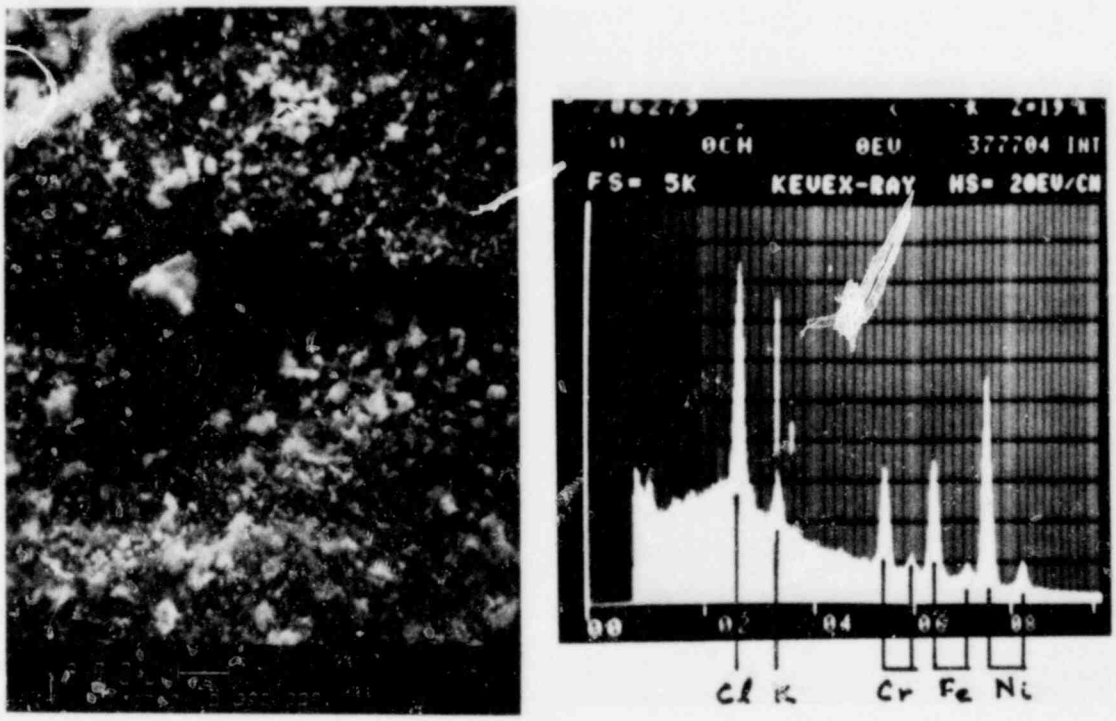

FIGURE F-12. LOCATION D. Crevice surface.

APPENDIX G

STRESS CORROSION CRACKING SUSCEPTIBILITY OF INCONEL 600 IN HIGH-PURITY ENVIRONMENTS

Literature Review

The Stress-Corrosion Cracking of Inconel 600 in High Purity Water Environments: A Literature Review

Inconel 600 is extensively used in the primary water circuits of Pressurized Water Reactors (PWRs), and its service performance has generally been good (1,2). The small number of service failures which have been reported can, in general, be attributed to caustic cracking (2-4). Failures have occurred at temperatures as low as 217°C (4), but contamination possible in PWR steam generator use accounts for the majority of these failures. To the author's knowledge, no failures attributable to pure water service have been reported.

The purpose of this review is to discuss those factors which may affect the service performance of Inconel 600 in Boiling Water Reactor (BWR) applications not involving heat transfer. In the absence of evidence of an upset in operating procedures involving an excursion in OH^- concentration, the performance of Inconel 600 in caustic environments is not at issue, since no mechanism of caustic concentration, such as that operative on heat transfer surfaces (5), is involved. No attempt will, therefore, be made to include a detailed appraisal of caustic cracking, although some mention will be made of the similarities between caustic and high purity water cracking. The major object here is to give a concise account of the expected influence of

a) Environment,

b) Geometry,

c) Stress Level, and

d) Metallurgical Condition

on service performance. It must be realized that the major use of Inconel 600 has been in PWRs, so that much of the data discussed has been collected at temperatures in excess of the normal operating temperatures of BWRs (290°C, 550°F). The compilation of Cowan & Gordon (2) shows that increasing temperature does increase susceptibility, but there is sufficient evidence of cracking at 290°C to suggest that the data derived at higher temperatures, up to 350°C, should be considered pertinent to the case in hand. Coriou and coworkers (10) consider the performance at 300°C to be similar to that at 350°C.

Effect of Environment

As early as 1959, laboratory studies showed that Inconel 600 was susceptible to intergranular stress-corrosion cracking (SCC) when exposed at high stress levels to high-purity water (8). Since that time, numerous workers have duplicated these results in pure water with oxygen contents ranging from the detection limit (< 3ppb) to levels above those experienced during normal BWR operation (i.e. 100-200 ppb) (8-17, 25, 27). There can now be no doubt that Inconel 600 can be cracked in water of a purity level typical of BWR service without the introduction of contaminants such as Pb^{2+} or OH^-. Although

cracking can be produced at oxygen levels approaching zero (9,10, 27), it is well documented that high oxygen contents accelerate attack (2, 13-17).

Various contaminants, apart from oxygen, are also of pertinence. Lead additions have been shown to accelerate the SCC of Inconel 600 and to cause a transition to transgranular fracture (13, 15). Contamination by halides (Cl^- and F^-) is also a common concern. Hydrofluoric acid is a constituent in commonly employed pickling baths, so that carry-over is a possibility. Chloride ions are known to have been involved in several service failures of stainless steels (1). Performance of Inconel 600 is not greatly influenced by Cl^- and F^- contamination (9, 10, 13, 15), although some pitting may occur. However, the observation that cracking is favored by acidic conditions (13, 14, 20) raises the question of the role these anionic species, which facilitate pit and crevice acidification, might play in in-service cracking. The existence of a crevice geometry, in combination with halide contamination, could conceivably accelerate SCC.

The role of electrochemical potential in the SCC of Inconel 600 is not well understood. Experimental evidence strongly supports the view that cracking is accelerated under oxidizing conditions (13-17, 20), and thus contamination by oxidizing species, such as O_2, H_2O_2 or Cr^{6+}, may be expected to be detrimental. Of major interest in regard to operating systems is the observation (1) that coupling with a type 304 alloy does not appear to significantly influence cracking behavior. Coupling is only of concern in practice on a local basis, since the high impedance (typically > $1\Omega M\ cm^{-1}$) of the solution prohibits long range galvanic effects.

In summary, the published data indicates that Inconel 600, when stressed to a sufficiently high level, is susceptible to intergranular SCC in typical PWR environments. No out-of-control conditions are necessary to cause SCC, although highly oxidizing conditions and low pH will probably stimulate the reactions causing SCC.

The Effect of Geometry

Two different geometric configurations deserve consideration, the occluded cell and the clean surface. The presence of an occluded region, such as a crevice, pit or lap, can significantly accelerate corrosive attack by concentrating aggressive species. In addition, such geometries act as points of stress concentration, increasing the local stress and thus favoring stress-corrosion cracking.

It has been conclusively shown that the presence of crevices (produced either by grain boundary attack or by specimen geometry) greatly accelerates the intergranular SCC of Inconel 600, particularly in the presence of high oxygen content and low pH solutions (2, 13-15). Results obtained by GE also clearly indicate that crevices are detrimental in pure water containing 200 ppb O_2, typical of reactor environments (27).

The mechanism of the crevice effect is not completely clear. In the low conductivity, low oxygen content solutions of interest, the conventional mechanism of crevice attack is of questionable relevance. It is highly unlikely that the classical deaeration cell can operate, since the high IR drop effectively isolates the interior and exterior of the crevice. It is, perhaps, instructive to note that during plant shutdown oxygen concentration will rise to 8 ppm, and some workers claim that levels of 100 ppm can be found in occluded regions such as the anular gap between the thermal sleeve and safe-end (18). These high levels could accelerate corrosion in such regions, and lead to the concentration of anionic species (e.g., Cl^-, F^-, $SO_4^=$) in the crevice, with the accompanying decrease in pH caused by hydrolysis of the dissolved metal ions. Since the concentration of anionic species in reactor water is very low, the classical scheme, of hydrolysis within the crevice and inward diffusion of anionic species to maintain charge neutrality, would be extremely sluggish. Once initiated, however, crevice corrosion would proceed, just as it does in the classical case, essentially independent of the bulk solution.

The Effect of Stress

Although some workers (27) have had difficulty cracking smooth specimens of Inconel 600 at stresses well above the yield stress, failures have been reported in uncreviced geometries at stresses as low as the 0.5% proof stress (7, 9, 10). Thus, it seems likely that the threshold stress lies near the yield stress. This parallels the behavior of sensitized type 304 stainless steel under similar conditions (21). The cracking of Inconel 600 is, therefore, not likely in BWR environments unless stresses exceed the yield stress.

The Effect of Metallurgical Condition

The familiar problems associated with the use of austenitic stainless steels in the sensitized condition has contributed to a wide suspicion of all alloys which may develop a similar condition. The Ni-Cr-Fe alloys also depend to a large extent on a passive chromium-based spinel for corrosion and oxidation resistance. The precipitation of carbides, particularly at grain boundaries, is therefore a potential source of problems, since this causes depletion of the (local) chromium level. Cause for concern is heightened, as the equilibrium solubility of carbon in Inconel 600 is significantly below that in iron-based austenitic alloys such as 304 (6, 24). Hence the matrix chromium content in equilibrium with carbides at any temperature is less than that in 304. A large effort has, therefore, been expended in the study of the effect of sensitization on the behavior of Inconel 600 in high purity water.

Mill-annealed Inconel 600 is generally in the sensitized condition, since practicable cooling rates for mill processes, and for large forged parts, are too slow to prevent carbide precipitation. Additional carbide precipitation can result from stress relieving heat treatment applied to pressure vessel components after fabrication. It should be pointed out that this treatment, commonly 1150-1200°F for several hours, is <u>not</u> a stress relief anneal of Inconel 600, but of the associated steel pressure-vessel components. Only slight stress relief of Inconel 600 results after heating to 1200°F or lower (23).

There is no evidence that a stress-relief sensitization treatment is detrimental to the stress-corrosion cracking resistance of Inconel 600 exposed to either high-purity water or caustic solutions. Coriou and co-workers (9, 10) have conclusively shown that lowering the carbon content and elimination of intergranular carbide precipitation have no apparent affect on the mechanism of cracking in high-purity water. Subsequently, others (11, 12, 14, 15) have shown that furnace sensitization of commercial Inconel 600 appears to increase resistance to SCC, both in high-purity water and in caustic solutions. However, as with the austenitic stainless steels, low sensitization temperatures are potentially more deleterious, since the equilibrium chromium and carbon levels are lower, and the diffusion rate is less, than at high temperatures. Therefore, prolonged aging at service temperatures could conceivably enhance chromium depletion. The effect of enhanced depletion is unknown. Alloys with increased chromium content (~30%) are known to be superior to Inconel 600 in high-purity water (10, 15, 26), but a simultaneous reduction in the nickel level, to ~60%, could be the main factor in improving resistance. The failure of sensitization at 1100-1200°F to reduce SCC performance of Inconel 600 suggests that low temperature aging may have little effect, despite fears to the contrary (3).

The above discussion is pertinent to the present failure, since welding produces zones of carbide re-solution and partial re-solution. On cooling, the region near the weld may be in a solution annealed or lightly sensitized condition. Further from the weld, a zone of heavier sensitization will be produced, regardless of the initial condition of the base metal. In initially solution-annealed base material the structure will, therefore, go through the transition from solution annealed (or slightly sensitized) near the fusion line to heavily sensitized in the heat-affected zone (HAZ), and back to the solution-treated condition. In base material which is initially sensitized, the degree of sensitization may be increased in the HAZ, because of the effect of the zone in which partial re-solution of the carbides has occurred (28). However, the structure will still consist of a solution annealed (or lightly sensitized) region at the fusion line and a heavily sensitized zone further out in the HAZ. Thus, the prior condition of the base material (sensitized or fully solution annealed) is not expected to have a significant effect on service performance.

The effects of welding and cold working have not been extensively investigated. The behavior of weld metal does not appear to be appreciably different from that of heat-affected zone of the base metal. The heat-affected zone may be slightly more resistant than the base material, but insufficient data is available to be positive (14, 15). The results of work investigating the effect of cold-work are conflicting, so it is unlikely that cold-work has a significant effect (2).

In conclusion, a literature review has established that:

1) Inconel 600 is susceptible to IGSCC in high purity water typical of BWR environments at stress levels above the yield strength.

2) The previous heat treatment is not critical in determining susceptibility. Specifically, sensitization associated with typical stress relief treatments is not detrimental.

3) The presence of a crevice can enhance the susceptibility to cracking at normal and above-normal oxygen levels.

4) Although contamination is not necessary to cause cracking of Inconel 600, caustic concentration, oxidizing agent concentration or acidification within a crevice could enhance failure.

5) Weld metal is not more susceptible to SCC than is the base metal.

REFERENCES

1. S. H. Bush and R. L. Dillon, "Stress-Corrosion Cracking and Hydrogen Embrittlement of Iron-Base Alloys," p 61, NACE, Houston (1977).

2. R. L. Cowan, II and C. M. Gordon, "Stress-Corrosion Cracking and Hydrogen Embrittlement of Iron-Base Alloys," p 1023, NACE, Houston (1977).

3. J. Weber and P. Sury, Materials Performance, 15, 34 (1976).

4. B. Gronwall, L. Ljungberg, W. Hubner and W. Stuart, Nuclear Eng., 6, p 383 (1967).

5. R. E. Hall, Trans. ASME, 66, p 457 (1944).

6. C. H. Wagner, H. Spahn and H. Schenk, Discussion of Ref. 25, p 1200.

7. H. Coriou, L. Grall, C. Mahieu and M. Pelas, Corrosion, 22, p 280 (1966).

8. H. Coriou, L. Grall, Y. L. Grall and A. Vettier, Third Metallurgy Conference on Corrosion, p 161, Saclay, North Holland Pub. Co., Amsterdam (1959).

9. H. Coriou, L. Grall, P. Olivier and H. Willermoz, "Fundamental Aspects of Stress-Corrosion Cracking," p 352, NACE, Houston (1969).

10. J. Blanchet, H. Coriou, L. Grall, C. Mahieu, C. Otter and G. Turbuer, "Stress-Corrosion Cracking and Hydrogen Embrittlement of Iron-Base Alloys," p 1149, NACE, Houston (1977).

11. H. A. Damian, R. H. Emanuelson, L. W. Sarver, G. J. Theus and L. Katz, Corrosion, 33, p 26 (1977).

12. F. W. Pement and N. A. Graham, "Corrosion Problems in Energy Conversion and Generation," The Electrochemical Society, Inc., Princeton (1974).

13. H. R. Copson and S. W. Dean, Corrosion, 21, p 1 (1965).

14. H. R. Copson and G. Economy, Corrosion, 26, 55 (1968).

15. H. R. Copson, D. van Rooyen and A. R. McIlree, "Proceedings of the Fifth International Congress on Metallic Corrosion," p 376, NACE, Houston (1974).

16. W. E. Berry, Discussion of Ref. 7, Corrosion, 22, p 287 (1966).

17. A. R. McIlree, H. T. Michels and P. E. Morris, "Corrosion Problems in Energy Conversion and Generation," Electrochemical Society, Princeton (1974).

18. T. Kondo, Y. Ogawa and H. Nakajima,"Corrosion Problems in Energy Conversion and Generation,"Electrochemical Society, Princeton (1974).

REFERENCES (Continued)

19. G. J. Theus and R. W. Staehle, "The Stress-Corrosion Cracking and Hydrogen Embrittlement of Iron-Base Alloys," p 845, NACE, Houston (1977).

20. D. A. Vermilyea, Corrosion, 29, p 442 (1973).

21. C. S. Tedmon, Jr., and D. A. Vermilyea, Corrosion, 27, p 376 (1971).

22. I. L. Wilson and R. G. Aspden, "Stress-Corrosion Cracking and Hydrogen Embrittlement of Iron-Base Alloys," p 1189, NACE, Houston (1977).

23. "Inconel 600," Huntington Alloy Products Division data sheet.

24. G. J. Theus, Nuclear Technology, 28, p 388 (1976).

25. G. J. Theus, Corrosion, 33, p 20 (1977).

26. A. J. Sedriks, J. W. Schultz and M. A. Cordovi, "Alloy 690 - a New Corrosion Resistant Material For High Temperature Applications," Presented at the 15th INCO Power Conference, Lausanne, Switzerland, Oct 5-7 (1977).

27. "Recirculation Inlet Safe-End Repair Program - Duane Arnold Energy Center," Iowa Electric Light and Power Company Report dated December 8, (1978).

28. H. D. Solomon, Corrosion, 34, p 183, (1978).